ICE XI:

THE ORDERED FORM

OF ICE Ih

by

RACHEL HOWE

A thesis submitted to the
Faculty of Science
of the
University of Birmingham
for the degree of
DOCTOR OF PHILOSOPHY

School of Physics and
Space Research
University of Birmingham
P O Box 363
Birmingham
B15 2TT
England

September 1988

SYNOPSIS

The history of the development of the understanding of the statistical arrangement of hydrogen bonds in ice Ih and the discovery of the transition at 72 K to the ordered phase, ice XI, catalysed by alkali hydroxide doping, is reviewed. Possible ordered arrangements of hydrogen bonds are discussed and enumerated. A theory is presented relating the entropy and permittivity of partially ordered ice to the degree of order. The apparatus developed for dielectric experiments on KOH-doped ice is described. The results of such measurements for polycrystalline specimens and one single crystal are presented. Measurements above the transition reveal that the main charge carriers are OH^- ions, with a temperature-independent mobility of approximately 10^{-10} m^2 V^{-1} s^{-1}. The transformation to the ordered phase starts when the sample is cooled below about 65 K, and once started can be speeded up by heating the sample to 67-70 K: the static permittivity and the a.c. conductivity slowly decrease. Neutron powder diffraction experiments were performed on HRPD at ISIS. After one unsuccessful experiment, dielectric measurements on powder samples showed the importance of excluding CO_2 during preparation. In a second experiment the structure of ice XI was confirmed and the lattice parameters determined for the first time.

DEDICATION

IN AFFECTIONATE MEMORY OF MY FATHER

WHO TAUGHT ME

(AMONG OTHER THINGS)

TO LOVE PHYSICS

ACKNOWLEDGEMENTS

I would like to acknowledge the invaluable assistance of, and offer thanks to, the following people:

Dr. R. W. Whitworth, for patient and stimulating supervision throughout the course of the work;

Dr. J. W. Glen, Prof. A. J. Leadbetter and Dr. A. I. M. Rae, for helpful discussions and encouragement;

Dr. S. Ahmad and Dr. M. Ohtomo, former colleagues in the Ice Physics Group, who taught me many things about the practicalities of research;

Dr. P. H. Borcherds, for permission to use the non-linear least squares fitting routine in the software for the dielectric measurement system;

Mr. D. J. Ives, who as a Vacation Student in the group carried out some useful work on KOH-doped single crystals of ice;

Dr. W. I. F. David, Mr. W. T. A. Harrison, Mr. R. M. Ibberson and Dr. R. C. Ward at the Rutherford Appleton Laboratory, for much advice and practical help with the neutron diffraction experiments and the associated computing;

Dr. P. Jovanovic and Mr. R. Staley, for the design and construction of the fast ADC unit;

The staff of the Condensed Matter Workshop, in particular Mr. E. L. Parker and Mr. G. R. Walsh, and Mr. R. Pflaumer, for advice on the design of apparatus and the skilled construction of the same once designed.

I am also grateful to the S.E.R.C. for the award of a Research Studentship and for the use of the facilities at the Rutherford Appleton Laboratory.

Finally, I would like to thank my landlady, Mrs. J. S. Goode, for providing a roof over my head and the minimum of domestic distractions, and, last but not least, my mother, who put up with three years of highly technical letters and was always there when needed.

CONTENTS

LIST OF FIGURES

Chapter 1

Chapter 2

Chapter 6

LIST OF TABLES

CHAPTER 1

THE ORDERED PHASE OF ICE: INTRODUCTION AND HISTORICAL BACKGROUND

1.1 Introduction

Ice can exist in many forms, depending on temperature and pressure: as well as ordinary hexagonal ice Ih and its metastable cubic counterpart ice Ic, there are the crystalline high-pressure phases, ice II to ice X, and at least two amorphous or vitreous forms. Some of these phases have ordered hydrogen bonds, while in others the bonds are disordered or symmetrical. Ice XI, the subject of this thesis, is the recently-discovered low temperature equilibrium version of the familiar ice Ih, with ordered bonds. The aim of the work presented in this thesis is to investigate the ordering transition by dielectric and neutron diffraction experiments, and by combining these with theoretical considerations to attempt to further the understanding of the structure of the ordered phase and the mechanisms by which it is achieved.

The history of the development of the current understanding of the arrangement of the protons in ice Ih, and of the transition to the ordered phase known as ice XI, is complex. To assist in tracing this development over more than sixty years of experiment, theory and speculation, a summary of the present position is essential.

Ice Ih, the ordinary hexagonal form of ice, consists of water molecules so arranged that the oxygen nuclei are tetrahedrally co-ordinated in a wurtzite-type structure. The four hydrogen bonds

joining each oxygen to its neighbours are disordered in their arrangement, subject to the conditions (the Ice Rules) that each molecule has two protons associated with it and there is only one proton on each bond. Above about 100 K this disorder is dynamic and in equilibrium: below this temperature one disordered configuration is 'frozen in', the disorder giving rise to a residual entropy of $Nk_B \ln(3/2)$, where N is the number of molecules. A small amount of local short-range order may occur at about this temperature, particularly in impure ice. The freezing in of the disorder, a kind of glass transition, occurs because the defects which allow rearrangement of the protons are thermally activated, becoming less numerous and less mobile with decreasing temperature. If the ice rules were ideally obeyed at all temperatures, no reorientation of isolated molecules or bonds could take place, and it would be difficult to change the proton configuration. Because the response of the ice to an electric field requires reorientation of molecules, in this case the dielectric constant and conductivity of ice would be low. It is believed that the observed dielectric properties can be explained by introducing four types of point defects constituting local violations of the ice rules, which can migrate around the lattice and so reorient molecules or bonds.

The defects are the ions OH^- and H_3O^+ and the so-called Bjerrum or orientational defects, the L-defect being a bond lacking a proton and the D-defect a doubly occupied bond. In pure ice these defects are created intrinsically as pairs of ions or Bjerrum defects, with an activation energy for their generation, while in ice 'doped' by the addition of small amounts of acidic or alkaline

FIGURE 1.1

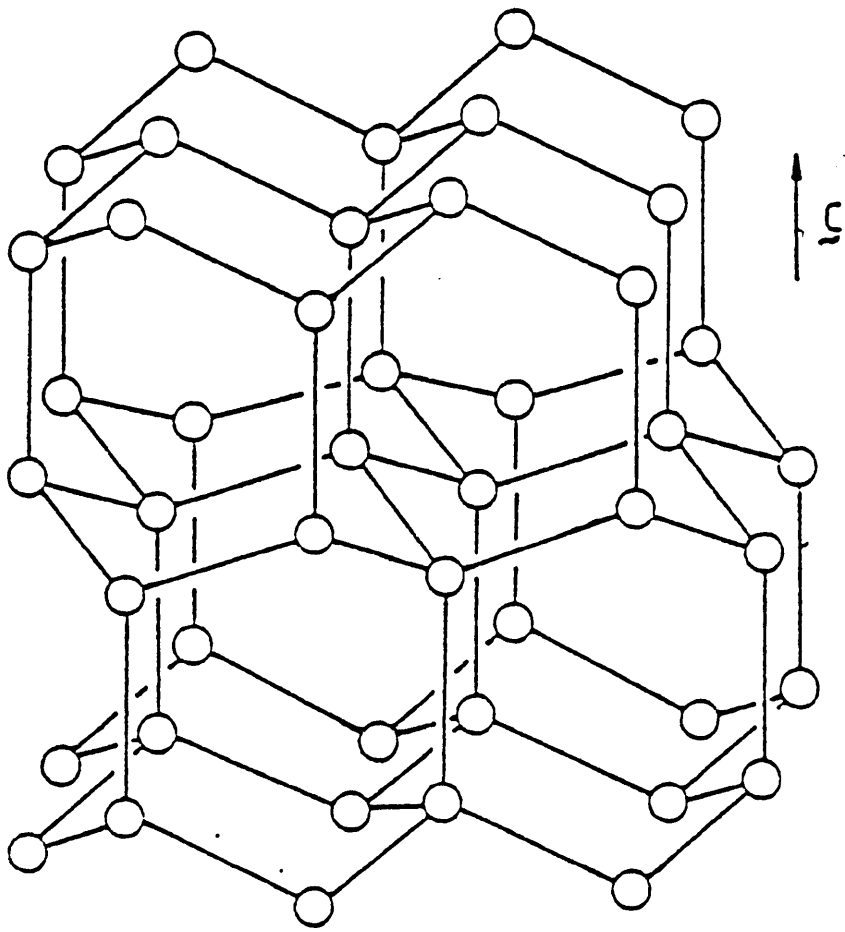

The arrangement of the oxygen nuclei in the hexagonal ice structure

impurities the defects may be introduced in other combinations and with lower activation energies. If the ice is doped with alkali hydroxides (in particular KOH), the extra defects introduced are sufficiently numerous and mobile at low temperatures to allow at least a partial transition to the equilibrium low-temperature phase, ice XI, to take place within laboratory timescales. The transition, to a phase in which the oxygen lattice is essentially unchanged but the protons are ordered, giving a polar structure with the space group $Cmc2_1$, proceeds over a period of days as the doped ice is held below the transition temperature of 72 K, and is of first order.

1.2 History

1.2.1 Proton disorder in ice Ih

The arrangement of the oxygen atoms in ice was first definitely determined by Barnes (1929), who used X-ray diffraction on both powder and single crystal specimens. The structure was found to contain four oxygen atoms per unit cell, with the hexagonal, centrosymmetric space group $P6_3/mmc$. The structure (shown in figure 1.1) is such that each oxygen is surrounded by four others at the corners of an approximately regular tetrahedron: the unit cell is divided into two layers perpendicular to the *c*-axis. Each layer in the structure consists of a network of puckered hexagonal rings, joined by bonds parallel to the *c*-axis in such a way that, if the *c*-axis is considered to be vertical, the rings of one layer are directly above those of the next but have their sides sloping in the opposite sense. This structure is equivalent to that

suggested by Bragg (1922). There was at that time no means of determining the positions of the hydrogen atoms in the structure, but Barnes suggested that one should lie at the centre of each oxygen-oxygen axis, forming ionic bonds.

In 1933 Giauque and Ashley, by careful measurement of the heat capacity of ice, confirmed what was already suspected: there existed a discrepancy of approximately 4 J mol^{-1} K^{-1} between the entropy of ice at low temperatures as calculated by such measurements and that calculated from studies of the band spectra of water vapour. They suggested that this was due to the rotation of water molecules so that the distinction between 'ortho' and 'para' molecules with different spin quantum numbers was preserved. Such a situation, with three out of four molecules having j=1 and one having j=0, would give rise to an entropy discrepancy of $(3/4)R\ln 2$ per mole (4.32 J mol^{-1} K^{-1}), where R is the gas constant.

At almost the same time, and probably not knowing of the work of Giauque and Ashley, Bernal and Fowler (1933) suggested yet another possible arrangement for the hydrogen atoms. This was based on the idea that ice consisted of intact water molecules, modelled as tetrahedra with two positive and two negative corners, arranged such that the two hydrogen nuclei of each molecule lay opposite negatively charged corners of two of the four neighbouring molecules, while the negative corners of the original molecule lay opposite the two hydrogen nuclei of the remaining neighbour molecules. On the basis of these conditions, which have become

known as the Bernal-Fowler rules or ice rules, the authors proposed a regular arrangement of hydrogen atoms, the simplest to have hexagonal symmetry, with twelve molecules in a cell and the (polar) space group $P6_3mc$. They also suggested that it was...

> "quite conceivable and even likely that at temperatures just below the melting point the molecular arrangement is still partially or even largely irregular, though preserving at every point tetrahedral coordination and balanced dipoles. In that case ice would be crystalline only in the position of its molecules but glass-like in their orientation."

Pauling (1935) carried the suggestion of Bernal and Fowler an important step further. To their assumptions of tetrahedrally coordinated intact water molecules and exactly one hydrogen per oxygen-oxygen bond, he added the further assumption that all configurations obeying these rules would have the same energy. The large number of such configurations would then give a contribution to the entropy which, if one configuration became 'frozen in' at low temperatures, could give rise to the observed residual entropy. Pauling calculated the size of this contribution as follows. Every molecule has six possible orientations if the requirement for correctly formed bonds is neglected, but for each of its two hydrogens the probability that there is no hydrogen at the other end of the bond is 1/2. The probability that a molecule can be correctly joined to its neighbours is thus 6/4 = 1.5, and the entropy per mole is R ln 1.5, or 3.37 J K^{-1}.

Giauque and Stout (1936) made more precise measurements of the heat capacity of ice down to 15 K. When compared with an improved calculation of the entropy by spectroscopic methods, these

measurements gave a value for the entropy discrepancy of 3.42 J mol^{-1} K^{-1}. This was closer to the value of Pauling than to that calculated for the rotating-molecule model. A more critical test of the two models was provided by Long and Kemp (1936), who measured the heat capacity of deuterated ice. According to the Pauling model the residual entropy should be isotope-independent, whereas in the rotating-molecule model the value for D_2O should be $(R \ln 2)/3$ per mole or 1.92 J mol^{-1} K^{-1}. The experimental value of 3.23 J mol^{-1} K^{-1} provided further support for Pauling's statistical model of the ice structure.

In the absence of any more direct evidence as to the proton positions, the matter rested at this point until the development of neutron diffraction techniques. In 1949 Wollan, Davidson and Shull carried out neutron diffraction measurements on powdered D_2O ice at 183 K, D_2O being chosen because of the higher coherent cross section and lower diffuse scattering for deuterium compared with hydrogen. The results were compared with the symmetrical-bond model of Barnes, the ordered arrangement of Bernal and Fowler, the rotating-molecule model and Pauling's statistical model (which would appear from diffraction measurements as though every possible deuteron site were occupied by half a deuteron and is therefore sometimes known as the half-hydrogen model). The statistical model was found to be in the best agreement with the data.

The assumption of Pauling that all configurations of molecules obeying the ice rules would have the same energy and probability was first seriously challenged by Bjerrum (1951) on the basis of a

FIGURE 1.2

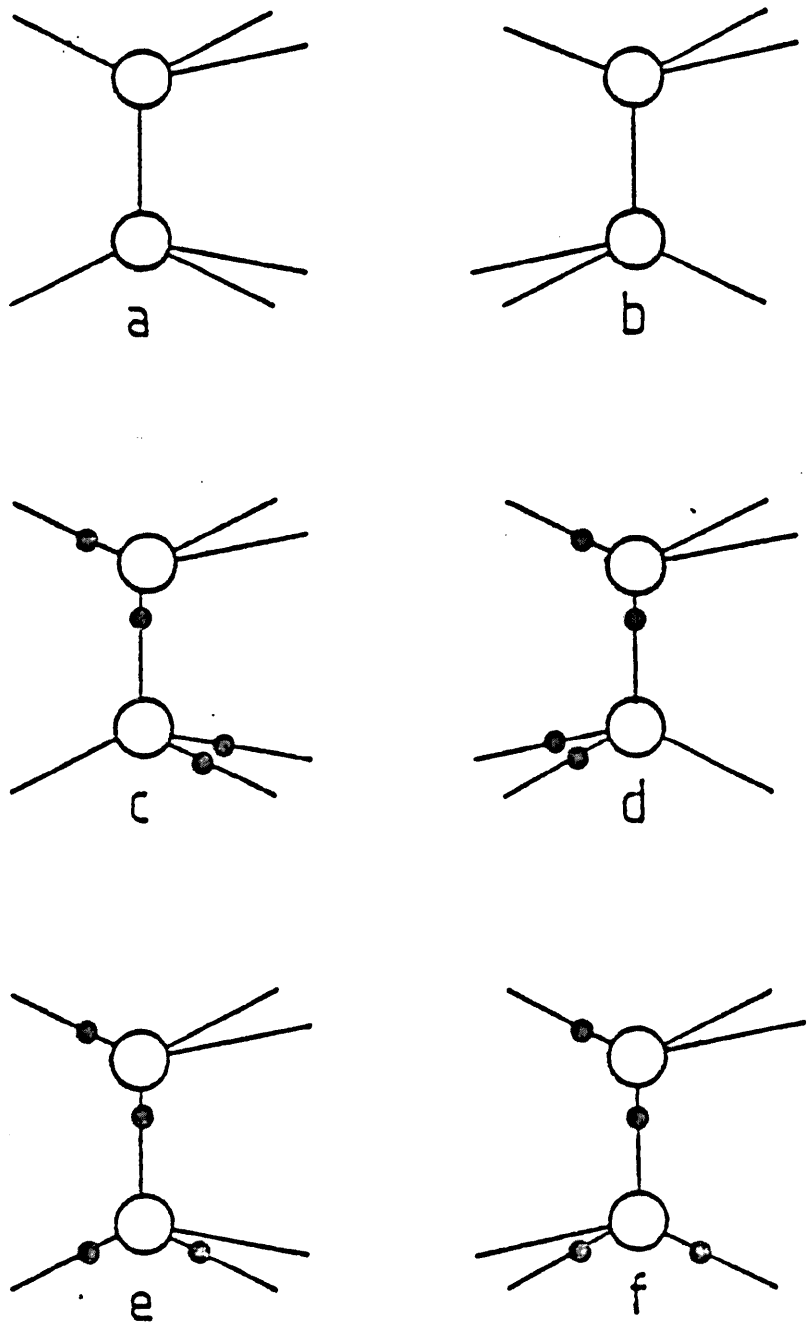

The possible molecule-molecule interactions:
a) Mirror symmetry
b) Centre symmetry
c) Inverse mirror symmetry
d) Inverse centre symmetry
e) Oblique mirror symmetry
f) Oblique centre symmetry

consideration of the interactions between nearest-neighbour molecules, modelled as tetrahedral arrangements of point charges. Bjerrum argued as follows: all pairs of neighbouring molecules in the ice lattice are either mirror-symmetric (figure 1.2 (a)) or centre-symmetric (figure 1.2 (b)). For each type of pair there are two possible relationships between the arrangements of protons on the bonds, known as inverse (figure 1.2 (c) and (d)) and oblique (figure 1.2 (e) and (f)). Of the three possible orientations of the second molecule of a pair when the first is fixed, one is inverse and two are oblique. Bjerrum calculated the electrostatic energy of each configuration and concluded that the inverse-mirror and oblique-centre combinations were energetically favourable, the differences being large enough to invalidate the assumption of equal probabilities even close to the melting point.

In the same paper, Bjerrum postulated the existence of the orientational defects (L and D) which bear his name and which became a vital component of later theories of the dielectric properties of ice. A detailed discussion of this area would be beyond the scope of this chapter: the relevant consequences of the theory will be dealt with in section 5.3.

Owston (1953) found an arrangement of protons in which all the nearest neighbour interactions would be those favoured by Bjerrum's calculation. This arrangement has an eight-molecule orthorhombic unit cell. Owston erroneously assigned it to the monoclinic space-group *Pc* and claimed it to be polar. In fact the correct space-group, $Pna2_1$, is geometrically polar but the arrangement of

the protons is such that the cell would have no net dipole moment unless the atomic coordinates were altered from those of the disordered ice structure. The neutron diffraction data of Wollan et al. were not of sufficient quality to discriminate against this model, but Owston's own X-ray work (at about 263 K) showed no evidence of order in the proton system. This led to the sugestion that the ordered structure was an ideal arrangement, not realised in practice, but which might be attained if the ice were kept at low temperatures for a sufficiently long time.

Pitzer and Polissar (1956) modified the calculations of Bjerrum by including an interaction omitted by him, and thereby considerably reducing the energy differences between the different types of configuration, though not changing their sign. The prediction by these authors of a lamda-type transition to an ordered phase with a critical temperature of about 60 K was accompanied by the suggestion that the sluggish thermal equilibrium observed by Giauque and Stout between 85-100 K might be associated with a slight shift towards an ordered structure, while the time to reach equilibrium at the hypothetical Curie temperature must be very long. The validity of their calculation is put in some doubt by the fact that they predict a positive Curie temperature for what, according to their model, would be an antiferroelectric transition.

A completely different suggestion for ordering in the proton system was made by Rundle (1955), who proposed a structure in which the bonds parallel to the *c*-axis would be polarised while some disorder remained in the planes perpendicular to this direction. This model

was an attempt to explain the apparent polar properties of ice reported by some workers, but failed to account for the observed residual entropy.

Peterson and Levy (1957) carried out a single-crystal neutron diffraction study on D_2O ice at 223 K and 123 K, which provided more definite evidence for the half-hydrogen model, ruling out those of Rundle and Owston.

Giguère (1959) considered the available data on the heat capacity of ice in some detail, comparing it with that for crystalline hydrogen peroxide (H_2O_2), and with a theoretical calculation based on the Debye model, and pointed out that

> "...the calculated entropy of ice in the neighbourhood of 100 K is smaller than the experimental quantity by about the same amount ... as the residual entropy. From this one might speculate that the disorder in ice contributes equally to the zero-point entropy and the 'excess' calorimetric entropy over the range 0-100 K."

On this basis Giguère endorsed the suggestion by Pitzer and Polissar of an unrealised lamda transition at some temperature below 100 K, though his own calculations suggested a transition temperature of about 80 K. This work made no attempt to speculate on the nature of the ordered phase or the interactions which would make a particular configuration more energetically favourable.

1.2.2 The 'transition' at 100 K

The claim by Dengel, Eckener, Plitz and Riehl (1964) to have found evidence of a ferroelectric transition at about 100 K in "ice which

was not highly pure" prompted a number of experiments looking for anomalies in this temperature region. These workers used two different techniques, one involving the measurement of the current induced when the ice sample was heated in an electric field, the other the measurement of the current flowing in response to a step voltage applied at constant temperature. The latter type of experiment is prone to errors due to the difficulty of extrapolating an exponential decay to an unknown baseline, so that the claim to have found a maximum in the static dielectric constant at 100 K by this method must be open to question.

Van den Beukel (1968), following a suggestion by Onsager (1967), measured the heat capacity of ice doped with HF and annealed for several hours at 95 K. Some anomalies were found, but the amount of entropy removed by the apparent ordering was small. Similar experiments by Pick (1969) and Pick, Wenzl and Engelhardt (1971) also found small anomalies at around 100 K in the heat capacity of doped ice.

Helmreich (1969,1973) found small changes in the elastic constants (as measured by the velocity of ultrasound) in H_2O and D_2O ice at around 100 K: although the changes were not significant within the accuracy of the experiment, repeated cycling of the temperature caused a cumulative effect.

Sakabe, Ida and Kawada (1970) found that ice doped with NaOH showed a maximum in the static permittivity at about 80 K, below which temperature the permittivity (actually measured at 1 Hz) fell

steeply to zero. The measurements of Kawada (1972) on ice doped with KOH showed a discontinuity in the permittivity at about 70 K, which appeared to be associated with a latent heat as would be expected for a first-order transition. However, this work, probably the first to find the true ordering transition in ice, attracted little attention and was not followed up at the time.

The neutron diffraction work of Chamberlain, Moore and Fletcher (1973), on a single crystal of H_2O ice, lightly doped with HF and measured at 77 K, showed no evidence of any ordering transition.

The work of Haida, Matsuo, Suga and Seki (1974) on the heat capacity of pure ice provided an explanation for the anomalous behaviour of ice in the region around 100 K. These workers carefully examined the heat-capacity data of Giauque and Stout (1936) in the 85 to 100 K region in which the authors had reported slow thermal equilibrium, and found that the measured values had a small systematic deviation from those extrapolated from the high-temperature side. They then measured the heat capacity of ice paying particular attention to the effect of annealing in the temperature region of interest, and found an anomaly which was increased by annealing in this temperature range. These measurements, more accurate than those previously mentioned, suggested that there was indeed a slight shift towards an ordered state, but with no more than 2% of the residual entropy being removed. This group had pioneered the concept of 'glassy crystals', in which molecules are ordered in position but disordered in orientation, with the disorder freezing in to give a 'glass

transition' at a temperature where the relaxation time for approaching the equilibrium ordered state becomes long compared with the experimental timescale. (See, for example, Suga and Seki 1974). They now suggested that ice was an example of such a crystal, and that the anomalous behaviour in the 85-100 K region was due to the glass transition and the small degree of ordering taking place at that temperature, rather than to a genuine ferroelectric transition.

1.2.3 Theories for ordering, 1979-1981

Once the idea of a ferroelectric transition at 100 K had been discredited in this way, little further experimental progress was made for some time. However, three theoretical works published in the period 1979-1981 are of some interest.

Hentschel (1979) considered the evidence for a transition somewhere in the region 70-100 K, apparently in ignorance of the 1974 paper of Haida et al. He then calculated the free energy for a partially ordered structure (like that proposed by Rundle), polarized parallel to the *c*-axis, and predicted a second-order transition with a critical temperature of 73 K.

Barnes, Bliss, Finney and Quinn (1980) attempted to predict the non-existence of the ordering transition by a computer simulation. An ordered structure with a unit cell of eight molecules was first generated and its electrostatic energy calculated. The structure was then disordered by reversing bonds around closed paths, and the energy of the new configuration calculated. The disordered state

was found to be energetically favourable at all temperatures, and it was concluded that the ordered state would never be attained. However, the method depends on the initial ordering being antiferroelectric so that the loops used in the disordering process may be closed. The arrangement chosen appears to have been that proposed by Owston. Therefore, a ferroelectric ordered state is not in fact ruled out by this work.

The contribution of Minagawa (1981) will be discussed in detail elsewhere, but a summary is given here for completeness. Minagawa devised a model in which the water molecule is represented by four point charges at the corners of a tetrahedron and an additional quadrupole moment located at the site of the oxygen nucleus. Considering interactions between nearest neighbour molecules along with a long-range interaction modelled as a dielectric constant, and using the four-molecule unit cell, the author found an expression for the free energy as a function of the proton configuration. The Curie and Curie-Weiss laws found by Kawada (1978) for ice perpendicular and parallel to the *c*-axis were used to obtain the energy differences between the oblique and inverse symmetries for pairs of molecules and hence fix the size of the additional quadrupole term. The result of this calculation was that the favoured combinations were found to be inverse mirror and inverse centre, in contrast to the conclusions of Bjerrum and others. A first-order transition was predicted, with critical temperature 69 K: the ordered phase had a polar structure in which all interactions were of the favoured types. According to these calculations the equilibrium state for several degrees below the

FIGURE 1.3

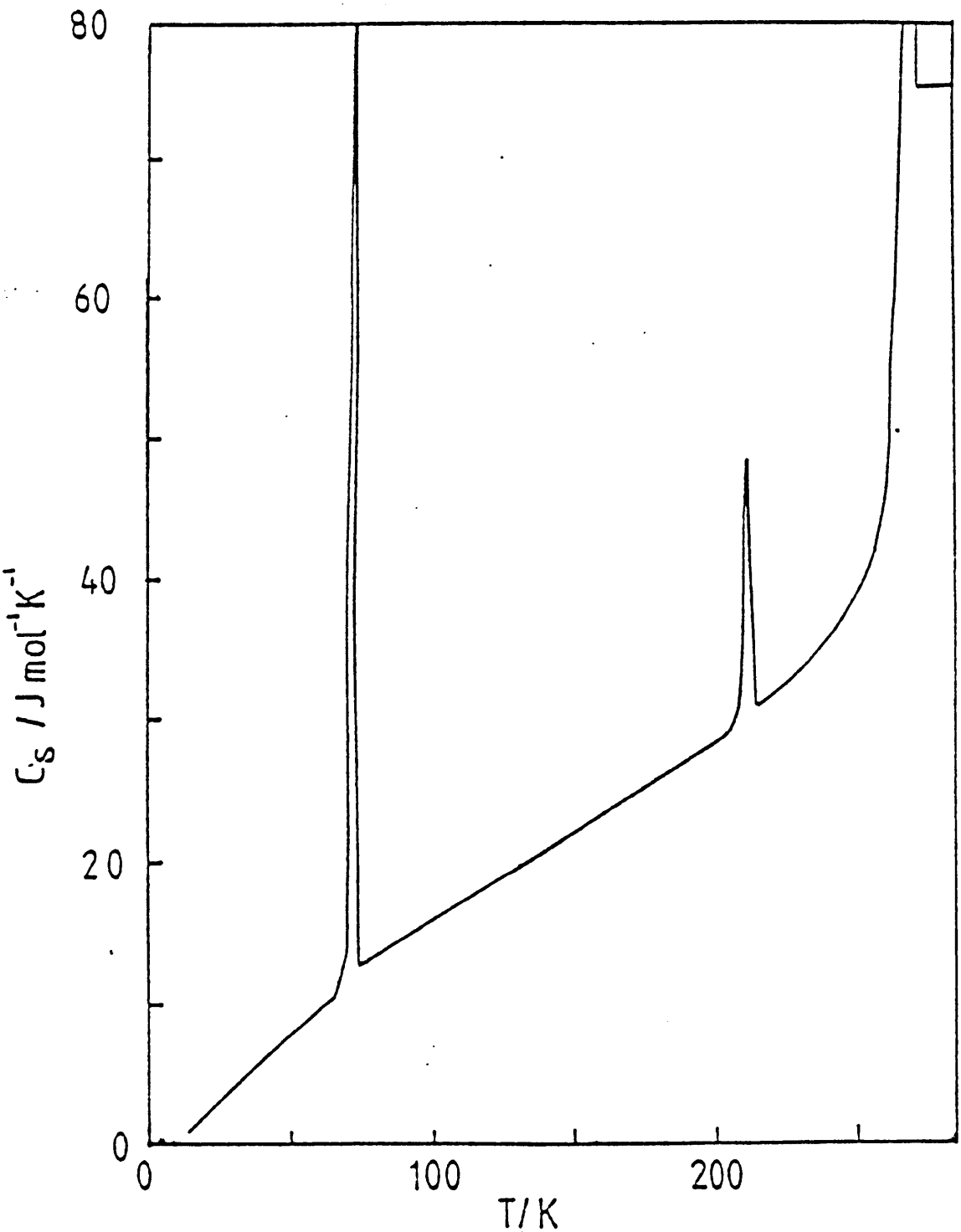

Variation of heat capacity C_s with temperature on heating, for a sample of ice doped with 0.1 M KOH and annealed below 72 K. (After Tajima et al.)

transition temperature would not be not completely ordered, about 85% of the bonds being in their correct orientation immediately below the transition.

1.2.4 Alkali hydroxide doping and the ice XI-Ih transition

The next interesting experimental development began with the work of Ueda, Matsuo and Suga (1982), who studied calorimetrically the effect of hydrogen fluoride doping. In common with previous workers, they found that the anomaly in heat capacity around 100 K was increased by the doping and by annealing in this temperature range. The doping decreased the relaxation time, in the best instance by a factor of about 30, but this was not enough to reveal the full ordering transition.

Tajima, Matsuo and Suga (1982;1984) investigated the effect of doping with alkali hydroxides and obtained dramatic results, particularly with potassium hydroxide which was used in the initial experiment. Solutions of KOH of the desired concentrations (0.1, 0.01 and 0.001 M) were frozen in the calorimeter cell to obtain polycrystalline samples. When the sample was cooled to about 60 K, a spontaneous heat evolution, continuing for about a week, was observed in the adiabatic calorimeter. When the sample was subsequently cooled to 13 K and then heated as the heat capacity was measured, a strong anomalous peak in this quantity appeared at 72 K. A typical heat-capacity plot for a sample frozen from a 0.1 M solution is shown in figure 1.3. The anomalies at 208 K and 273 K were attributed to the eutectic melting of concentrated KOH solution and to the melting of the ice, respectively. In the less

concentrated samples the eutectic anomaly was absent, which suggested that all the KOH had been incorporated in the bulk of the ice. The anomaly at 72 K was interpreted as evidence of a first order transition between the ordered phase at low temperatures and the disordered state. The peak had a high-temperature 'tail' extending about 40 degrees above the transition temperature, which was attributed to the short-range ordering which in pure ice would be frustrated by the glass transition. The size of the peak, which is related to the amount of entropy removed by the ordering process, was found to vary with the concentration of dopant in the specimen. The maximum amount of entropy lost, in a specimen frozen from a 0.1 M solution and annealed in the 60-65 K region for 256 hours, was 2.33 J mol^{-1} K^{-1} or about 68% of the total residual entropy. Less entropy was removed from the specimens with lower dopant concentration, but the amount of entropy removed per dopant ion increased with decreasing concentration. The degree of transformation to the ordered phase appeared also to depend on the thermal history of the sample and the temperature to which it had been heated after any previous transition, but this dependence was not easy to characterize.

The role of the KOH doping in catalysing the transition to the ordered phase was not well understood at this time: it was not even clear whether the K^+ or the OH^- ion was the important component. The authors pointed out that the doping would introduce a Bjerrum L-defect as well as the OH^- ion, but doping with HF, which would also introduce L-defects, was known not to be effective in producing the transition. They suggested that the presence of the

K^+ ion, incorporated interstitially in the lattice, would disturb neighbouring bonds and perhaps thereby enable large numbers of extra defects to be produced, allowing ordering to take place in a region around the ion.

In an attempt to establish the structure of the ordered phase, Leadbetter, Ward, Clark, Tucker, Matsuo and Suga (1985) performed a neutron diffraction experiment on a powdered sample of D_2O ice doped with KOD by dissolving the metal in high-purity D_2O. The sample was frozen by pouring the solution a little at a time onto a block of metal buried in dry ice, and dry ice was also used to cool the mortar used for grinding, which was carried out in a glove box under a dry atmosphere to avoid contamination of the D_2O by H_2O. The sample was then sealed in a vanadium cell for the annealing and diffraction experiment. Diffraction profiles were obtained at 5 K and 65 K, below the 76 K transition temperature for deuterated ice, and above it at 120 K.

The differences between the profiles were not dramatic, but the low-temperature spectrum showed one small additional peak as well as extra 'wings and shoulders' on some others. The extra peak could be indexed as (111) in the $P6_3/mmc$ space group of hexagonal ice, in which this is a systematically absent reflection. In an orthorhombic structure with 8 molecules per unit cell and the space group $Cmc2_1$, the reflection would be indexed as (131). This structure is the one predicted by Minagawa (1981). Profile refinement based on a partial order with this symmetry suggested that about 63% of the bonds had their 'correct' orientations. The

broadening of the extra peak indicated that the ordering took place in small, strained regions about 40 angstrom across. Some other possible ordered structures will be introduced in chapter 2: the relation of the diffraction results to the calorimetric experiments will be discussed in chapter 3.

Matsuo, Tajima and Suga published the results of experiments on doped D_2O ice in 1986, although the information was presumably available when the neutron diffraction experiment was carried out in 1982. The experiment was similar to that on H_2O. A sample of D_2O doped with 0.01 M KOH underwent only a small amount of transformation to the ordered phase. However, when D_2O was doped with 0.1 M KOD by dissolving the potassium metal in the liquid, the result was more satisfactory. The transition temperature was 76 K in both cases, and the maximum amount of entropy removed was 64% of the total residual entropy for D_2O. The heat capacity peak had an extended high-temperature tail, similar to that found with hydrogenous ice. The failure to achieve ordering in the specimen doped with KOH was unexpected: the authors suggested that the OH^- ions might be less mobile in D_2O than OH^- in H_2O or OD^- in D_2O. A tentative explanation of the isotope shift in the transition temperature was given by considering the effect of deuteration on the frequencies of vibrational modes of the water molecule in ice. This paper contains the first English reference to the new phase as 'Ice XI'. However, the name had previously been used in a Japanese publication (Suga, 1985).

Prompted by the success of Tajima et al., Kawada and Dohata (1985)

FIGURE 1.4

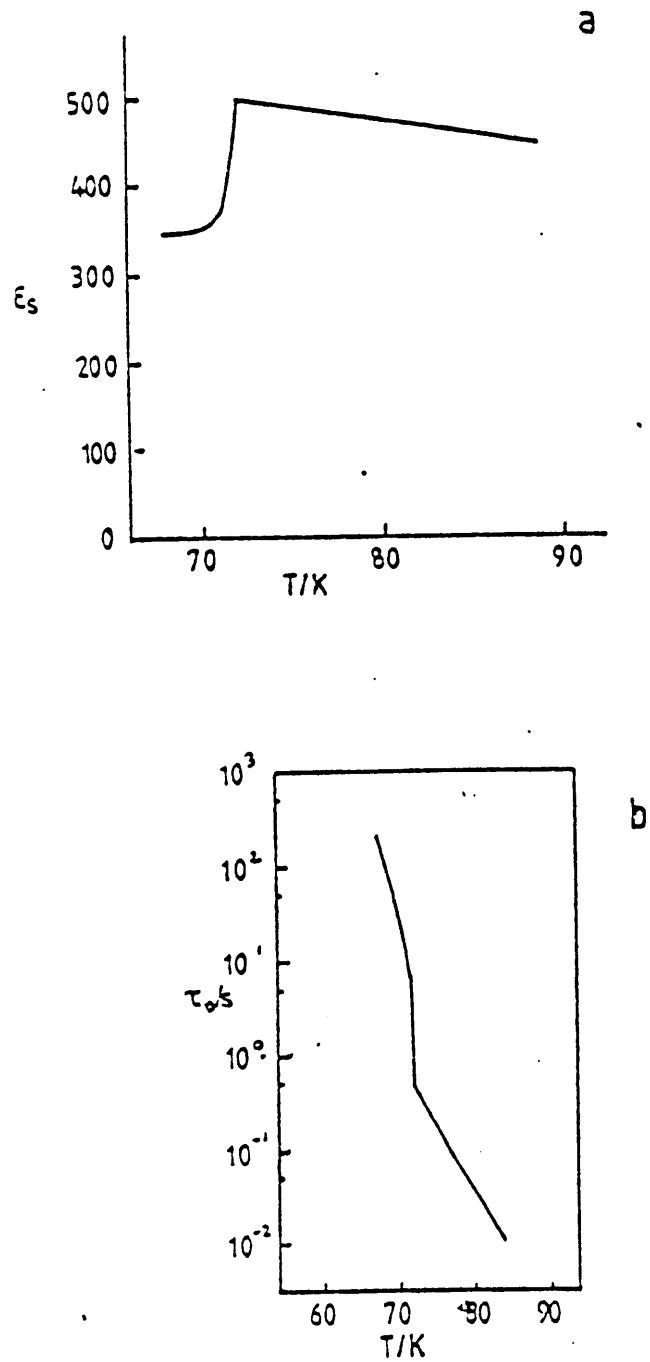

Results from dielectric measurements on KOH-doped ice on heating after annealing below 72 K.
a) Variation of static dielectric constant ε_s with temperature.
b) Variation of relaxation time τ_ϕ with temperature
After Kawada and Dohata (1986)

performed a more thorough investigation of the transition in KOH-doped ice by dielectric methods. Samples prepared by diluting commercial standard solutions were frozen in a cell between the parallel gold plates of a capacitor. The concentration of KOH was varied from 0.1 to 0.01 M, but the value of the dielectric relaxation time τ_D at 77 K remained constant at about 0.04 s. The components of the complex permittivity (permittivity and conductance) were measured over the frequency range 1 Hz to 10^{-3} Hz at temperatures between 55-90 K on cooling and heating. No anomaly in the dielectric properties was observed as the sample was cooled below 72 K at a rate of about 4 K per hour. The observed dielectric relaxation was found to be polydispersive (that is, not having a single clearly defined relaxation time but a distribution of times). The activation energy for the temperature variation of τ_D was found to be about 0.15 eV, much lower than the 0.57 eV typical for pure ice at temperatures above about 220 K.

When the sample was held below the transition temperature, an evolution was observed by which τ_D became progressively longer and the static permittivity ε_s (the measure of the strength of the dispersion) was reduced. The characteristic time for this evolution is quoted as 'about several days'. The variation of these quantities on heating is shown in figure 1.4: both showed discontinuous jumps at 72 K; the permittivity by about a factor of two, the relaxation time by a decade or more, the size of the discontinuities depending on the duration of annealing below the transition temperature. The fact that the dispersion below the transition temperature could not be entirely removed even after

annealing for some days suggested that the fully ordered state might be difficult to obtain. The results did not offer conclusive evidence that the ordered phase is ferroelectric.

The dependence on pressure of the transition temperature in KOH-doped hydrogenous ice has been studied by Yamamuro, Oguni, Matsuo and Suga (1987c). Two series of heat capacity measurements were made on a sample doped with 0.07 M KOH, first at the near-zero vapour pressure of the sample and then under 158.9 MPa pressure of helium gas. The transition temperature shifted from 71.6 to 74 K, giving a rate of variation with pressure of 0.015 K MPa^{-1}. The Clausius-Clapeyron equation was then used to deduce the volume increase associated with the disordering transition, which was calculated to be about 0.26% if the sample was assumed to be a mixture of completely ordered and disordered phases. If the maximum entropy loss obtained, 2.33 J mol^{-1} K^{-1}, was assumed to be that for a complete transformation to a partially ordered phase the volume change would be 0.18%. The former value, together with the cell dimensions found by Leadbetter et al., was used to obtain an estimate of the volume change of the ordered phase between 5 K and 72 K. The value obtained for this quantity was negative: the same trend is known to occur in disordered ice.

The effects of dopants other than KOH have also been investigated. Tajima et al. (1984) reported an experiment using rubidium hydroxide. The heat capacity data showed a large eutectic anomaly, suggesting that the RbOH was less soluble in ice than KOH, but an anomaly also occured at 72 K. The fact that the transition

temperature was independent of the dopant suggested that the transition was indeed an intrinsic property of the ice. Dielectric experiments on RbOH-doped ice were carried out by Kawada and Shimura (1987). The results were similar to those for KOH-doped ice, except that the relaxation times were longer and the dispersion appeared to be split into two branches about a decade apart in frequency. The lower-frequency branch behaved in the same way as the main dispersion in KOH-doped ice, while the higher-frequency component seemed largely unaffected by the transition. The author suggested that the high-frequency branch might arise because some OH^- ions, perhaps in grain-boundary regions, might be more tightly bound to the Rb^+ ion than those in the bulk of the ice.

Matsuo and Suga (1987) reported calorimetric measurements on ice doped with a number of different substances. In a sample doped with NaOH, a transition occured at 72 K, removing about 41% of the residual entropy. $Ba(OH)_2$, which was tried because it is the only divalent metal hydroxide reasonably soluble in water, was ineffective in producing the transition, probably because it did not dissolve in the ice. Ice doped with KF in order to include the K^+ without the OH^- ions did not transform to the ordered phase: neither did a sample doped with NH_4F. Matsuo (private communication, 1987) found that the transition took place in ice doped with LiOH, but only when the sample had first been annealed for some time at the eutectic temperature.

1.2.5 Analogous transitions in other systems

It is also of interest to consider the effect of KOH-doping on other hydrogen-bonded systems. Handa, Klug and Whalley (1987) found order-disorder transitions in ice V and ice VI by calorimetry. In the case of ice V the amount of entropy removed was increased and the transformation process accelerated by doping with KOH, although the transition occurred even in undoped ice. In ice VI, however, the transformation took place rapidly and the doping had no effect. These transitions were not of first order.

Yamamuro, Oguni, Matsuo and Suga (1987b) observed a first-order transition in tetrahydrofuran clathrate hydrate doped with 0.01 M KOH. The clathrate hydrates have a lattice of water molecules forming polyhedral cages containing the 'guest molecules', and this hydrogen-bonded system exhibits residual entropy in the same way as ice I. The transition took place at 62 K after the sample had been annealed for about two days around 55-60 K, and exhibited many of the same features as that from ice XI to ice Ih, including the high-temperature 'tail' due to short-range order. This tail was in fact more pronounced in the clathrate transition, suggesting that the local ordering takes place more easily in this system.

Yamamuro, Oguni, Matsuo and Suga (1987a) transformed a sample of KOH-doped ice to the cubic form by compressing and recovering at liquid nitrogen temperature. The temperature of the glass transition was substantially lowered, indicating that the doping had some effect in allowing the bonds to reorient, but the effect was not strong enough to reveal an ordering transition, perhaps

because most of the KOH was expelled from the ice during the formation of the cubic phase.

1.3 The implications of previous work

The implication of the results described above seems to be that doping with alkali hydroxides facilitates the rearrangement of the protons in a hydrogen-bonded system, by the introduction of the OH^- ion (or possibly the associated L-defect): the role of the interstitial cation would be unlikely to be equivalent in systems of such varying geometry. The variation in effectiveness among the various alkali hydroxides may be due to their different solubilities in ice. (The solid solution is not recognised in the standard phase-diagram studies, but evidently must be formed in these experiments.)

The existence of an ordering transition in the proton system of ice Ih at 72 K, catalysed by doping with alkali hydroxides, is now quite well established. However, the mechanism by which the ordering proceeds is not clear, and the structure of the new phase is not yet determined beyond doubt. The work described in this thesis is an attempt to address these issues.

CHAPTER 2

POSSIBLE ORDERED STRUCTURES FOR ICE Ih

2.1 Introduction

In the context of an investigation of the ordered phase of hexagonal ice it is interesting to consider the possible arrangements of the hydrogen bonds in such a phase. In this chapter the rules governing such arrangements will be considered, and an analysis given of the possible fully ordered arrangements for three hypothetical unit cells. Some other arrangements of interest will also be introduced, and the possibilities for isotropic or anisotropic partial ordering will be discussed. Simulated neutron diffraction profiles for the simpler structures obtained will be compared with the data of Leadbetter et al. (1985). Part of this work has been published (Howe, 1987).

Disordered ice has the space group $P6_3/mmc$ and the structure discussed in section 1.2.1 and illustrated in figure 1.1. The structure can be divided into crinkled layers perpendicular to the *c*-axis. For the purposes of the analysis in this chapter, it is convenient to consider the *c*-axis as vertical and these layers, of which there are two in the unit cell, as horizontal. Each of the possible proton sites is notionally occupied by a half-proton, or in other words has a 50% probability of being filled. The disorder of the proton positions is subject to the ice rules, and it is obvious that any regular arrangement must also obey these

conditions, both within the chosen unit cell and at its boundaries.

Certain constraints and simplifications arise from the combination of the ice rules with the requirement for a repeating structure. First, the unit of repetition chosen must clearly contain a whole number of the four-molecule unit cells of the oxygen lattice, and so must have an even number of layers each with an even number of molecules.

The choice of which *c*-axis sites in each layer are occupied is subject to the constraint that exactly one such site is occupied in each layer for each four-molecule cell making up the unit cell. (This is obvious if the whole structure is considered, for each *c*-axis bond must have exactly one proton.) From this it follows that a structure with an antiferroelectric arrangement of *c*-axis bonds must contain a whole multiple of eight molecules in its unit cell. Once the orientations of all *c*-axis bonds have been chosen, the oblique bonds in each layer are independent of those in adjoining layers and each layer can be treated separately.

For every layer constructed in accordance with the conditions, the layer above or below can always be formed so that every oblique bond is oriented oppositely to the corresponding bond in the next layer. (In a structure where the layers are related in this way, all mirror-symmetric molecule pairs are of the 'inverse' type.) Also, for every proton configuration obeying the ice rules, an equivalent configuration exists which can be formed by reversing the orientation of every bond.

FIGURE 2.1

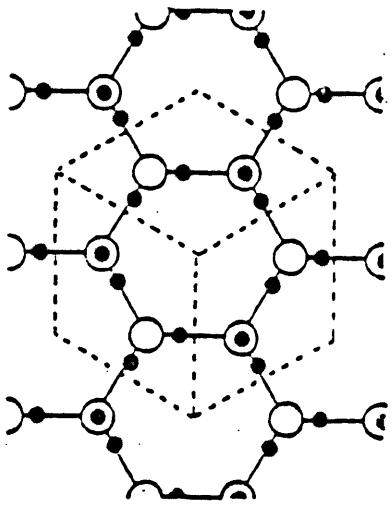

Ordered layer of four-molecule structure with three choices of unit cell

FIGURE 2.2

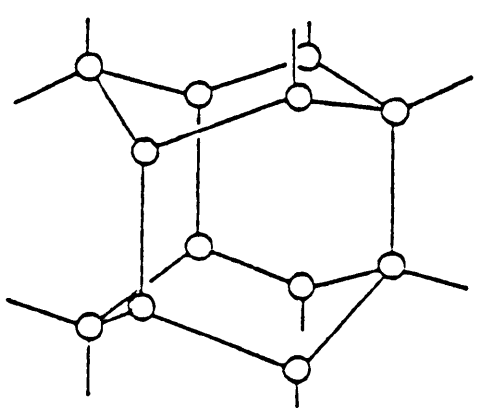

Oxygens and bonds involved in the eight-molecule cell

2.2 The four-molecule cell

Any attempt to order the protons in the four-molecule cell will result in the loss both of the centre of symmetry and, unless ordering occurs in the *c*-axis direction only, of the hexagonal symmetry of the disordered structure. There is only one arrangement of one puckered layer of the four-molecule cell which maintains the translational symmetry. In such an ordered layer, as shown in figure 2.1, the unit cell can be chosen in any of three orientations. The second layer can also have any of three orientations. There are therefore two distinct structures possible with the four-molecule cell, of which one, with the dipole moments of alternate layers antiparallel, has the orthorhombic space group $Cmc2_1$. The other, where the dipole moments of the layers make an angle of 60°, is monoclinic, with space group *Cc*. Both these structures are conventionally represented with an eight-molecule centred cell, as shown in figure 2.2. The $Cmc2_1$ structure is that proposed by Kamb (1973), predicted by Minagawa (1981) and used by Leadbetter et al. (1985) for the analysis of neutron diffraction data.

2.3 The eight-molecule cell

If the translational symmetry of the eight-molecule cell is preserved, other possible ordered structures can be found, as shown in figure 2.3, in which each rectangle represents the upper (001) layer. Here, the oxygen site at the left of the 'upper' layer is

FIGURE 2.3

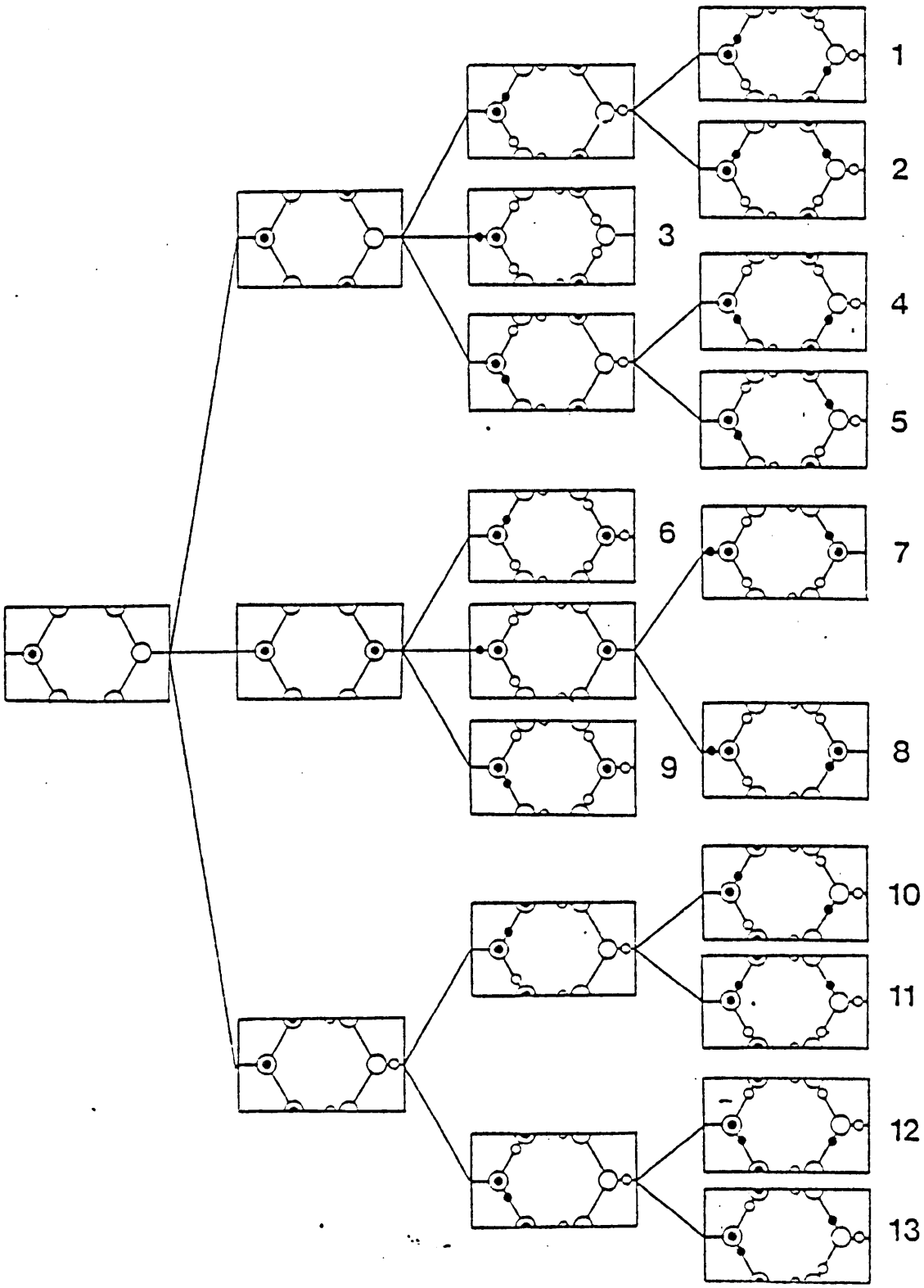

Construction of 13 upper layers for the eight-molecule cell

considered to be at the foot of a *c*-axis bond connected to the layer above, while the oxygen at the right is at the upper end of a *c*-axis bond connected to the layer below. In the 'lower' layer this is reversed and the slant of each oblique bond is opposite to that of the bond immediately above it. Those protons which are independently fixed are shown in the figure by small filled circles: the small open circles represent protons whose position is fixed as the result of the choice of the others. The first column shows the choice of a proton on the *c*-axis bond site at the left: the second column shows the three possible choices for the second occupied *c*-axis site in the layer. In the third column the possible ways of completing the molecule on the left are shown for each configuration of the *c*-axis bonds. In three cases, labelled 3, 6, and 9, the ice rules and the boundary conditions of the cell fix the positions of all the remaining protons in the layer. In the other cases, two orientations of the molecule at the right are possible: once these have been chosen all other protons are fixed. The configurations resulting from these choices are shown in the fourth column. The diagram is so arranged that each of the three sections defined by the choice of *c*-axis bonds has complete mirror symmetry.

There are thus 13 final arrangements of a single layer: there are of course a further 13 possible, each corresponding to one of those shown, with all occupied proton sites exchanged with empty sites. These 'converse' arrangements do not however increase the number of unique arrangements of the extended layer, of which there are five: 2, 3, and 4 are all equivalent by rotation through 120°; 1 and 5,

Table 2.1

Combinations of the upper and lower layers 1-13 of the 8-molecule cell to give the 17 structures A-S

		U	P	P	E	R		L	A	Y	E	R	S	
		1	2	3	4	5	6	7	8	9	10	11	12	13
L	1	A	B	C	D	E	.	.	.	.	.	.	.	.
O	2	B	F	G	G	D	.	.	.	.	.	.	.	.
W	3	C	G	F	G	C	.	.	.	.	.	.	.	.
E	4	D	G	G	F	B	.	.	.	.	.	.	.	.
R	5	E	D	C	B	A	.	.	.	.	.	.	.	.
	6	.	.	.	.	.	H	J	K	L	.	.	.	.
L	7	.	.	.	.	.	J	H	L	K	.	.	.	.
A	8	.	.	.	.	.	K	L	H	J	.	.	.	.
Y	9	.	.	.	.	.	L	K	J	H	.	.	.	.
E	10	.	.	.	.	.	.	.	.	.	M	N	P	Q
R	11	.	.	.	.	.	.	.	.	.	N	R	S	P
S	12	.	.	.	.	.	.	.	.	.	P	S	R	N
	13	.	.	.	.	.	.	.	.	.	Q	P	N	M

Table 2.2

Symmetry, polar properties and molecule-molecule interactions of the 17 eight-molecule structures

		Dipole moment parallel to *c*	Dipole moment perpendicular to *c*	Centre-inverse molecule pairs	Mirror-inverse molecule pairs
A	*Pca*2_1	Y	N	8	4
B	P_1	Y	Y	10	2
C	*Pc*	Y	Y	10	0
D	P_1	Y	Y	10	2
E	*Pna*2_1	Y	Y	8	0
F	*Cmc*2_1	Y	N	12	4
G	*Cc*	Y	Y	12	0
H	$P2_1$	N	N	8	4
J	$P2_1$	N	Y	8	0
K	*Pc*	N	Y	8	0
L	*Pc*	N	Y	8	2
M	*Pna*2_1	N	N	0	4
N	$P2_1$	N	Y	2	2
P	$P2_1$	N	Y	2	2
Q	$P2_12_12_1$	N	N	0	0
R	$P2_12_12_1$	N	N	4	4
S	*Pna*2_1	N	Y	4	0

10 and 13, and 11 and 12 are mirror-image pairs; 6, 7, 8, and 9 are all related by rotation and reflection.

For each upper layer shown, a lower layer may be constructed in projection by the same process as for the converse layers, remembering however that in three dimensions the bonds slant in the opposite sense. Each lower layer so constructed will be designated by the same number as its corresponding upper layer. Provided that the vertical bonds are compatible, any upper layer may be combined with any lower layer. There are thus 5x5 + 4x4 + 4x4 = 57 possible combinations of the upper layers shown with the corresponding lower layers. However, rotations and reflections severely restrict the number of unique structures: for example, the combination of upper layers 2, 3, and 4 with their appropriate lower layers all give the same structure, denoted by F in Table 2.1. Similar arguments apply to other groups of combinations: the possible combinations are shown in Table 2.1, where the upper layers are shown along the top line and the lower layers down the left-hand column. No combinations of layers shown in figure 2.3 with lower layers from the 'converse' set are permitted, as by the nature of these layers the *c*-axis bonds will not be compatible. The 17 unique structures are denoted by letters A-S, and their space groups, their polar or antiferroelectric nature and the number of molecule-molecule pairs of each type, are summarized in Table 2.2. F, the simplest and most symmetrical of these structures, is the *Cmc*2$_1$ structure discussed above: G is the only other possible centred structure with this unit cell. M is the structure proposed by Owston (1953) and also by Davidson and Morokuma (1984) on the grounds discussed in section

FIGURE 2.4

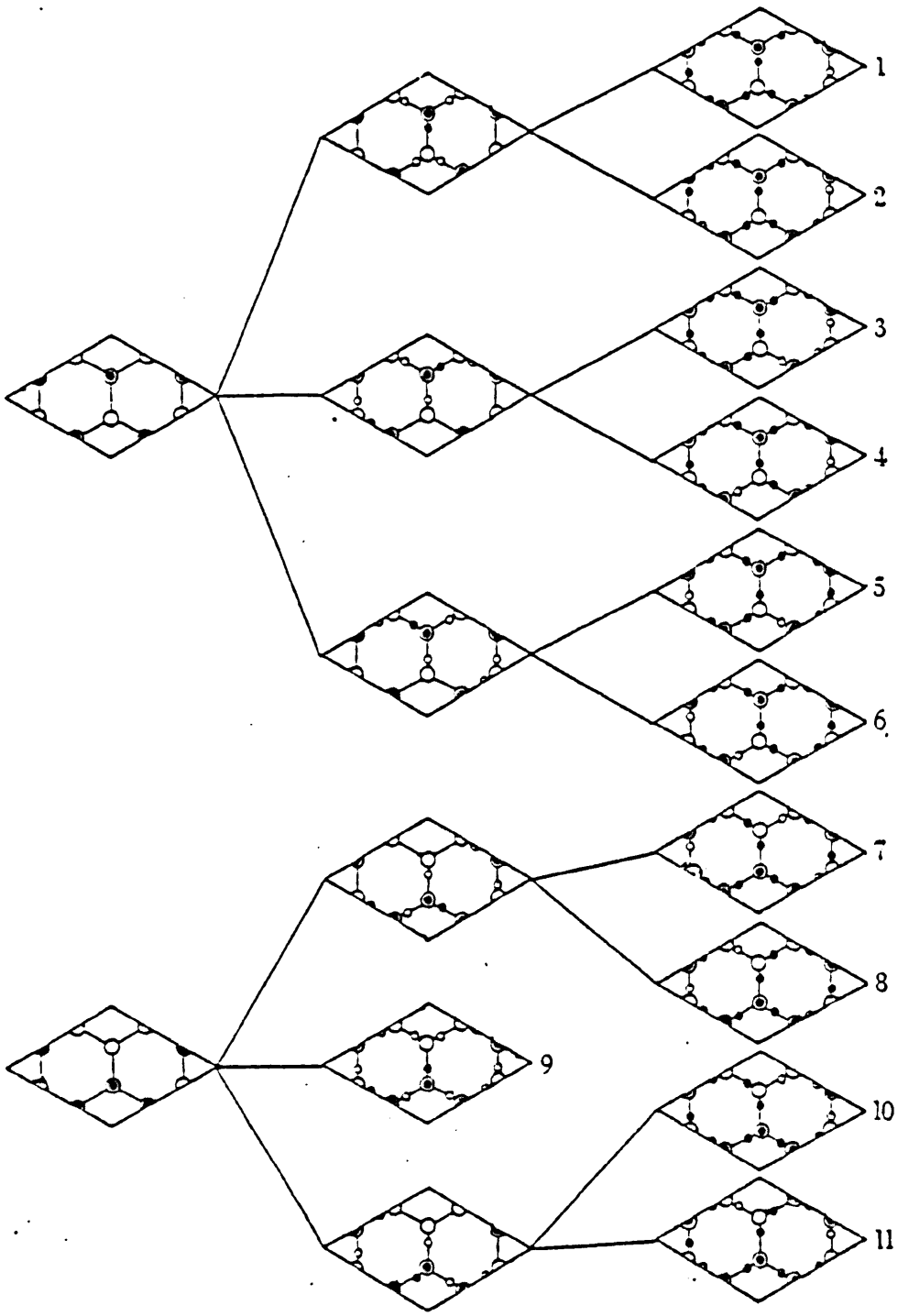

Construction of 11 upper layers for the twelve-molecule cell

1.2.1. Q and R are interesting in that, although not centro-symmetric, they are geometrically non-polar: all the other structures have polar space groups.

2.4 The twelve-molecule cell

The ordered structure proposed by Bernal and Fowler (1933) and mentioned in section 1.2.1 has a cell of twelve molecules, with the hexagonal space group $P6_3cm$. This is the smallest cell for which an ordered structure with hexagonal symmetry can be found. It is possible to analyse other structures with the translational symmetry of this cell, in a similar manner to that given above for the eight-molecule cell. In the diagram of figure 2.4, eight of the ten possible arrangements of the *c*-axis bonds in one layer of the cell have been omitted, as they are all equivalent to the second of the two arrangements shown in the left-hand column. There are 11 final arrangements shown for the layer, of which five are unique. Layers 2, 4 and 5 are all equivalent to the layer in figure 2.1: 8 and 10 are equivalent to each other by reflection, as are 7 and 11, while 9, which has a mirror axis in the layer, is unique. The four 'new' layers are shown in figure 2.5 (a) to (d). The structure proposed by Bernal and Fowler is formed by combining the layer in figure 2.5 (a) with a lower layer formed in the usual way. The other three layers have two out of three *c*-axis bonds in one orientation and the third in the other. The 15 possible combinations of the layers are shown in Table 2.3. The structure denoted by δ is equivalent to that denoted by F in table 2.1, while ε is equivalent to G and α is the structure proposed by

FIGURE 2.5

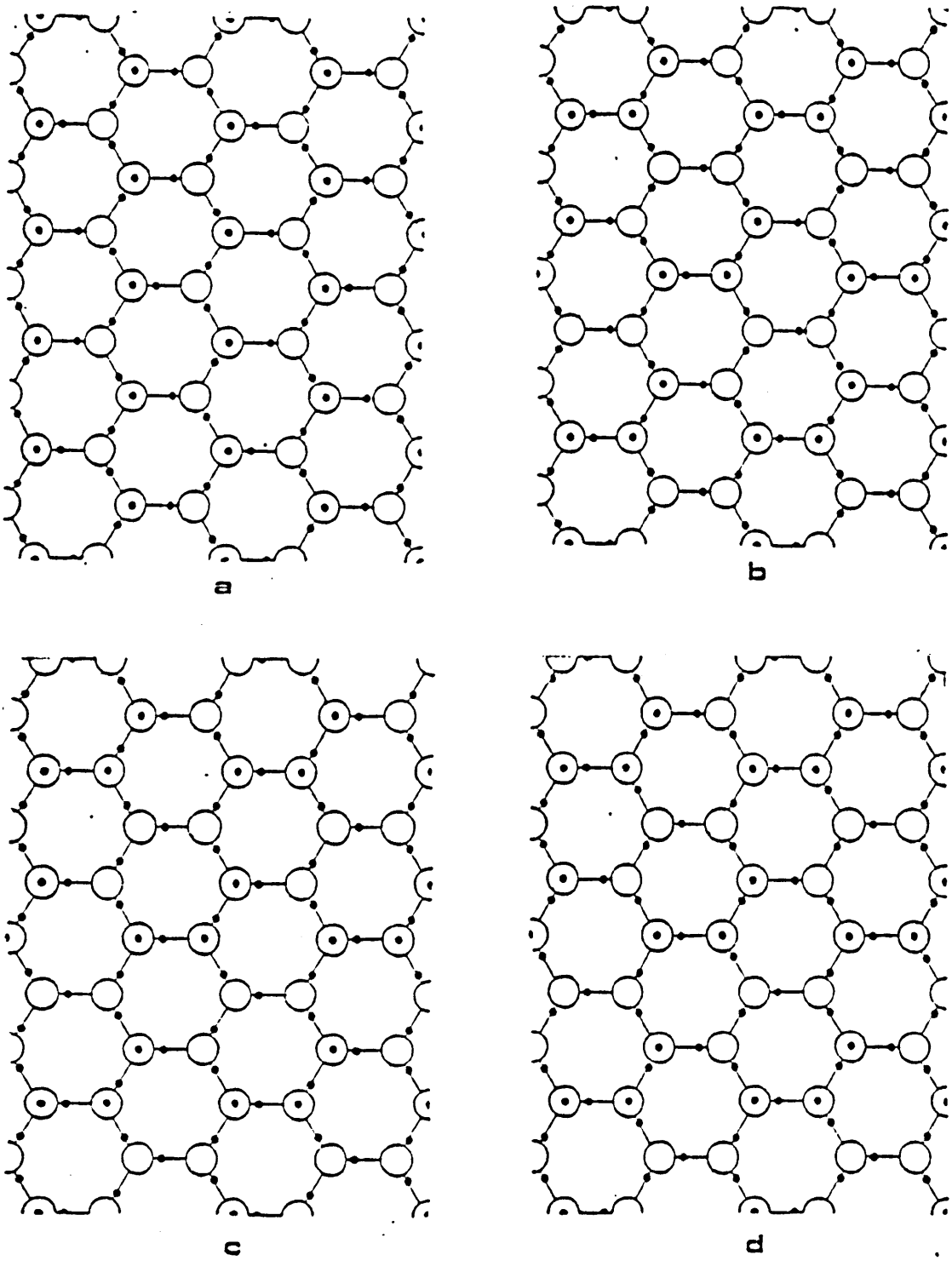

The four new layers for the 12-molecule cell
a)1, 3, 6
b)7, 11
c)8, 10
d)9

Following page 29

TABLE 2.3

Combinations of the upper and lower layers 1-11 of the 12-molecule cell to give the 15 structures α-ρ

		U	P	P	E	R		L	A	Y	E	R
		1	2	3	4	5	6	7	8	9	10	11
L	1	α	β	γ	β	β	γ	.	.	.	.	.
O	2	β	δ	β	ε	δ	β	.	.	.	.	.
W	3	γ	β	α	β	β	ζ	.	.	.	.	.
E	4	β	ε	β	δ	ε	β	.	.	.	.	.
R	5	β	δ	β	ε	δ	β	.	.	.	.	.
	6	γ	β	ζ	β	β	α	.	.	.	.	.
L	7	.	.	.	.	.	.	η	θ	κ	λ	μ
A	8	.	.	.	.	.	.	θ	ν	ξ	π	λ
Y	9	.	.	.	.	.	.	κ	ξ	ρ	ξ	κ
E	10	.	.	.	.	.	.	λ	π	ξ	ν	θ
R	11	.	.	.	.	.	.	μ	λ	κ	θ	η

Following page 28

FIGURE 2.6

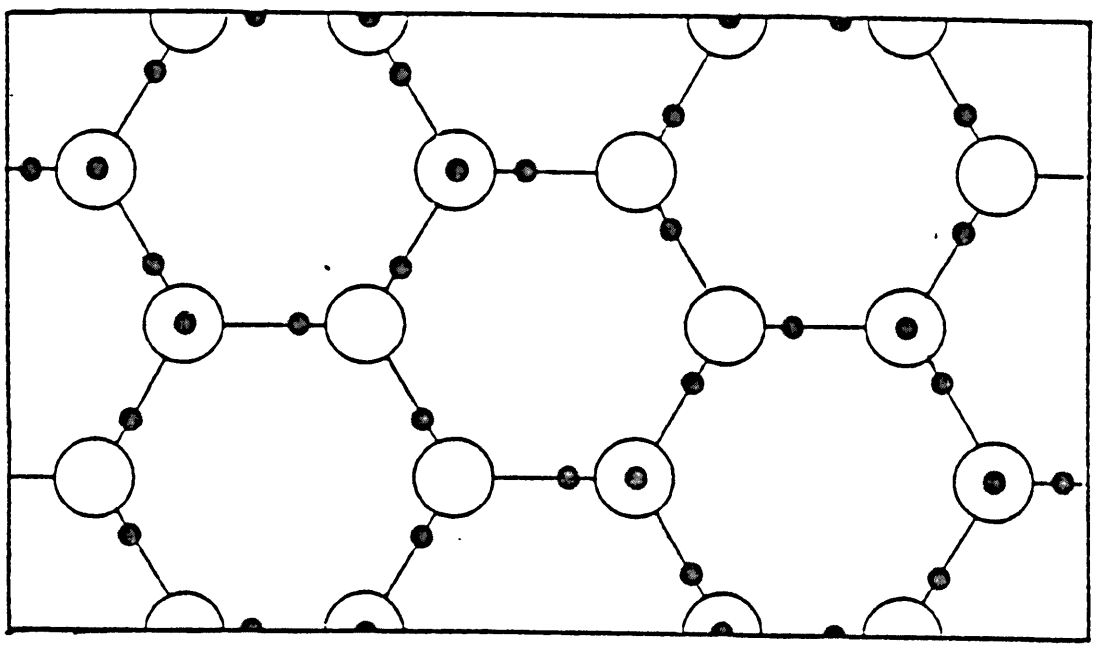

One layer of the 32-molecule centred cell of the centrosymmetric ordered structure

Bernal and Fowler. Most of the other structures are of low symmetry.

2.5 Other interesting arrangements

While this exercise could be continued indefinitely, there is little benefit in considering large and complicated cells which would be unlikely to occur in nature. However, two further structures are mentioned here for interest. The first, shown in figure 2.6, is the smallest ordered arrangement to have a centre of symmetry. Its space group is *C*2/*c*. The primitive cell contains 16 molecules, the centred cell 32 molecules.

The second interesting structure arises out of the claim of Bernal and Fowler to have found a structure with 96 molecules in the unit cell, antiferroelectric and with the symmetry of the trigonal space group $P3_1$. This claim appears to be in error for the following reasons. The space group requires a threefold screw axis, which in turn means that the unit cell must have at least six layers. The presence of the 3_1 axis also requires that the arrangement of the *c*-axis bonds in each layer have three-fold symmetry. This can only be achieved if the unit cell contains $6n^2$ molecules per layer, where n is an integer. An antiferroelectric structure must contain $4m$ molecules per layer, where m is also an integer. The smallest number of molecules per layer fulfilling both conditions is 24: the next is 96. A six-layered cell of ninety-six molecules would have sixteen molecules per layer. A structure has been found with a two-layer hexagonal unit cell of 48 molecules, which seems from the

FIGURE 2.7

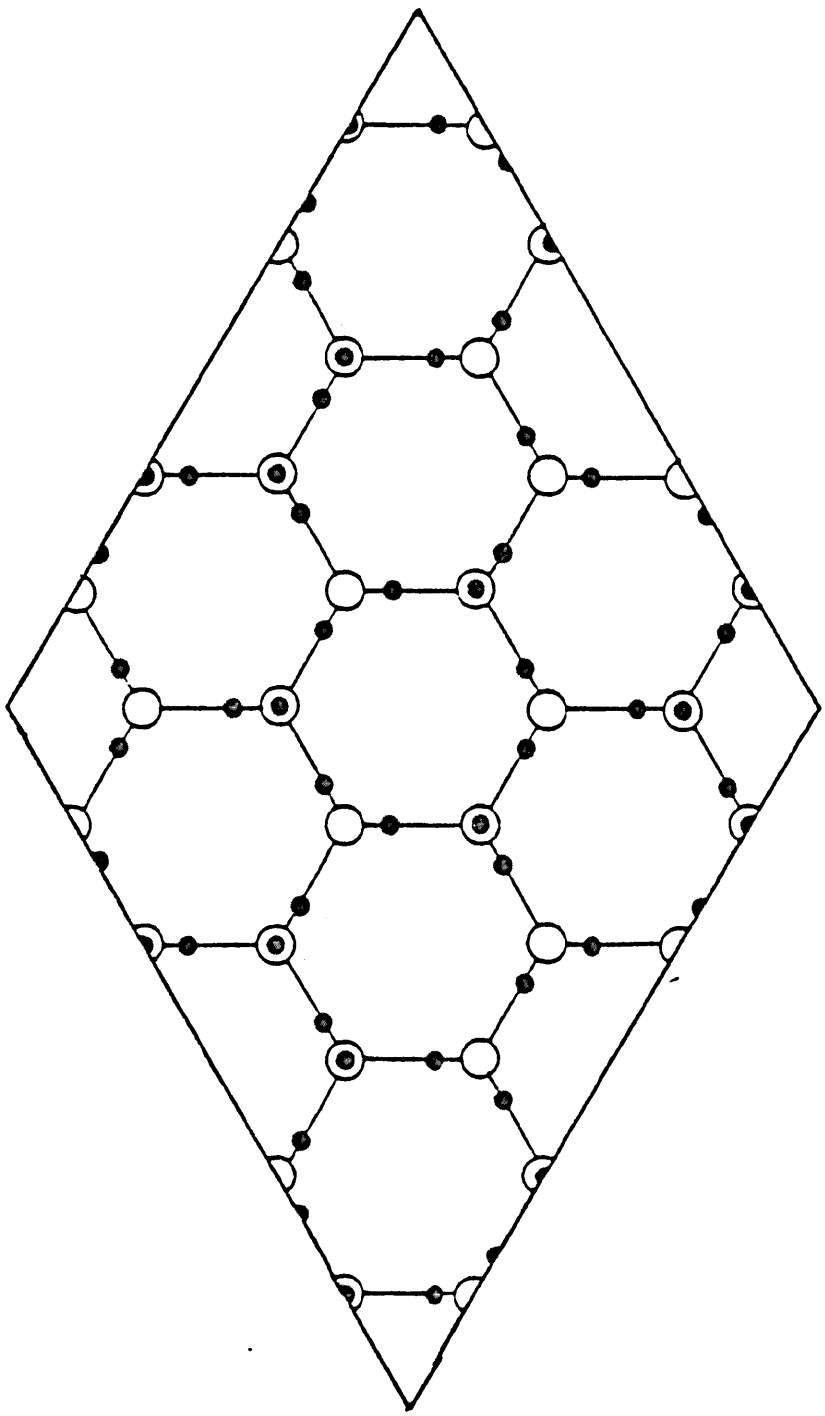

One layer of the 48-molecule cell of the antiferroelectric hexagonal structure

arguments given above to be the simplest to combine a fully ordered non-polar structure with hexagonal symmetry. One layer of this structure is shown in figure 2.7.

2.6 Partially ordered structures

In addition to the fully ordered structures, various kinds of partial order can also be envisaged. In the partially ordered case the occupancies of the proton positions can take any fractional value between 0 and 1, always subject to an extended version of the ice rules requiring that the total occupancy of the four sites surrounding any given oxygen be two and that the two sites on each bond have a total occupancy of one. The simplest case would be one where, if half the sites are labelled as 'correct', a single parameter described the probability of any labelled site being occupied. The implications of this case will be discussed in Chapter 3.

It is also conceivable that one direction might be completely or partially ordered while some disorder remained perpendicular to this direction: the obvious example is that proposed by Rundle (1955) and Hentschel (1979), in which the *c*-axis bonds are completely or partially ordered but the oblique bonds are disordered. In this case the fractional occupancies of the oblique sites are not independent of those for the vertical-bond sites. A calculation of the entropy of such a structure is given in section 3.3.1. This structure has the space group $P6_3mc$, differing from that of disordered ice only in the absence of a centre of symmetry,

and the same 4-molecule unit cell as the completely disordered structure. In a diffraction experiment, such a structure would produce no reflections not present in the completely ordered case.

Finally, a class of structures can be devised in which the bonds in two directions are ordered, dividing the lattice into a series of straight parallel chains each of which can have either of two directions: the entropy arising from this type of disorder is very small.

2.7 Simulated diffraction profiles

In order to compare the eight-molecule structures described above with the neutron diffraction data of Leadbetter et al., simulated diffraction profiles were computed for some of the structures, using the sample dimensions and instrument characteristics appropriate for that experiment, with a neutrom wavelength of 1.909 angstrom. The simulations were carried out using programs in the Cambridge Crystallography Subroutines Library. The lattice parameters used for these simulations were obtained by transforming those for hexagonal ice to the eight-molecule centred cell: the atomic co-ordinates were based on those found by Leadbetter et al., but with a slightly idealized geometry. No attempt was made to take account of changes in the cell dimensions which might arise from the breaking of the symmetry of the disordered structure.

Some examples of the results are shown in figures 2.8 to 2.11. In every case, the ordering introduces reflections not

FIGURE 2.8

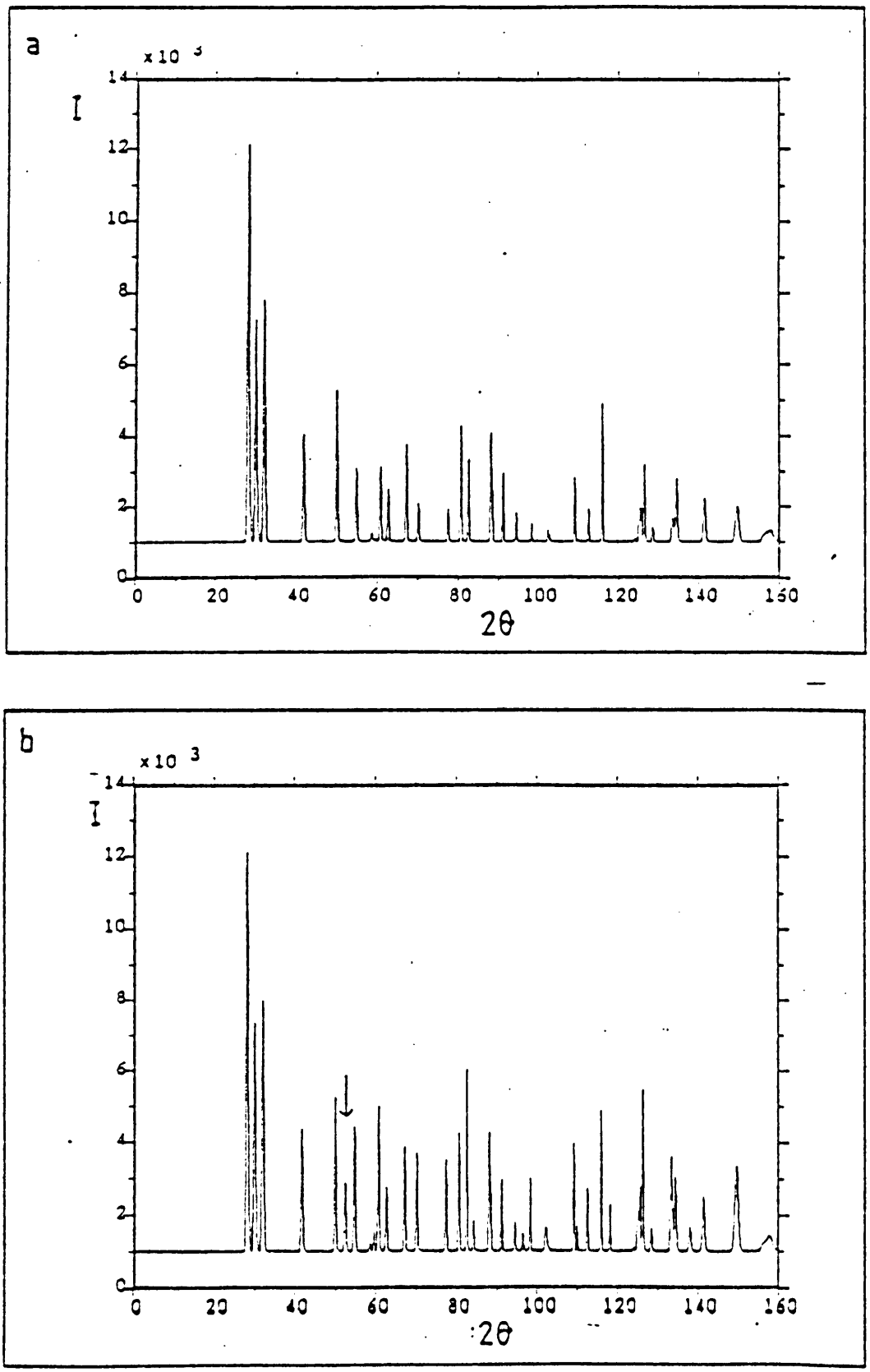

Simulated neutron diffraction profiles for (a) the disordered ice structure and (b) the ordered structure 'F'

Following page 3:

FIGURE 2.9

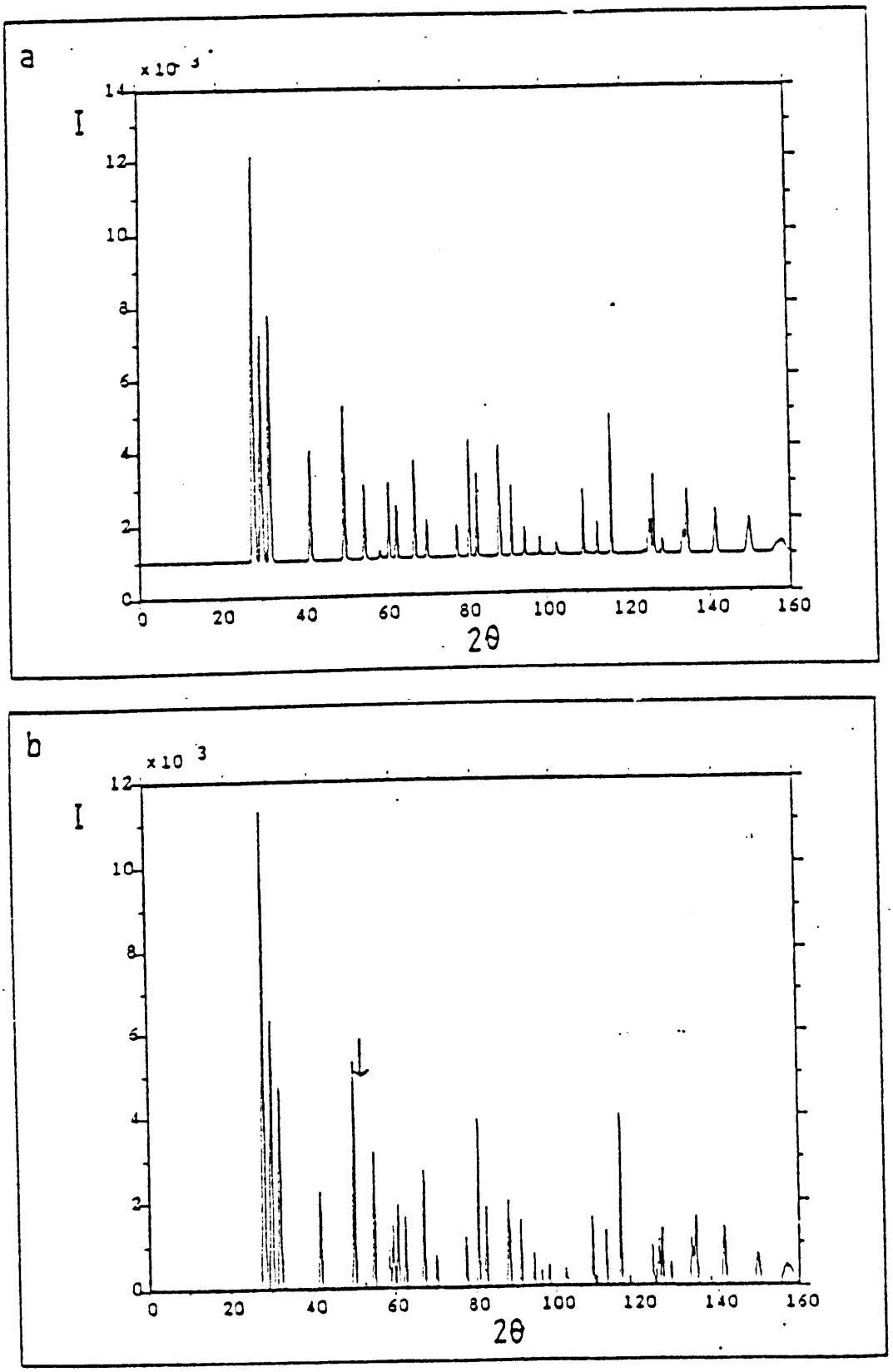

Simulated neutron diffraction profiles for (a) the disordered ice structure and (b) the ordered structure 'G'

Following page 31

FIGURE 2.10

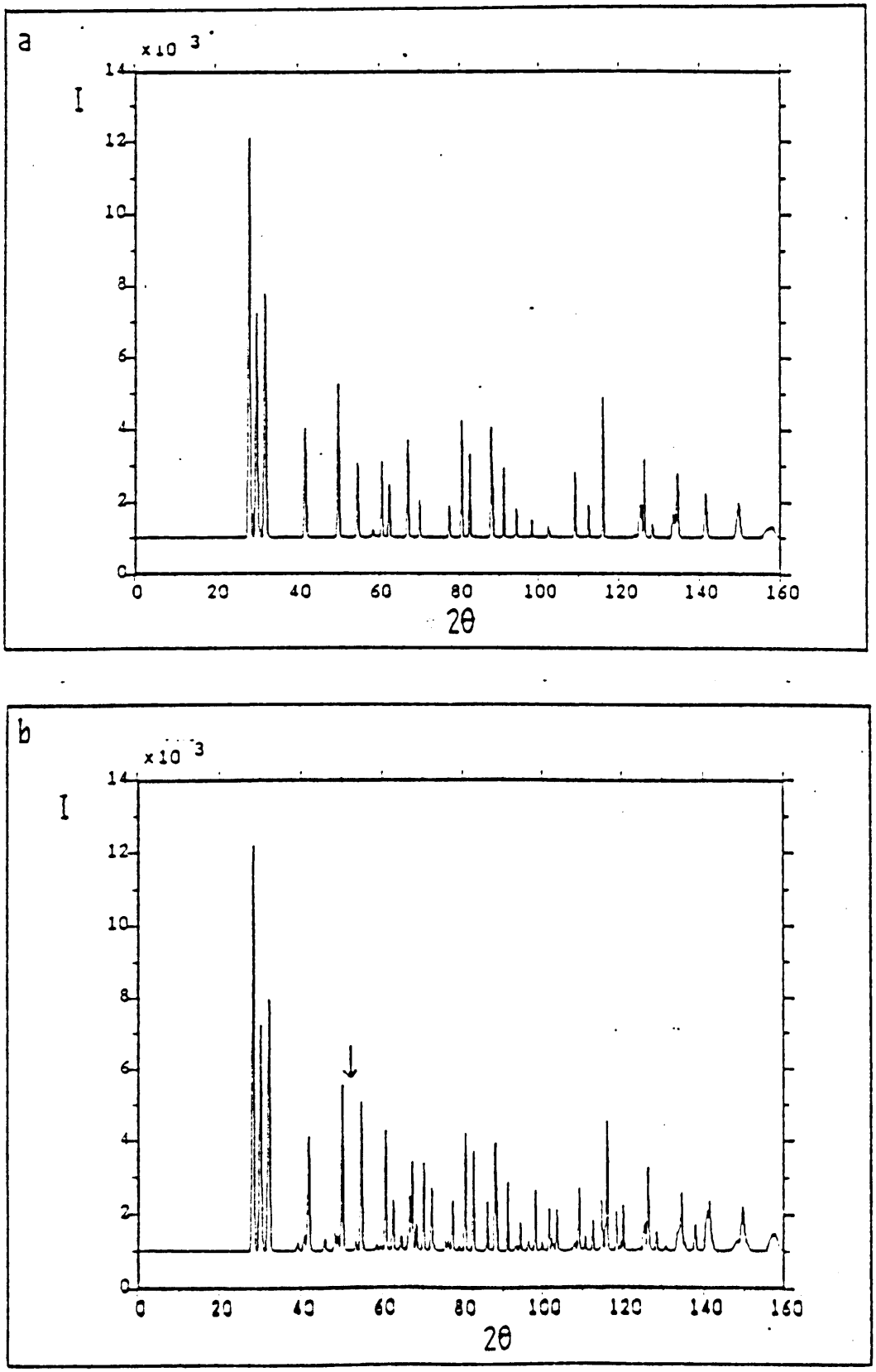

Simulated neutron diffraction profiles for (a) the disordered ice structure and (b) the ordered structure 'M'

Following page 31

FIGURE 2.11

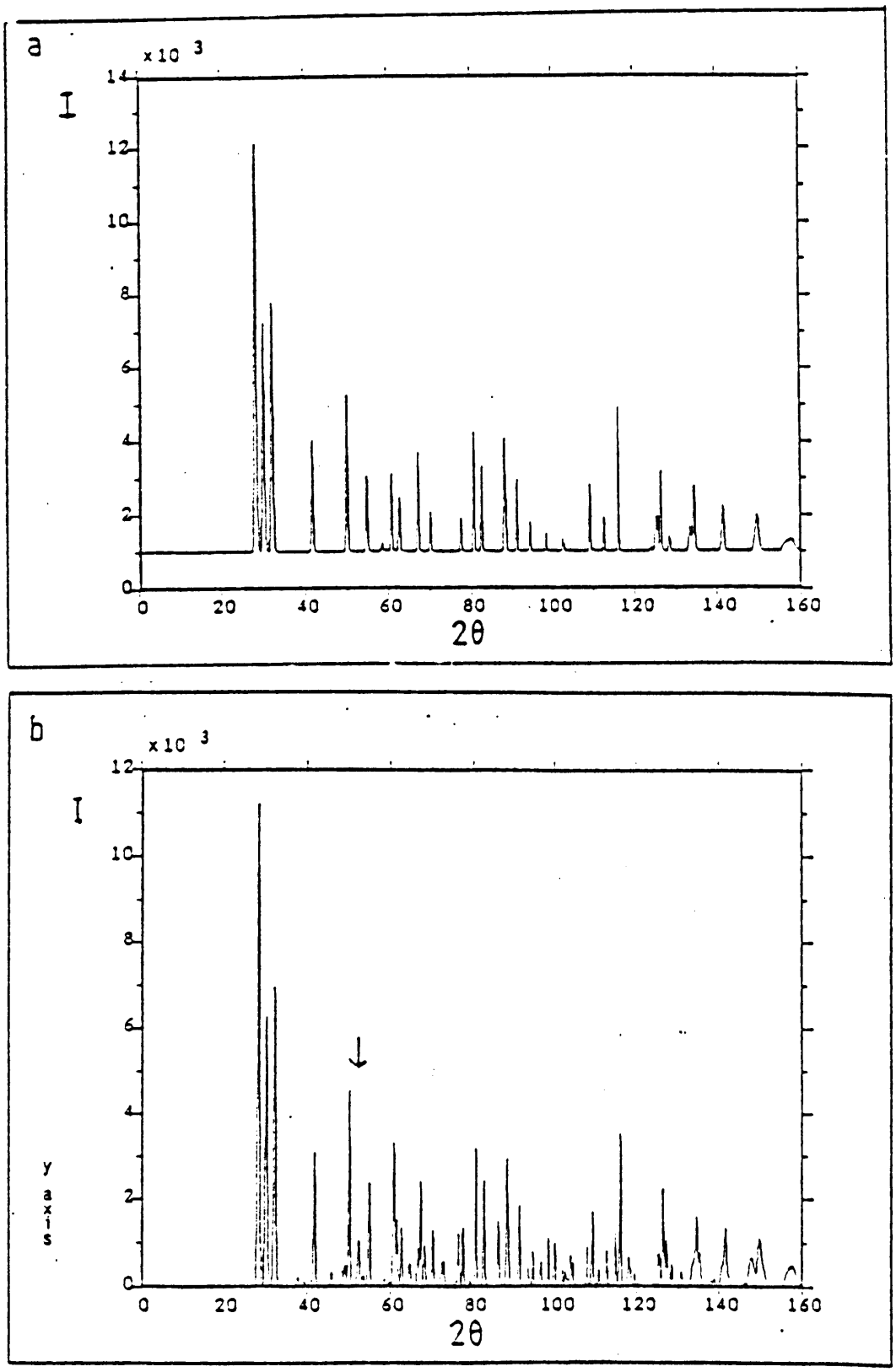

Simulated neutron diffraction profiles for (a) the disordered ice structure and (b) the ordered structure 'Q'

Following page 31

present in the disordered case. If the reflections from disordered ice are indexed in the orthorhombic cell, all reflections with $h+k \neq 2n$ are absent, as are those with indices (h $3h$ $2n+1$). In the two centred structures, the only reflections present which were not allowed in the hexagonal space group are those indexed (h $3h$ $2n+1$). Of these, only the (131) reflection is in a position where it would be visible in the experimental profile. In the non-centred structures, other reflections, which do not obey the condition $h+k=2n$, are also allowed. The profile for the $Cmc2_1$ structure is the most similar to the experimental data: those for the other structures show extra reflections which should have been detectable, being as strong as or stronger than the '(131)' reflection which is the only extra one clearly visible in the experimental data. The position of this reflection is marked on each of the simulated profiles for ordered ice.

CHAPTER 3

A THEORETICAL TREATMENT OF PARTIALLY ORDERED ICE

3.1 Introduction

The various experiments on the ordering transition in ice, discussed in section 1.2.4, measured three different indicators of the degree of order: the entropy removed; the number of bonds having their correct orientations, and the changes in the dielectric properties. In all cases it appeared that the transformation to the ordered phase was less than complete. In order to interpret and compare the results of such experiments, it is necessary to develop a theory relating the dielectric properties and the entropy loss to the proportion of correctly oriented bonds. There are two possible ways of approaching this problem: the crystal can be assumed to be either a mixture of ordered and disordered regions or a single, homogeneous domain of partial order. The first, simpler case will be considered in section 3.2 and the second in section 3.3. Finally, in section 3.4, the two approaches will be combined.

3.2 Theory for the two-phase model

In a crystal consisting of a mixture of completely ordered and completely disordered domains, the relationships between entropy, number of bonds correctly oriented and dielectric constant can be found as follows.

Let a fraction w of the volume of the crystal be completely

ordered. Then the fraction of bonds having their 'correct' orientation will be $f=(1+w)/2$, since in the disordered regions half of the bonds are in the correct orientations by chance. If the domains are sufficiently large that the entropy due to their arrangement can be neglected, the entropy of the crystal will be simply that of the disordered portion, $S=Nk_B(1-w)\ln(3/2)$, where N is the number of molecules and k_B is Boltzmann's constant. If the lattice parameter changes associated with the ordering are too small to be resolved by diffraction measurements, any extra reflections due to the ordered structure will have an intensity varying with w. If the two phases have significantly different lattice parameters, the profile may show splitting or broadening of the reflections common to both phases as well as extra reflections from the ordered phase.

The evaluation of the dielectric constant of a mixture of two phases is not a trivial problem. The treatment given here is taken from Davies (1971).

Let the sample consist of a mixture of two phases, a fraction v with dielectric constant ε_2 and a fraction w with dielectric constant ε_1, where $\varepsilon_2>\varepsilon_1$. In the case where the mixture consists of spheres of the material with dielectric constant ε_2 in a matrix of the material with dielectric constant ε_1, the effective dielectric constant ε^* is given by

$$\varepsilon^* = \varepsilon_1 \left\{\frac{\varepsilon_1(2-2v)+\varepsilon_2(2v+1)}{\varepsilon_2(1-v)+\varepsilon_1(2+v)}\right\}. \qquad (3.1)$$

When the roles of the two materials are reversed, the effective

dielectric constant is

$$\varepsilon^* = \varepsilon_2 \left\{\frac{\varepsilon_2(2-2w)+\varepsilon_1(2w+1)}{\varepsilon_1(1-w)+\varepsilon_2(2+w)}\right\}. \quad (3.2)$$

These formulae are exact lower and upper bounds to ε^*, but only give its exact value when the geometry fulfills particular conditions. Two formulae are available for interpolating between the two extreme cases.

The first formula is due to Böttcher, and is applicable to a case where it cannot be said that one phase is matrix and the other inclusion. ε^* is a solution of the equation

$$\frac{3\varepsilon^*}{\varepsilon_1+2\varepsilon^*} w + \frac{3\varepsilon^*}{\varepsilon_2+2\varepsilon^*} v = 1. \quad (3.3)$$

The formula of Looyenga is appropriate where there are continuous paths of each phase, for example in a compressed powder. It takes the form

$$\varepsilon^{*\frac{1}{3}} = \varepsilon_1^{\frac{1}{3}} w + \varepsilon_2^{\frac{1}{3}} v. \quad (3.4)$$

Both these formulae are symmetrical between v and w and make a smooth interpolation between the upper and lower bounds.

In the absence of any direct evidence as to the geometry of the hypothetical two-phase system in ordered ice, the formula of Looyenga will be adopted. Davies suggests that this formula is the more useful in real systems, and in any case the differences between the two expressions are not large compared with the accuracy of the available experimental data. Suppose that the ordered phase has a dielectric constant ε_1 equal to the

FIGURE 3.1

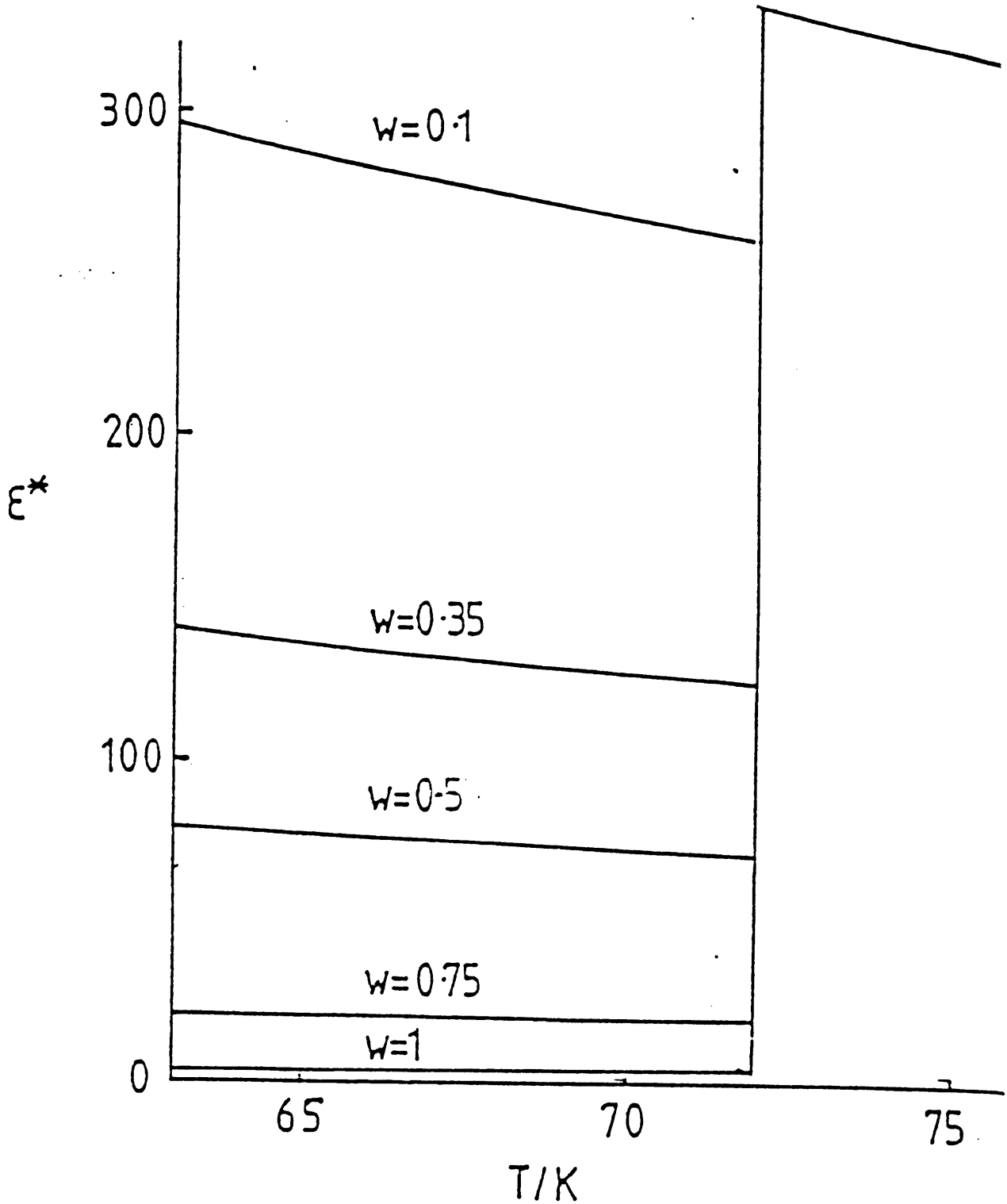

Variation of the effective static dielectric constant ε^* with temperature in the two-phase model, for different values of w, the fraction of material transformed

Facing Page 36

high-frequency dielectric constant for ice, while the disordered phase obeys a Curie Law, $\varepsilon_2 \propto 1/T$. Then, if w has a constant value below the transition temperature and is equal to zero above the transition, the variation of ε^* with temperature will be of the form shown in figure 3.1: even below the transition, ε^* falls with increasing temperature. If the value of w is allowed to fall as the temperature increases towards the transition, ε^* will increase below the transition. However, if the sample is at a uniform temperature it seems unlikely that macroscopic regions would undergo spontaneous disordering below the transition temperature.

3.3 Theory for the homogeneous model

The calculations of the variation of the residual entropy and the dielectric constants in the case of homogeneous partial order are more interesting than those in the two-phase model.

3.3.1 The entropy of partially ordered ice

The following calculation of the entropy of partially ordered ice is an extension of the work of Pauling (1935), discussed in section 1.2.1, to the case of homogeneous partial order. This work has been published (Howe and Whitworth 1987). As in Pauling's calculation, the existence of rings of molecules is neglected.

We consider a crystal consisting of N molecules and $2N$ hydrogen bonds, within which the ordered structure is assumed to have a single domain such that every bond has a 'correct' orientation. It

is assumed that the degree of ordering can be described by a single order parameter f, the fraction of bonds having their correct orientation, which applies equally to all bonds within the unit cell. For completely ordered ice f=1, while f=1/2 corresponds to complete disorder and f=0 to an ordered domain oriented in the opposite direction.

For each oxygen site within the unit cell there are six possible orientations of the water molecule. As shown in figure 3.2, these fall into three categories: one (a) in which all four bonds are correct, one (b) comprising the four orientations with two bonds correct and two incorrect, and the third (c) with all four bonds incorrect. (The diagram represents the situation in 'square ice', a two dimensional arrangement of water molecules useful for illustrating points which depend only on their four-fold coordination.) In our crystal of N molecules, we let fractions p, q and r belong to these three categories, respectively. It is obvious that

$$p + q + r = 1, \qquad (3.5)$$

and since the number of correct bonds in the crystal, by definition equal to $2Nf$, is $(4p+2q)N/2$, the condition

$$2p + q = 2f \qquad (3.6)$$

must always be satisfied.

The number of different ways of placing these N molecules on the N oxygen sites is given by

FIGURE 3.2

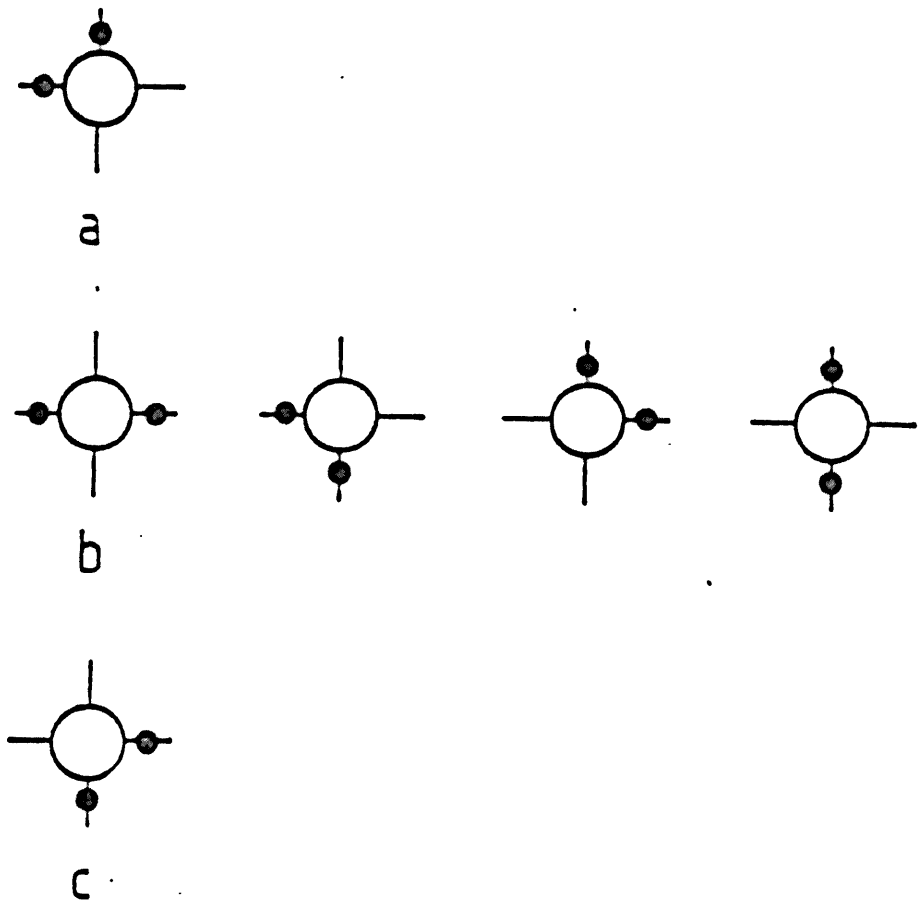

The six possible orientations of a water molecule
a) all bonds correct
b) two bonds correct
c) no bonds correct

$$W_1 = \frac{N!4^{qN}}{(pN)!(qN)!(rN)}, \quad (3.7)$$

where the factor 4^{qN} arises because there are four orientations for the half-correct molecules. Only a fraction of these configurations will satisfy the rule requiring each bond to have one proton. If two adjacent molecules are to form a correctly oriented bond, the proton sites on each end of the bond must be in their correct states. For each end, this condition is fulfilled by a molecule having all bonds correct and by two of the four possible molecules with two bonds correct, so that the probability of the bond being properly formed and correctly oriented is $(p+q/2)^2$. Similarly, the probability that a single bond is properly formed but incorrectly oriented is $(r+q/2)^2$. There must be $2Nf$ correct bonds and $2N(1-f)$ incorrect bonds: the number of ways of arranging these is given by

$$W_2 = \frac{(2N)}{(2Nf)![2N(1-f)]}. \quad (3.8)$$

The number of configurations for a given value of f which satisfy the ice rules is therefore

$$\Omega = W_1 W_2 (p+q/2)^{4Nf}(r+q/2)^{4N(1-f)}. \quad (3.9)$$

Using Stirling's approximation and Eqs. 3.5 and 3.6 this becomes

$$\Omega = \left[\frac{f^{2f}(1-f)^{2(1-f)}2^{2(f-p)}}{p^p(f-p)^{2(f-p)}(1+p-2f)^{(1+p-2f)}} \right]^N \quad (3.10)$$

Equation 3.10 involves both f and p. In order to determine the entropy as a function of f it is necessary to sum Ω over the values of Np compatible with a given f. As is common in statistical mechanics, in the limit of large N this sum may be replaced, for the purposes of calculating $\ln \Omega$, by the maximum value of Ω as a

FIGURE 3.3

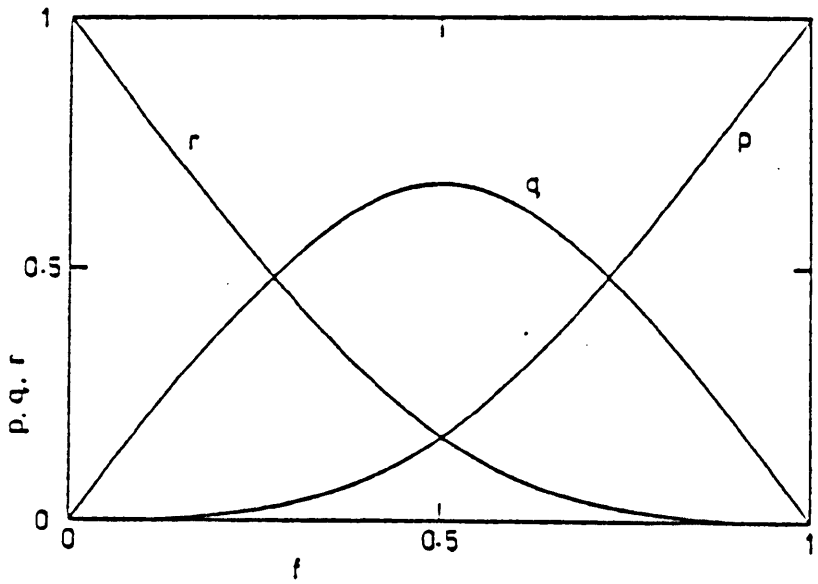

The variation of the fractions p, q and r of molecules with four, two and no bonds correct respectively, with the fraction f of correct bonds.

FIGURE 3.4

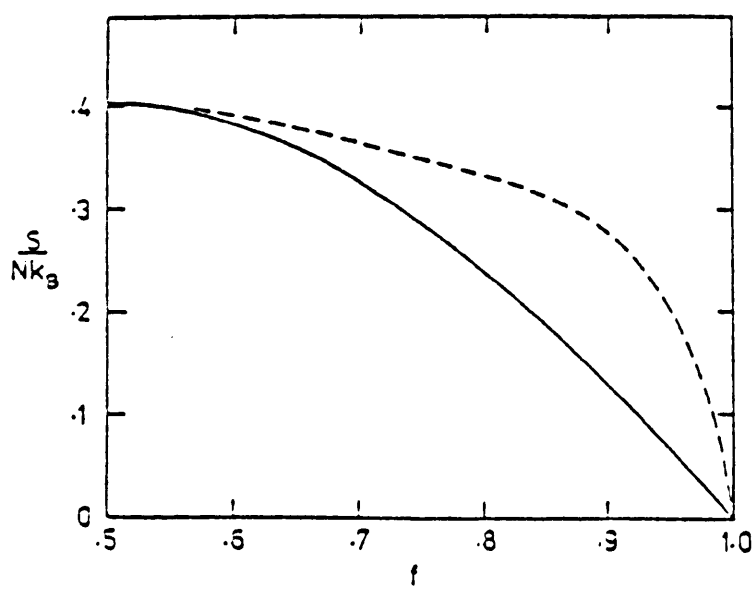

The variation of the calculated entropy S with the fraction f of correctly oriented bonds
solid line; present theory
dashed line; Nagle's expression.

function of p. This maximum occurs at the value

$$\langle p \rangle = f - 2[1 - (3f^2 - 3f + 1)^{1/2}]/3, \quad (3.11)$$

which will be the expected value for p in a crystal of given f. As expected, $\langle p \rangle = 1/6$ for $f = 1/2$. The dependences of $\langle p \rangle$ and of the corresponding values of q and r on f are shown in fig. 3.3.

The entropy $S(f) = Nk_B \ln \Omega$ may be calculated by substituting Eq. 3.11 into Eq. 3.10: the result is shown in fig. 3.4. The same result can be obtained by placing $2Nf$ correct and $2N(1-f)$ incorrect bonds randomly in the crystal and finding the fraction of such configurations in which all the molecules have two protons and the relations 3.5 and 3.6 are also satisfied.

A different approximate expression for the entropy of partially ordered ice was proposed by Nagle (1973), as follows. If the probabilities of occupation of the four hydrogen sites close to a given oxygen are $p_1 \ldots p_4$, the number of configurations per molecule is estimated as

$$W \approx \left[\prod_{i=1}^{4} \left[p_i^{-p_i} (1-p_i)^{p_i - 1} \right]^{1/2} \right] \times \left[\sum_{\substack{i \neq j \neq k \neq m \\ i<j,k>m}} p_i p_j (1 - p_k)(1 - p_m) \right]. \quad (3.12)$$

When this expression is applied to the case of homogeneous partial order and written in terms of our single order parameter f, putting $p_1 = p_2 = f$, $p_3 = p_4 = 1-f$, the entropy becomes

$$S = Nk_B \ln\left[\frac{f^4 + 4f^2(1-f)^2 + (1-f)^4}{f^{2f}(1-f)^{2(1-f)}}\right], \quad (3.13)$$

which is shown as the broken line in figure 3.4. While both calculations give Pauling's entropy of $Nk_B\ln(3/2)$ at $f = 1/2$ and zero entropy at $f = 1$, Nagle's value is higher at intermediate values of f than that obtained from the present model and approaches $S = 0$ at $f = 1$ with a much steeper slope.

It is not difficult to see how Nagle's expression was obtained. The denominator in the logarithm in Eq. 3.13 arises from counting all possible configurations of $2N$ bonds with one proton on each, $2Nf$ of these being correct and $2N(1-f)$ incorrect. The numerator in the logarithm is the sum of of the probabilities that at a particular molecular site in such an arrangement all the bonds are correct, two are correct and two incorrect, or all are incorrect. Nagle's formula is obtained by taking this to be the probability that the ice rules are satisfied at every oxygen site, but this step is not valid. The expression in the numerator is dominated by the most probable case (the first term f^4 as $f \to 1$), but the full analysis requires definite proportions of molecules, q and r, to be in less probable configurations. Nagle's calculation overestimates the fraction of all possible bond configurations which have two protons in each molecule, and thus gives too large an entropy, especially in cases of fairly large f. Nagle (private communication, 1986) has agreed that the present calculation is correct.

A simple argument can be used to support the calculation given above, in cases where f is close to 1. Disorder cannot be

introduced into a perfectly ordered crystal by reversing single bonds or rotating isolated molecules, as these processes would result in violations of the ice rules. A small amount of disorder can only exist in the form of strings of reversed bonds, such as would be produced on the path followed through the crystal by an ion or Bjerrum defect. These strings cannot form closed loops in a ferroelectric ordered structure, and the probability of their doing so in an antiferroelectric structure is negligible. The strings, therefore, pass from one surface point to another, and we may suppose that in a cube of $N = M^3$ molecules a string has typical length M. The $n = 2N(1-f)$ incorrect bonds will lie on n/M strings each starting on one of the $6M^2$ surface sites. The possible paths of a string branch in two directions at every molecule along its length, and the number of possible configurations for a single string is therefore 2^M. The number of ways of choosing the n/M starting points is of the order of $(6M^2)^{n/M}$. The total number of configurations of the crystal is then $\Omega \approx (6M^2)^{n/M} 2^n$ and the entropy is

$$S = k_B \ln \Omega \approx k_B \left[\frac{2N(1-f)}{M} \ln (6M^2) + 2N(1-f)\ln 2 \right]. \quad (3.14)$$

As $N \to \infty$, this takes the form

$$S \approx Nk_B(1-f)\ln 4,$$

which for $f \to 1$ has the same slope as the asymptote to our function shown in fig. 3.4.

In the structure proposed by Rundle (1955), the bonds parallel to the c-axis are ordered while some disorder remains in the planes perpendicular to c. It is of interest to consider the residual

entropy associated with such a structure.

We again consider a crystal of N molecules and $2N$ bonds. There are $N/2$ c-axis bonds, of which $fN/2$ are in their 'correct' orientation and $(1-f)N/2$ are in the other orientation. The probability of occupation of each of the non-c-axis sites on a molecule are assumed to be equal. Each oblique bond has two possible states which will be designated 'up' and 'down'. If the c-axis is considered to be vertical, and the correctly oriented vertical bonds have their proton at the bottom end, then in order to complete each molecule correctly, the two states must have probabilities of occupation given by $(2-f)/3$ and $(1+f)/3$, respectively.

The N molecules are divided into two categories, one containing the molecules with the c-axis bond correct and the other those where it is incorrect: each category contains molecules of three equally likely orientations. The number of ways of distributing the molecules between these categories is given by

$$W_1 = \frac{N! \quad 3^N}{(Nf)![N(1-f)]!}. \qquad (3.15)$$

For a c-axis bond the probability of being correctly oriented and properly formed is f^2, while the probability of being incorrectly oriented but properly formed is $(1-f)^2$. For an oblique bond the probability of being 'up' and properly formed is $[(2-f)/3]^2$, and the probability of being 'down' and properly formed is $[(1+f)/3]^2$. The $3N/2$ oblique bonds are distributed between two groups with populations of $(2-f)N/2$ and $(1+f)N/2$, while the $N/2$ c-axis bonds

FIGURE 3.5

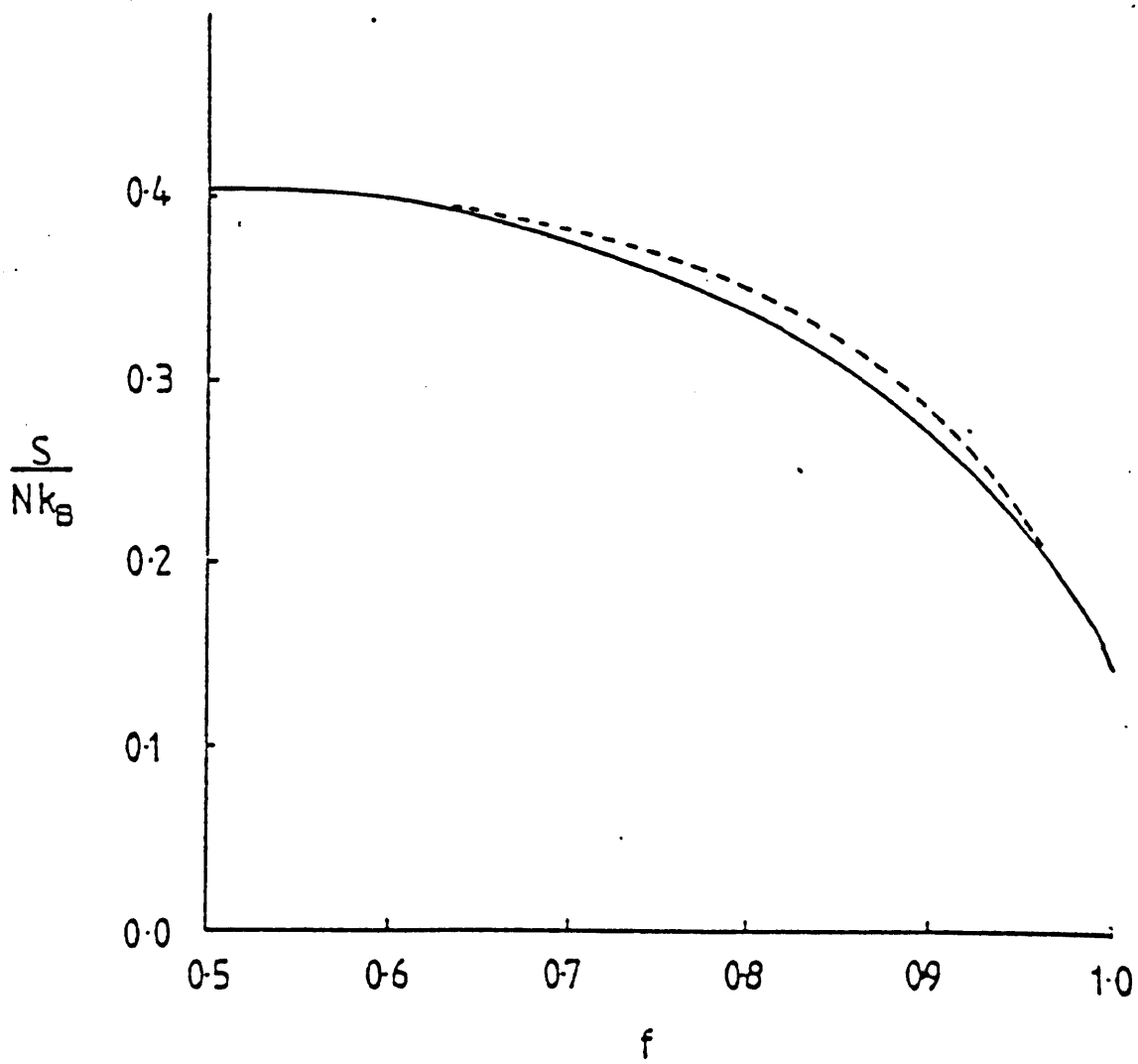

Variation of the entropy S with the fraction f of correctly oriented c-axis bonds in the Rundle model
solid line; present theory
dashed line; Nagle's expression.

are distributed between two groups with populations $fN/2$ and $(1-f)N/2$. The number of ways of distributing all the bonds between the two pairs of groups is given by

$$W_2 = \frac{\left[\frac{N}{2}\right]!}{\left[\frac{Nf}{2}\right]!\left[\frac{(1-f)N}{2}\right]!} \times \frac{\left[\frac{3N}{2}\right]!}{\left[\frac{N(2-f)}{2}\right]!\left[\frac{N(1+f)}{2}\right]!}. \quad (3.16)$$

Using Stirling's approximation and the relations 3.15 and 3.16, the number of allowed configurations is given by

$$\Omega = \left[\frac{(2-f)^{(2-f)}(1+f)^{(1+f)}}{3f^f(1-f)^{(1-f)}}\right]^{N/2}. \quad (3.17)$$

When f = 1 the residual entropy is $Nk_B[\ln(4/3)]/2$, or approximately 36% of the entropy for complete proton disorder. The variation of the entropy with f is plotted in figure 3.5 as the solid line. The dashed line shows the result obtained by putting $p_1=f$, $p_2=p_3=p_4=(2-f)/3$ in Nagle's expression. The two results are less dissimilar in this case than in the isotropic case: both give the same value for the entropy at f=1. This calculation suggests that the failure of Tajima et al. (1984) to remove more than 68% of the residual entropy is not due to the ordered phase being ordered in one direction only as this hypothesis cannot completely account for the entropy loss.

3.3.2 The dielectric constant of partially ordered ice

The model for the dielectric constant of partially ordered ice is based on the work of Minagawa (1981), which was introduced in section 1.2.3, and uses the notation designed by that author for

FIGURE 3.6

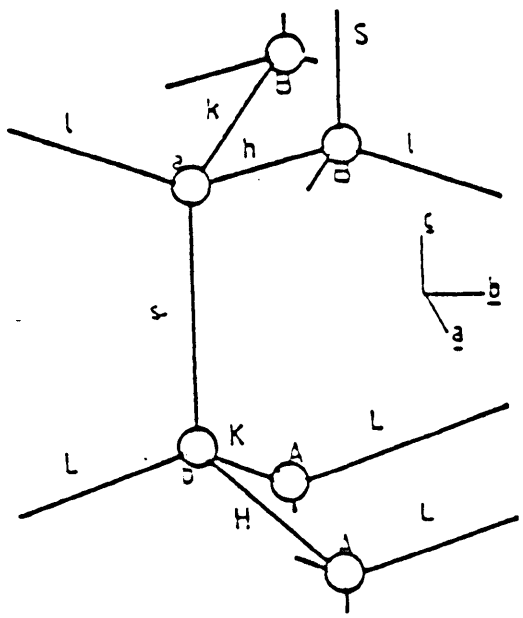

Labelling of bonds, molecules and crystal axes in the theory of section 3.3.2 (after Minagawa)

the description of the populations of each type of bond and molecule. The bonds and molecules within the four-molecule unit cell of hexagonal ice are labelled as shown in figure 3.6. The population of molecules of type A which have their protons on the bonds H and K is denoted by A_{HK}, while the populations of bonds labelled H with protons at the upper and lower ends are denoted respectively by H^+ and H^-. In all there are 24 'molecule variables';

$$A_{HK},\ A_{KL},\ A_{HS},\ A_{KS},\ A_{HL},\ A_{LS},$$
$$B_{hK},\ B_{kL},\ B_{hS},\ B_{kS},\ B_{hL},\ B_{lS},$$
$$a_{hK},\ a_{kL},\ a_{h*},\ a_{k*},\ a_{hL},\ a_{l*},$$
$$b_{HK},\ b_{KL},\ b_{H*},\ b_{K*},\ b_{HL},\ b_{L*};$$

and 16 'bond variables';

$$H^+,\ H^-,\ h^+,\ h^-,$$
$$K^+,\ K^-,\ k^+,\ k^-,$$
$$L^+,\ L^-,\ l^+,\ l^-,$$
$$S^+,\ S^-,\ s^+,\ s^-.$$

Because of the restrictions imposed by the ice rules, however, these variables are not all independent.

Minagawa gives two types of relation among the variables. The first arises from the requirement that each bond have one proton, and gives 8 equations of the form

$$H^+ + H^- = n, \quad (3.18)$$

where n is the number of unit cells in the crystal. The second type of relation is of the form

$$A_{HK} + A_{HL} + A_{HS} = b_{L*} + b_{KL} + b_{K*} = H^-, \quad (3.19)$$

and is required in order to maintain consistency between the bond

and molecule variables. There are four further relations, not explicitly mentioned by Minagawa, which are required in order to ensure that each molecule has two protons. These are

$$\begin{aligned} s^+ + l^- + k^- + h^- &= 2n \\ s^- + L^+ + K^+ + H^+ &= 2n \\ S^+ + L^- + K^- + H^- &= 2n \\ S^- + l^+ + k^+ + h^+ &= 2n. \end{aligned} \qquad (3.20)$$

In the present work, the number of independent variables has been effectively reduced to one or two by the use of appropriate symmetry conditions.

The only electrostatic interactions considered in the model are those between nearest-neighbour molecules. As was discussed in section 1.2.1, for two molecules meeting through a c-axis bond, the interaction is either inverse mirror symmetric, with energy E_{mi}, or oblique mirror symmetric with energy E_{mo}. For two molecules meeting through an oblique bond, the interaction is either inverse centre symmetric with energy E_{ci} or oblique centre symmetric with energy E_{co}. For our purposes, only the differences $E_m = E_{mo} - E_{mi}$ and $E_c = E_{co} - E_{ci}$ are of interest.

The full expression for the entropy of a configuration is then given by $S = k_B \ln\Omega$, where

$$\Omega = \left[\frac{(h^+)^{h^+}(k^+)^{k^+}\ldots\ldots(s^-)^{s^-}}{a_{hs}^{a_{hs}} a_{ks}^{a_{ks}} \ldots B_{hk}^{B_{hk}} n^{4n}} \right]. \qquad (3.21)$$

This is the expression given in equation 4.13 of Minagawa's paper, with two misprints corrected. It can be obtained by an argument

Table 3.1

Bond variables and their changes in an applied field

	Equilibrium value in partially ordered state	Excess with field parallel to *a*	Excess with field parallel to *b*	Excess with field parallel to *c*
S^+	$n(1-f)$	0	0	$-v$
S^-	nf	0	0	v
s^+	$n(1-f)$	0	0	$-v$
s^-	nf	0	0	v
H^+	$n(1-f)$	v	$v/2$	$-v/3$
H^-	nf	$-v$	$-v/2$	$v/3$
h^+	$n(1-f)$	$-v$	$-v/2$	$-v/3$
h^-	nf	v	$v/2$	$v/3$
K^+	$n(1-f)$	v	$v/2$	$-v/3$
K^-	nf	$-v$	$-v/2$	$v/3$
k^+	$n(1-f)$	$-v$	$-v/2$	$-v/3$
k^-	nf	v	$v/2$	$v/3$
L^+	nf	0	$-v$	$-v/3$
L^-	$n(1-f)$	0	v	$v/3$
l^+	nf	0	v	$-v/3$
l^-	$n(1-f)$	0	$-v$	$v/3$

similar to that used in section 3.3.1 except that all the molecules and bonds in the unit cell are considered separately.

The electrostatic energy is calculated by counting the occurences of each type of interaction in a given configuration, and is given by the following expression (after Minagawa).

$$U/n =$$

$$-E_m\{(a_{h*}b_{KL}+a_{k*}b_{HL}+a_{l*}b_{HK}+a_{k1}b_{H*}+a_{h1}b_{K*}+a_{hk}b_{L*})/(s^+s^++s^-s^-)$$

$$+(A_{Hs}B_{k1}+A_{Ks}B_{h1}+A_{Ls}B_{hk}+A_{kL}B_{hs}+A_{HL}B_{ks}+A_{HK}B_{ls})/(S^+S^++S^-S^-)\}$$

$$-E_c\{(a_{h*}B_{k1}+a_{k*}B_{h1}+a_{l*}B_{hk}+a_{k1}B_{hs}+a_{h1}B_{ks}+a_{hk}B_{ls})$$

$$\times[1/(h^+h^++h^-h^-)+1/(k^+k^++k^-k^-)+1/(l^+l^++l^-l^-)]$$

$$+(A_{Hs}b_{KL}+A_{Ks}b_{HL}+A_{Ls}b_{HK}+A_{kL}b_{H*}+A_{HL}b_{K*}+A_{HK}b_{L*})$$

$$\times[1/(H^+H^++H^-H^-)+1/(K^+K^++K^-K^-)+1/(L^+L^++L^-L^-)]\}. \quad (3.22)$$

The Helmholtz free energy, $U-TS$ where T is the absolute temperature and S is the entropy, is denoted by nf in Minagawa's paper. In the present work, to avoid confusion with the order parameter f, it will be denoted by A.

We consider a crystal which is in equilibrium in the absence of an electric field, and which is assumed to be homogeneous and isothermal. Initially it will be assumed that the equilibrium state is completely disordered and so has no spontaneous polarization. When an electric field is applied along one of the axes of the crystal, it is assumed that the excess polarization induced is small and parallel to the direction of the applied field, and is proportional to ν, the number of extra bonds which become aligned with the field. It can be shown (see for example Mitsui et al. 1974) that the dielectric constant in the direction of the

Table 3.2

Molecule variables and their changes in an applied field

	Equilibrium value in partially ordered state	Excess with field parallel to *a*	Excess with field parallel to *b*	Excess with field parallel to *c*
A_{HK}	np	0	$-v/2$	$v/3$
A_{HL}	$nq/4$	$-v/2$	$v/4$	$v/3$
A_{KL}	$nq/4$	$v/2$	$v/4$	$v/3$
A_{Ls}	nr	0	$v/2$	$-v/3$
A_{Hs}	$nq/4$	$-v/2$	$-v/4$	$-v/3$
A_{Ks}	$nq/4$	$v/2$	$-v/4$	$-v/3$
B_{hk}	nr	0	$-v/2$	$-v/3$
B_{hl}	$nq/4$	$-v/2$	$v/4$	$-v/3$
B_{kl}	$nq/4$	$v/2$	$v/4$	$-v/3$
B_{ls}	np	0	$v/2$	$v/3$
B_{hs}	$nq/4$	$-v/2$	$-v/4$	$v/3$
B_{ks}	$nq/4$	$v/2$	$-v/4$	$v/3$
a_{hk}	np	0	$v/2$	$v/3$
a_{hl}	$nq/4$	$v/2$	$-v/4$	$v/3$
a_{kl}	$nq/4$	$-v/2$	$-v/4$	$v/3$
a_{ls}	nr	0	$-v/2$	$-v/3$
a_{hs}	$nq/4$	$v/2$	$v/4$	$-v/3$
a_{ks}	$nq/4$	$-v/2$	$v/4$	$-v/3$
b_{HK}	nr	0	$v/2$	$-v/3$
b_{HL}	$nq/4$	$-v/2$	$-v/4$	$-v/3$
b_{KL}	$nq/4$	$v/2$	$-v/4$	$-v/3$
b_{Ls}	np	0	$-v/2$	$v/3$
b_{Hs}	$nq/4$	$-v/2$	$v/4$	$v/3$
b_{Ks}	$nq/4$	$v/2$	$v/4$	$v/3$

field is then proportional to

$$\frac{1}{\frac{\partial^2 A}{\partial v^2}\Big|_{v=0}} .$$

This is equivalent to finding the shift in the minimum of the free energy $G=U-TS+EP$ as a function of polarization P when a field E is applied. A can be found as a function of v by the substitution of appropriate values into equations 3.21 and 3.22. The changes in the molecule and bond variables for an applied field parallel to each axis are shown in tables 3.1 and 3.2. The changes in the bond variables not parallel to the field are determined by the requirement for symmetry about the applied field and the relations 3.18 and 3.20. The expectation value of the polarization at a given applied field will be that for which the entropy is maximised. This condition and the relations 3.19 have been used to calculate the changes in the molecule variables. In the disordered state with no applied field, all bond variables are equal to $n/2$ and all molecule variables are equal to $n/6$. Then the dielectric constants ε_a, ε_b, ε_c are given by

$$\begin{aligned} \varepsilon_a &\propto 1/k_B(T-\theta_a) \\ \varepsilon_b &\propto 1/k_B(T-\theta_b) \qquad (3.23) \\ \varepsilon_c &\propto 1/k_B(T-\theta_c). \end{aligned}$$

The Curie-Weiss temperatures are

$$\begin{aligned} \theta_a = \theta_b &= (5/3)E_c/k_B - E_m/k_B, \qquad (3.24) \\ \theta_c &= (8/3)E_c/k_B. \end{aligned}$$

These results are obtained by Minagawa by a different but equivalent method. In the present work, the dielectric constants ε are defined such that the static permittivity in the chosen

FIGURE 3.7

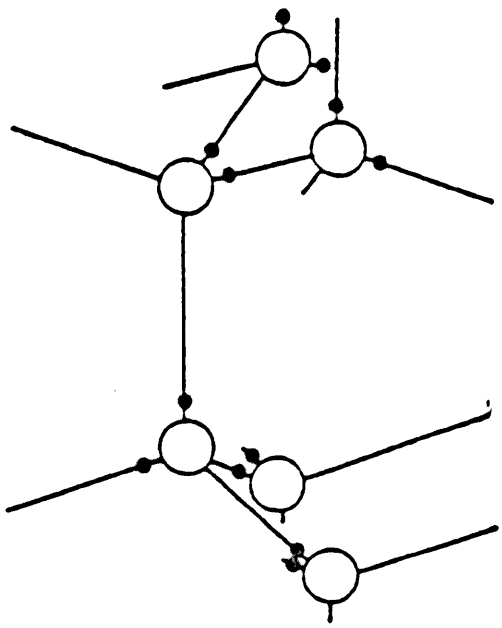

The chosen ordered arrangement of protons

direction is equal to $\varepsilon+\varepsilon_\infty$. This convention has been maintained throughout, and in particular in section 5.3.

Widely different experimental values of the Curie-Weiss temperatures perpendicular and parallel to the *c*-axis have been found by various workers, as summarised, for example, by Hobbs (1974). However, two recent sets of measurements appear to be reliable and consistent. Kawada (1978) found θ_a = 0 K and θ_c = 46 K, while Takei and Maeno (1987) found θ_a = 0 K and θ_c = 48.7 K. From these values the energy differences E_m and E_c can be obtained for use in the consideration of the ordered and partially ordered states. Minagawa uses the value θ_c = 46 K, giving a temperature for the transition to the ordered state of 69 K. In the present work, the value θ_c = 48.6 K has been chosen so that the transition temperature has its experimental value of 72 K.

Since, from equations 3.24 and the experimental Curie-Weiss temperatures, E_m and E_c are both positive, the equilibrium ordered state must be one in which as many interactions as possible are of the inverse mirror or inverse centre type. There is only one structure in which all interactions are of these types: this is the *c*-axis polar structure, with the space group $Cmc2_1$, found by Leadbetter et al (1985) and described elsewhere. This structure remains the most favourable even when the model is extended to an eight-molecule unit cell. For the purposes of the calculation, it will be assumed that the fully ordered structure is as shown in figure 3.7, while the partially ordered state is one in which a fraction *f* of bonds have the orientations chosen as 'correct'. The

FIGURE 3.8

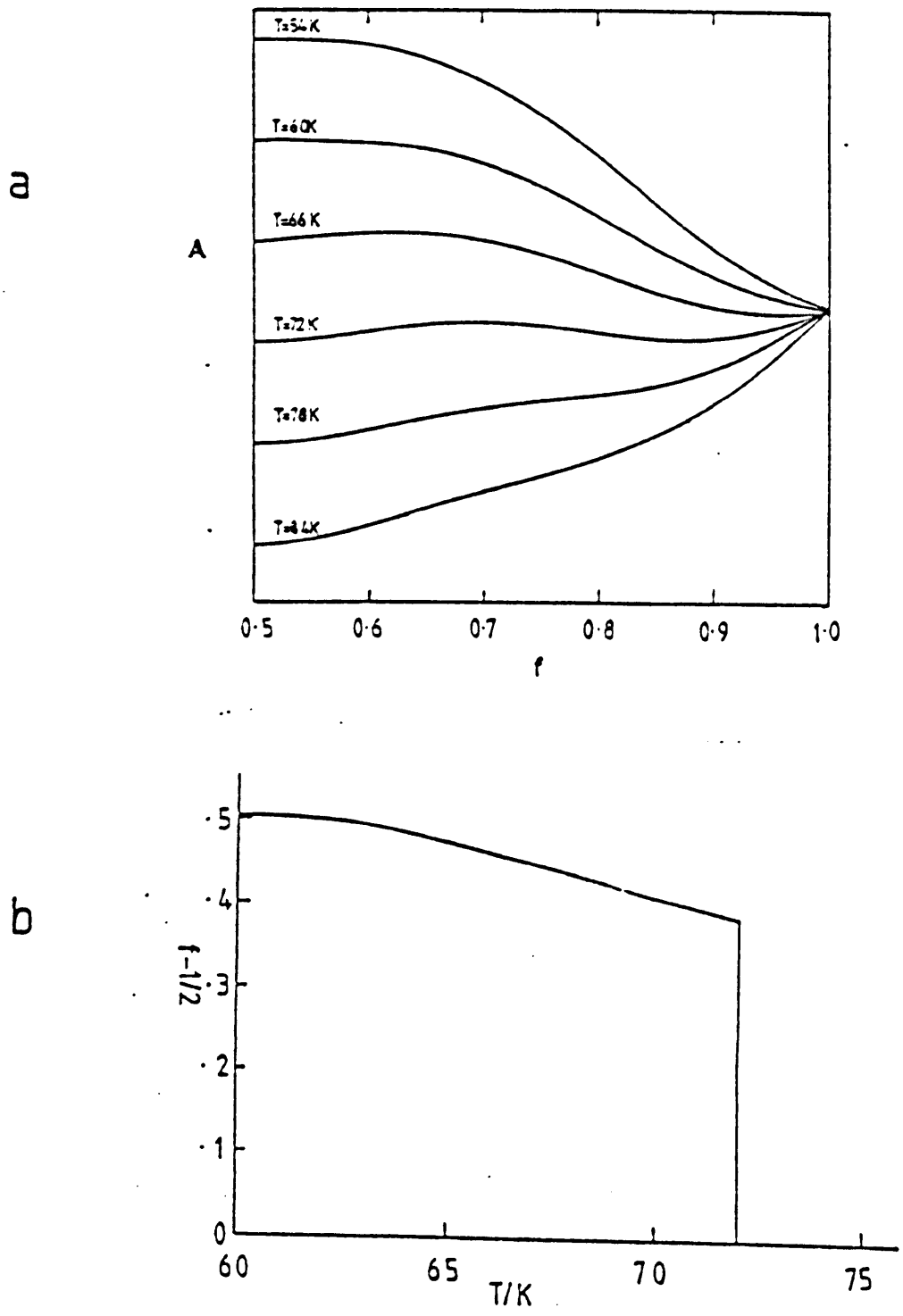

a) Variation of the Helmholtz free energy A (arbitrary scale) with the fraction f of correctly oriented bonds, at various temperatures

b) Variation of the equilibrium value of f with temperature

values of the bond and molecule variables corresponding to this situation are shown in tables 3.1 and 3.2, where p, q, and r have the same meanings as in section 3.3.1.

The entropy expression is as in equations 3.10 and 3.11, with $N = 4n$. The expression for the contribution of the energy differences E_m and E_c to the electrostatic energy per unit cell, $u=U/n$, becomes

$$u = -E_0 \left[\frac{p^2 + r^2 + q^2/4}{2f^2 - 2f + 1} \right], \quad (3.25)$$

where $E_0 = 2E_m + 6E_c$.

The equilibrium value of f at a given temperature is that at which the free energy A is minimized. Figure 3.8 (a) shows the variation of A with f at various temperatures, where θ_a = 0 K and θ_c = 48.6 K. At temperatures above about 80 K, the only minimum is at f=1/2 and the equilibrium state is completely disordered. As the temperature is reduced, a second minimum appears at $f \approx 0.8$, but with a higher value of A than that at f=0.5. When T $\approx$ 72 K, the values of A at the two minima are equal: this is the condition for a first-order transition. At lower temperatures the equilibrium phase is partially ordered, approaching f=1 as the temperature falls still further. Until the temperature reaches $\approx$ 60 K, the free energy curve still has two minima, so that there is a potential barrier for ordering. Figure 3.8 (b) shows the variation of the equilibrium value of f with temperature.

FIGURE 3.9

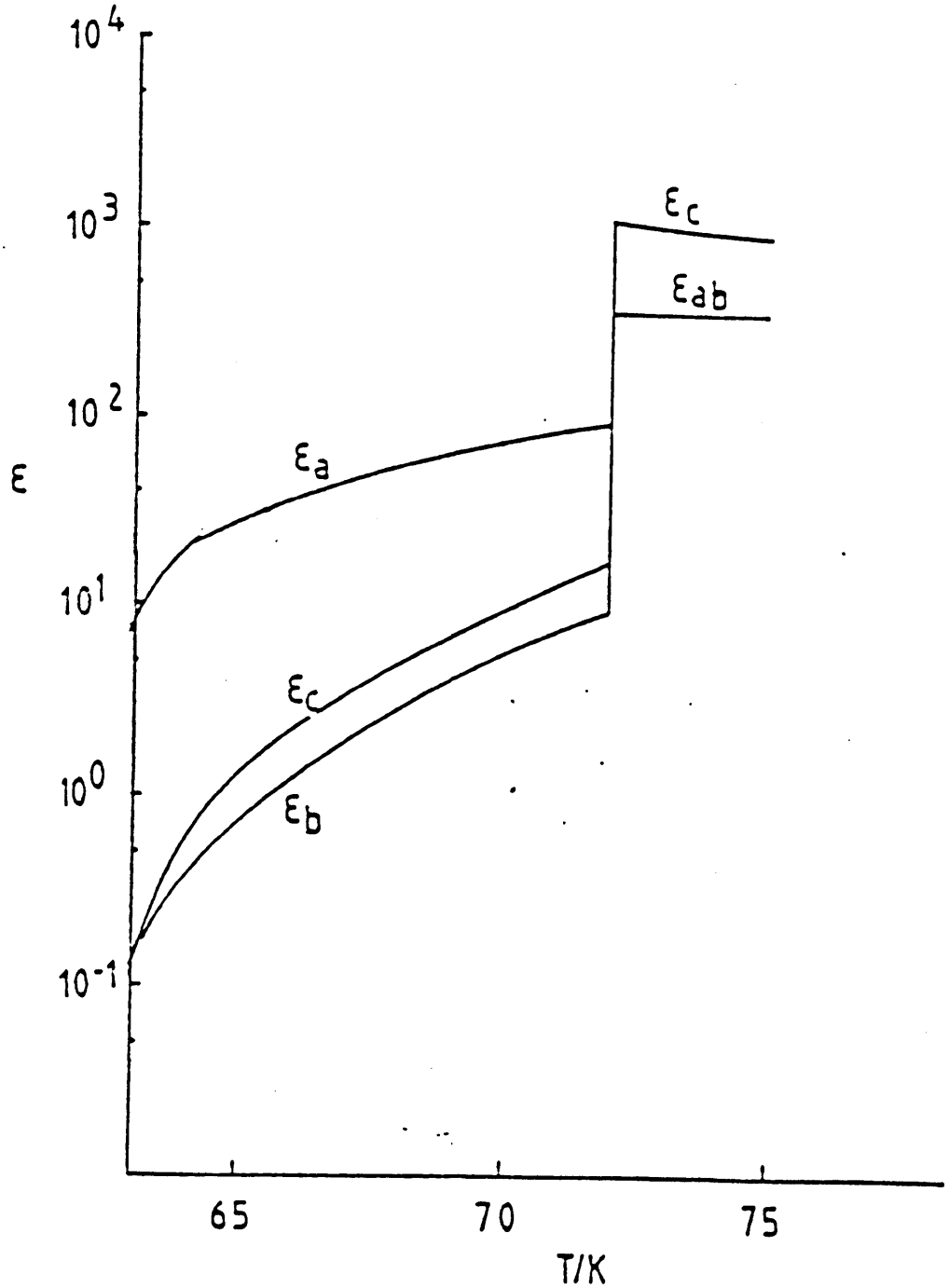

Temperature dependence of the dielectric constants along the three orthorhombic crystal axes

The dielectric constants in the equilibrium partially ordered phase have been calculated in the same way as those for the paraelectric phase, except that v is now proportional, not to the total polarization in the chosen direction but to the additional polarization caused by the applied field. The dielectric constants were calculated at the equilibrium value of f, found by numerical differentiation of the expression for $A(f)$. Because the ordered phase is orthorhombic, ε_a and ε_b are distinct. However, in real specimens, it would be unlikely that a whole crystal would be ordered so that its a- and b-axes were distinguishable: different domains would have the b-axis in different directions. Fig 3.9 shows the permittivity in the three directions as a function of temperature. The absolute values are obtained by using the Curie constant, 24000, found by Kawada (1978). In all directions, the equilibrium static permittivity falls to a low value immediately below the transition temperature and continues to fall with decreasing temperature, tending to 0 as the equilibrium value of f approaches 1. The higher value of ε_a immediately below the transition reflects the fact that even within one (001) layer the ordered structure has no spontaneous polarization along this axis.

3.4 The 'mixed' model

It is likely that in practice neither of the extremes discussed above is realised, but that a partially ordered sample close to the transition temperature consists of a mixture of regions of homogeneous partial order and complete disorder. The degree of order and the dielectric constants in the ordered regions are

FIGURE 3.10

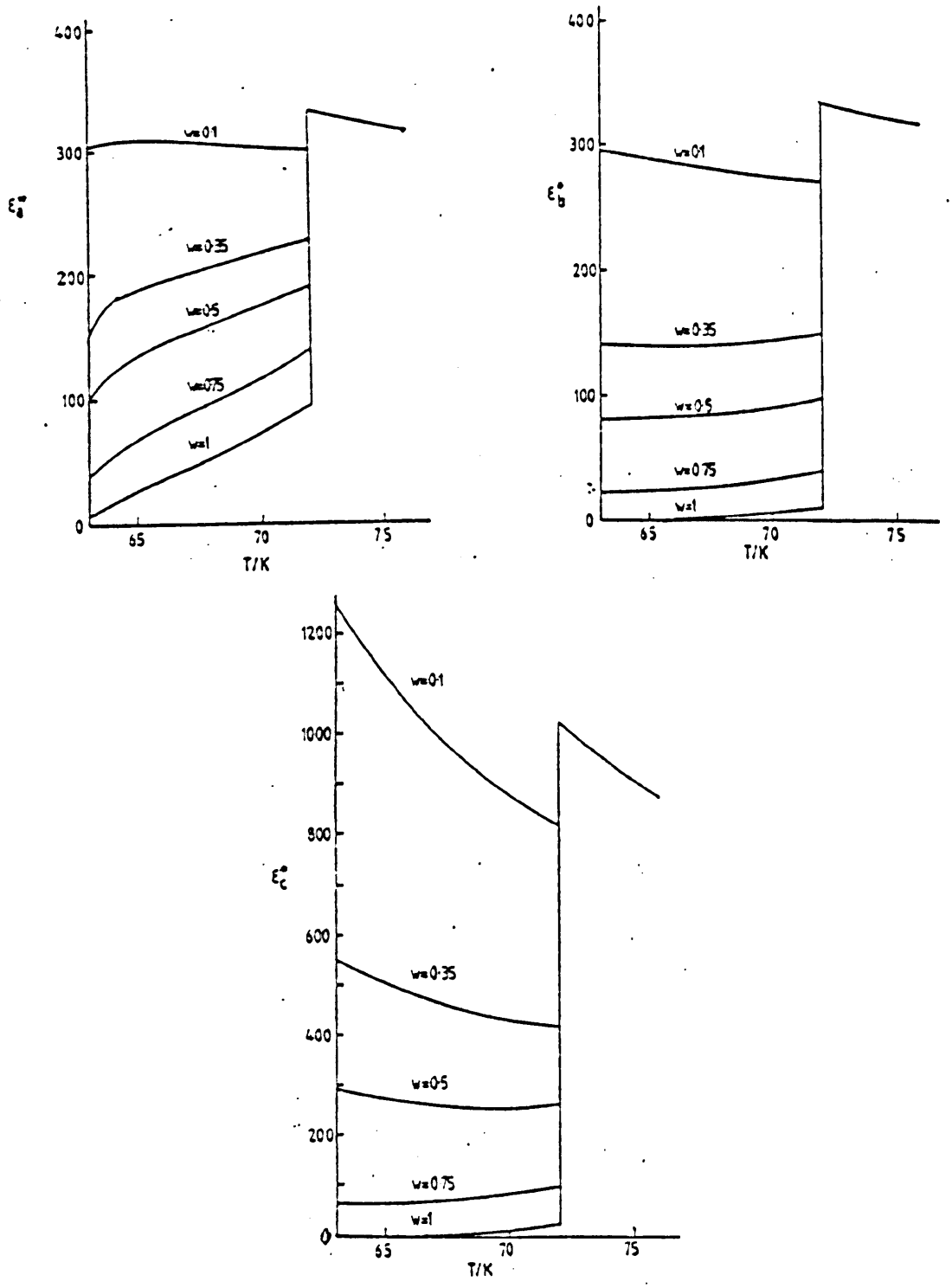

Temperature dependence of the effective static dielectric constants along the three crystal axes, for a mixture of which a fraction w is in equilibrium and a fraction (1-w) is disordered.

assumed to vary with temperature following the theory discussed in section 3.3, while the disordered regions have dielectric constants varying according to the appropriate Curie and Curie-Weiss laws. The variation of ε_a^*, ε_b^* and ε_c^* with temperature are shown in figure 3.10 for various values of w, the fraction of the sample which is in the equilibrium phase below the transition.

In a polycrystalline sample there will be grains with their crystal axes at all angles to the field. For simplicity, the arrangement of grains will be approximated as a mixture, with equal volumes having *a*, *b*, and *c* axes parallel to the applied field. The effective dielectric constant of such a mixture for various values of w may be estimated using equation 3.4, and is plotted as a function of temperature in figure 3.11.

3.5 Application of the theory to published results

We are now in a position to compare the results of the experiments mentioned in section 3.1. The maximum entropy loss found in the calorimetric measurements by Tajima et al. (1984) was 68% of the total residual entropy. In the two-phase model this would correspond to w=0.68, or f=0.84, and in the homogeneous model to $f\simeq$0.9. For any mixed model the value of f will be intermediate between these two extremes. The value f=0.63 found by Leadbetter et al. (1985) by neutron diffraction would correspond to w=0.26 with the loss of 26% of the entropy in the mixed-phase model, or to the loss of about 10% of the entropy in the homogeneous model. In this case the two-phase model is probably the more appropriate as

FIGURE 3.1:

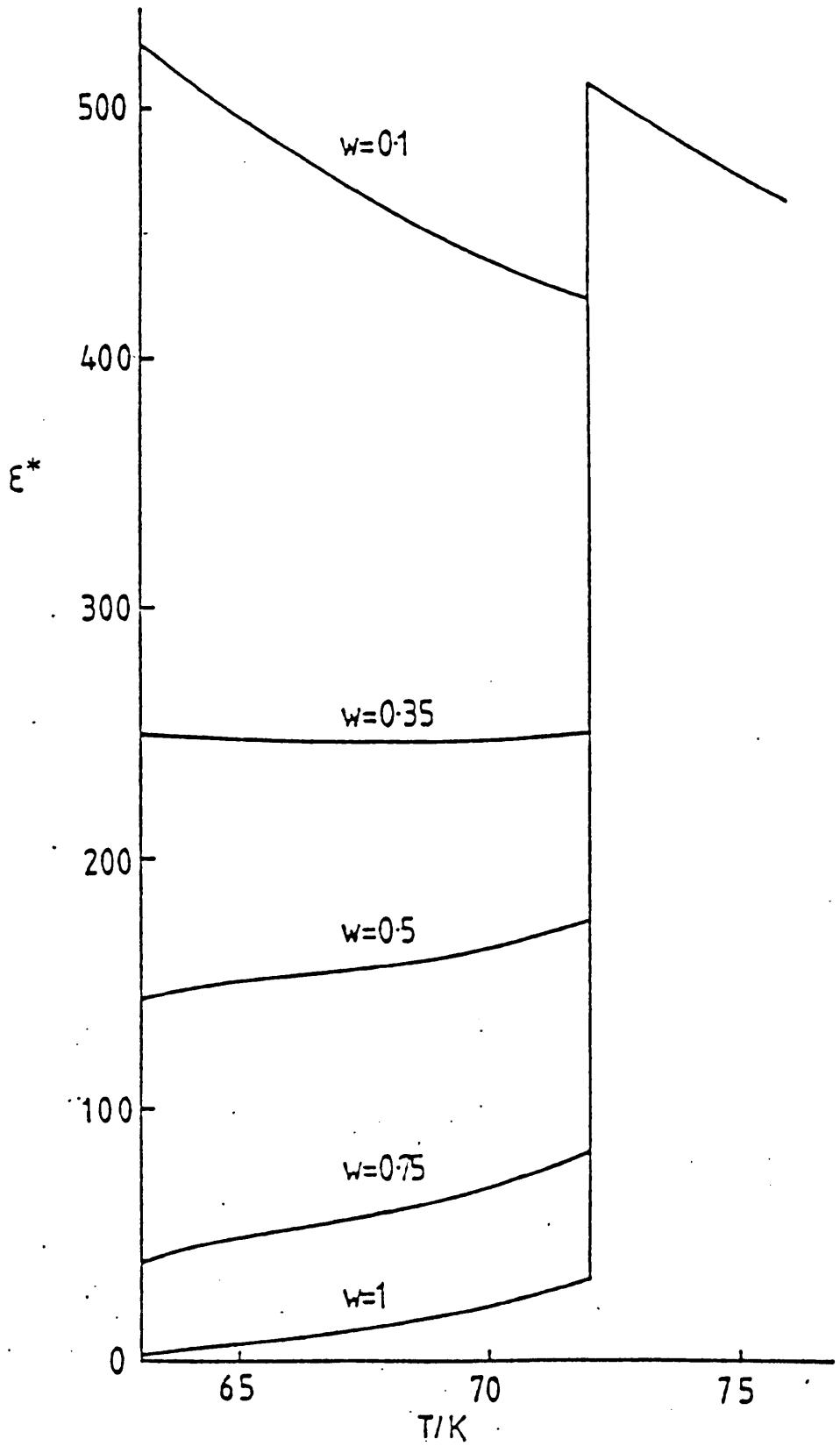

Temperature dependence of the effective static dielectric constant of polycrystalline ice, for a mixture of which a fraction w is in equilibrium and a fraction (1-w) is disordered.

Facing Page 52

homogeneous partial order has little physical meaning in a crystal with such a low degree of order. It is evident that the degree of order achieved in the powdered specimen used in the diffraction experiment was much less than that attained in the calorimetric measurements on a sealed solid polycrystalline specimen.

Kawada and Dohata (1985) found that the static dielectric constant immediately below the transition temperature was never less than about 250, 50% of its value immediately above. If we assume that the samples consisted of a mixture of transformed material in equilibrium with $\varepsilon_s \simeq 30$ and 'supercooled' disordered regions with $\varepsilon_s \simeq 500$ just below the transition, and apply equation 3.4, this means that the volume fraction w of transformed material is approximately 0.34. If the order parameter in the ordered regions has its theoretical equilibrium value, 0.88, at the transition temperature, this corresponds to $f \simeq (0.88 \times 0.34) + (0.5 \times 0.66) \simeq 0.63$. If w remained constant with temperature while the ordered regions became completely ordered at lower temperatures, the maximum value of f would be $(1 \times 0.34) + (0.5 \times 0.66) = 0.67$ and the maximum entropy loss would be 34%. This represents a relatively poorly transformed sample.

FIGURE 4.1

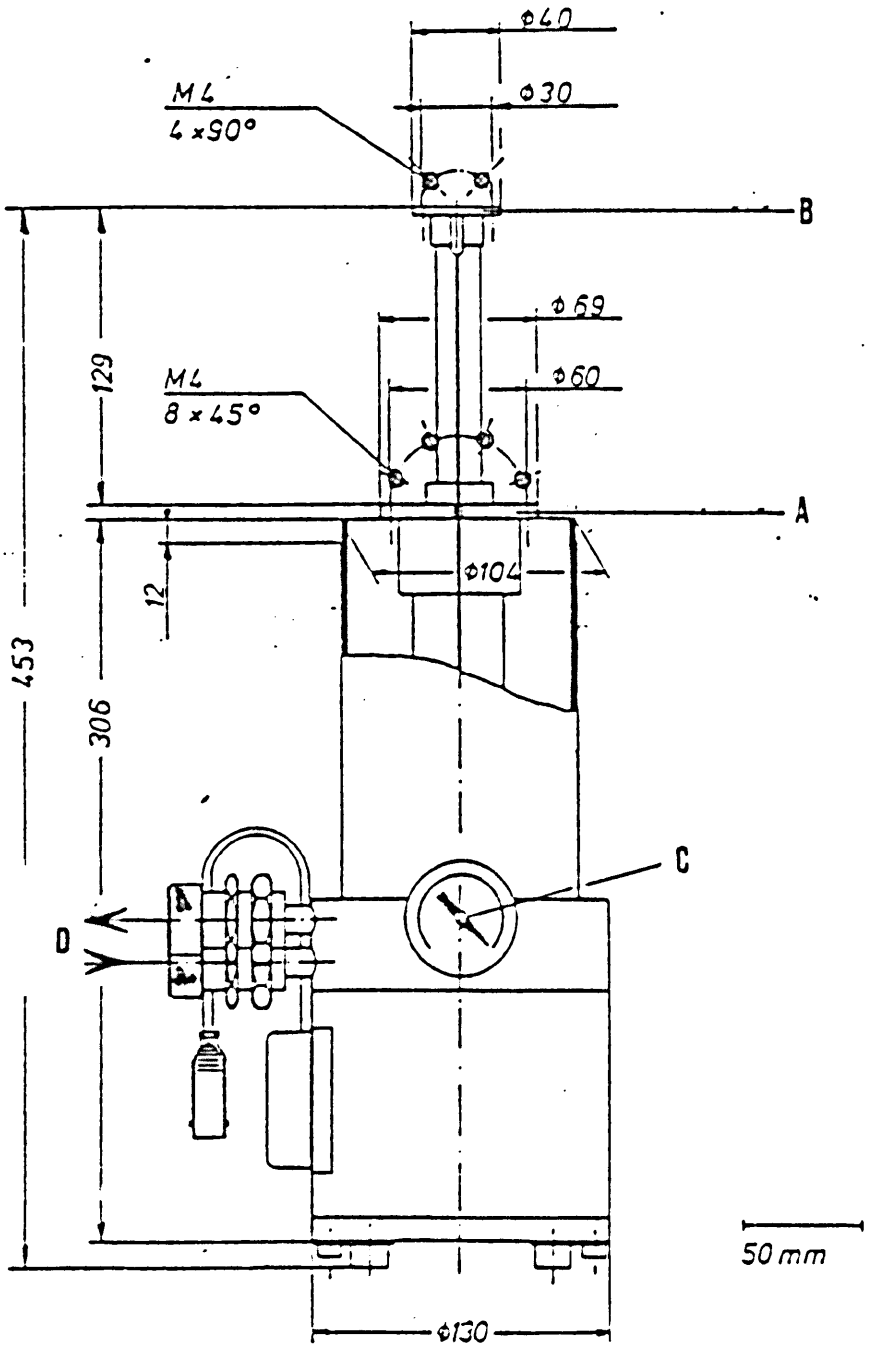

The cold head of the cryogenerator

CHAPTER 4

APPARATUS FOR THE DIELECTRIC MEASUREMENTS

Measurements of the dielectric properties of KOH-doped ice have been carried out in solid and powdered polycrystalline samples and in one single crystal. For these experiments, a cryostat has been designed and a measuring system with associated software has been developed.

4.1 The refrigerator

The major requirement for experiments on the ordering transition is the ability to maintain the sample at temperatures around 60-70 K for periods of days or even weeks. For this purpose a Leybold-Heraeus cryogenerator was chosen (model RG2): this is a small two-stage closed-cycle helium refrigerator. Since no external gas supply is required, the refrigerator can run unattended for extended periods. The unit, which is driven by a separate, air-cooled compressor, is shown in figure 4.1. The first stage cold head A runs at about 80 K, the second stage B at about 20 K. The temperature at the second stage cold head is measured by a hydrogen vapour-pressure thermometer C. The helium is carried to and from the compressor by flexible pipes entering at D. The refrigerating capacity varies with the heat input to the cold head: in order to reach its bottom temperature the second stage cold head must have a heat input of no more than about 2 W. Vacuum insulation is therefore essential for the proper operation of the refrigerator.

FIGURE 4.2

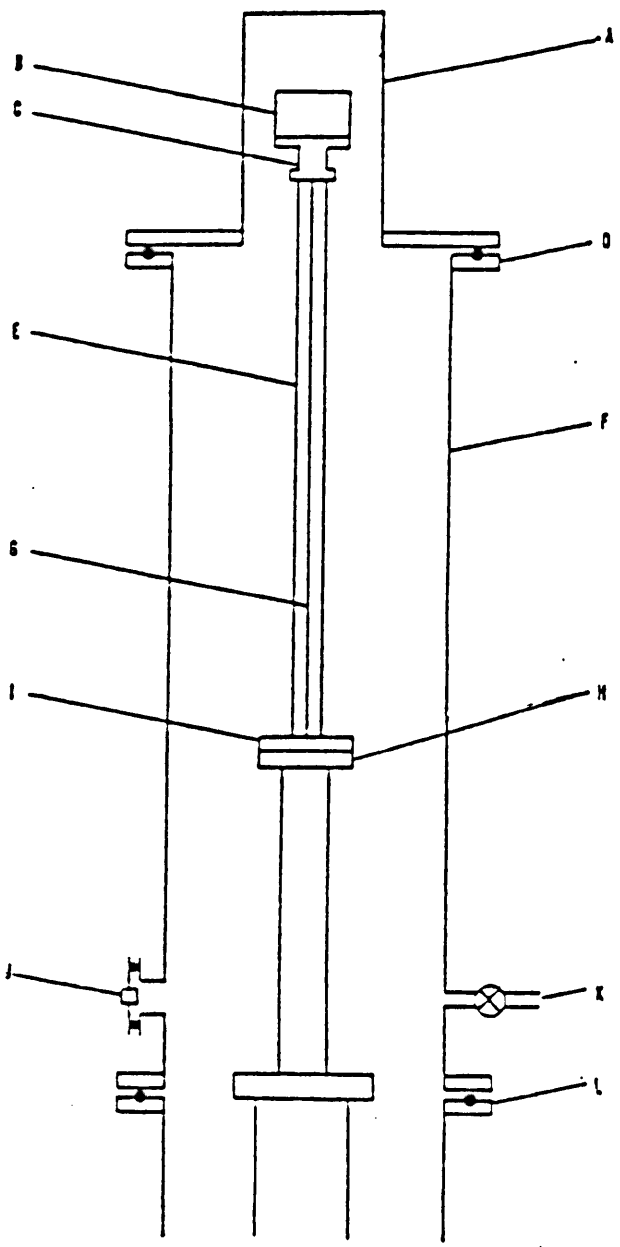

The first mode of use of the cryostat (not to scale): the letters refer to the text of section 4.2.1

The base of the cryogenerator stands on a rubber mat and is supported by a wooden 'nest' in order to reduce the mechanical vibration caused by the two pistons in the cold head.

4.2 The cryostat

The cryostat which has been designed around the cold head can be used in two modes, which will be described separately. In both cases, the cold head is enclosed in an evacuated vessel.

4.2.1 The first mode

In the first mode, shown in figure 4.2, the cryostat takes a sample in a sealed cell, which is mounted in the vacuum vessel before evacuation and freezes as the refrigerator cools. The vacuum vessel consists of a brass cylinder F bolted at its base to a flange L on the shell of the cold head and closed at the top by a blind cover A bolted to a flange on the cylinder, the seals being made by rubber O-rings in both cases. Around the base of the cylinder are three ports J with glass-metal seals for electrical connections and three quarter-inch copper pipes K fitted with HOKE valves. Of these, one is connected to the rotary pump used for preliminary evacuation and one to a Pirani gauge, while the third is generally used to admit air to the vessel before disassembly.

No suitable pump is available to maintain the thermal vacuum required for the cold head to function effectively. However, the operating temperature of the cold head is such that it will 'cryopump' by condensing residual gas in the vessel, once the

pressure has been reduced to about 100 Pa by the use of a single-stage rotary pump. The cryostat is therefore designed with only a weak thermal link between the cold head and the sample on its temperature-controlled platform, so that the cold head remains cold enough to maintain its own vacuum even with the sample close to the melting point. The link consists of a strand of 18 s.w.g. copper wire G inside a cupro-nickel tube E which provides mechanical support while having a low thermal conductance. At its base is a copper disc I bolted to the cold head H, while at the top is a copper platform C to which the sample cell B is attached. Layers of vacuum grease are used to ensure good thermal contact between the parts. Both ends are fitted with heating coils, of approximate resistance 30 ohm, wound from 36 s.w.g. Eureka wire and bonded to the metal with epoxy resin ('Araldite'). A cylinder of aluminized Melinex film is placed around the link and the sample to shield them from thermal radiation.

The internal wiring comprises power leads for the two heating coils, four-wire connections for the platinum resistance sensor used to monitor the sample temperature and two leads for the measurement of the dielectric properties of the sample. Of these, that for the 'high-impedance' side incorporates a small polystyrene capacitor and is sleeved in PTFE for most of its length, emerging at a single-way lead-through. All the wires are of 30 s.w.g. enamelled copper, and are anchored to the central tube near its base. The leads are fitted with miniature plugs and sockets near the exit ports, so that when these are disconnected the outer vessel can be lifted clear leaving the central tube in position.

FIGURE 4.3

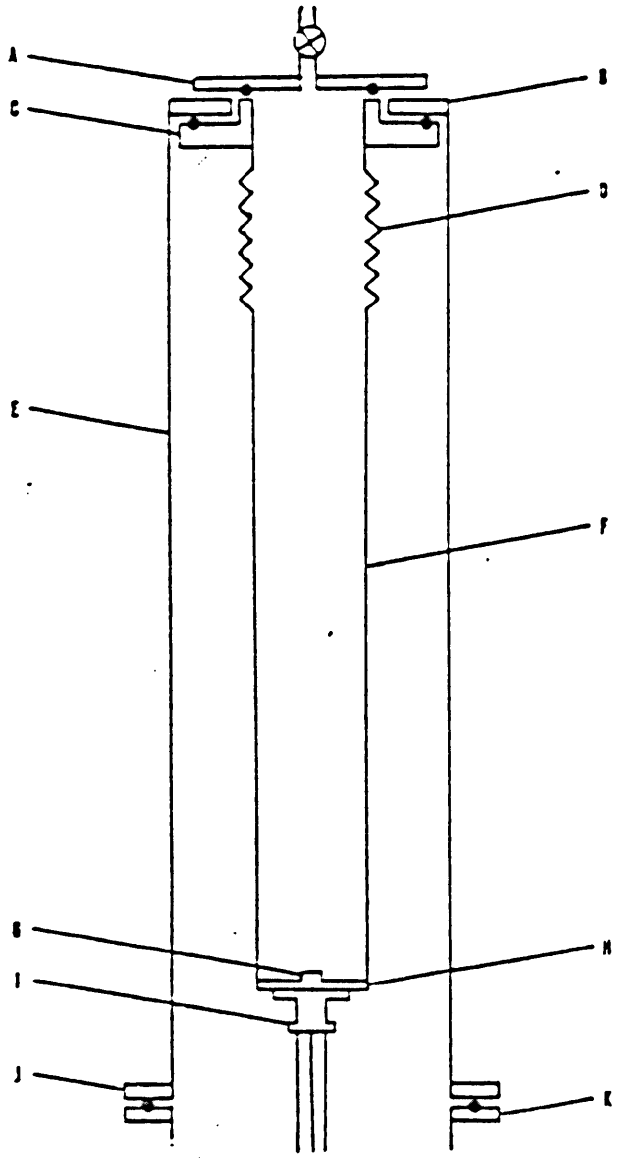

The extension of the cryostat for the second mode of use (not to scale): the letters refer to the text of section 4.2.2

4.2.2 The second mode

In the second mode, which was developed at a later stage, already-frozen samples (powder or single crystal) are placed in the cryostat as it is running: the sample is outside the main vacuum vessel, but sufficiently isolated from the surroundings that it can be cooled effectively. The design was constrained by the wish to disturb the existing body and wiring as little as possible, so that experiments could still be carried out as in the original cryostat: as a result, the adapted vessel was perhaps taller than necessary.

The adaptation to the second mode of operation involves the addition of three main parts, of which the first two are shown in figure 4.3. The inner part of the extension consists of a stainless-steel tube F, closed at its bottom end by a copper plate H which is fixed to the sample platform by six screws and has on its inside a threaded boss G designed to accept the sample holder. The upper end of the tube is attached to a bellows D to accomodate the differential contraction between the inside and outside of the vessel. Above this is a brass flange C carrying a rubber O-ring. A layer of aluminized Melinex film is loosely wrapped around the steel tube to provide radiation shielding. The outer shell consists simply of a brass cylinder E with an outward flange J at the base and an inward flange B at the top, with appropriate holes. Once the inner part has been fixed to its platform, the outer shell is lowered over it, closing the vacuum chamber and sealing against the O-ring on the top of the inner vessel. The upper flange of the outer vessel has six countersunk holes, through which bolts are

fastened into blind tapped holes in the flange of the inner vessel. In the lower flange of the outer shell are six slotted holes which are used to secure the shell to the upper flange K of the original vessel (where the blind cover is attached in the first mode).

The cryostat as described above forms a closed vacuum chamber in which the cold head can be run, with an open, insulated vessel about 400 mm deep to hold the sample. When the sample assembly is not in position, the vessel can be closed by a blank cover A. The sample holder with its associated wiring is incorporated in a lid which closes the open vessel, as follows. The top of the sample holder is fixed to a cupro-nickel tube which is made in two parts, one sliding on a length of brass tube which is fixed to the other, so that its length is adjustable. This 'centre-stick' carries two copper radiation baffles, with holes through which the wires pass. The top of the centre-stick is attached to the brass disc which forms the lid, and through which pass pipes leading to two electrical ports and a HOKE valve. This lid has six 30° slots, so that it can always be fixed using six of the twelve blind holes in the upper flange of the outer shell, whatever the angle reached by screwing the sample holder down on its threaded boss. An O-ring in the underside of the lid seals against the top of the inner vessel. If necessary, the sample vessel can be evacuated using the rotary pump.

The wiring for experiments in the adapted cryostat consists of the four leads for the platinum resistance sensor in the sample cell and a low- and high-impedance connection for the dielectric

FIGURE 4.4

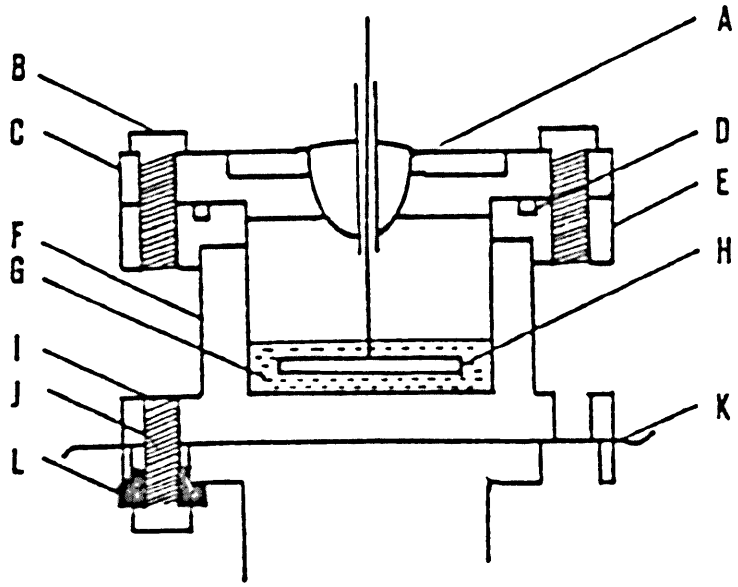

The sample cell for polycrystalline ice (twice actual size): the letters refer to the text of section 4.3

measurements, the latter being sleeved and brought out to a single-way glass-metal seal. A second platinum resistance sensor is mounted in the base of the cryostat, within the vacuum vessel, and used in conjunction with the platform heater to control the sample temperature.

In order that the sample may be cooled sufficiently, the thermal link between the sample platform and the cold head is strengthened by the addition of four extra lengths of 18 s.w.g. copper wire soldered into plates which are clamped at the top between the heater platform and the cryostat base, and at the bottom between the cold head and the base of the original link. The cryostat can be operated in this mode for about ten days before the internal screws become loose due to thermal contraction and the vibration of the cold head so that the link is no longer effective.

4.3 The sample cell for polycrystalline ice

The cell used for the experiments on polycrystalline samples is shown in figure 4.4. It consists of a copper body F with a stainless steel flange E and a stainless steel cover C which contains a single-way glass-metal seal A. The inside of the body is gold-plated to prevent contamination of the sample. The low-impedance electrode is formed by the cell body, which is fixed to the sample platform in the cryostat by three screws J but electrically insulated from it by a layer of greased Melinex film K and the use of plastic washers L. The high-impedance electrode is a gold disc H immersed in the sample solution G and attached to a

central lead which enters the cell through the glass-metal seal in the cover and is soldered into its tube to provide a good seal. The lead to this electrode, incorporating a polystyrene capacitor, is connected to the central lead by a miniature socket. The capacitor serves the same purpose as the more usual insulating layer on the electrode: no suitable material for such a layer could be found because of the need for the insulation to remain intact over a wide range of temperatures. The cover is sealed with an indium ring D and held in place by six stainless steel screws B, one of which is also used to secure the low-impedance connection.

4.4 Temperature measurement and control

The sample temperature is monitored using small platinum resistance sensors, (PT100) which have a resistance of 100 ohm at 0°C. The resistance of the sensors falls almost linearly with temperature between 273 K and 73 K. No definite calibration is available below 73 K, so the following system has been adopted. The temperature of the ordering transition, 72 K, is taken as a fixed point and the temperature variation assumed to be linear, with a known coefficient (deduced from published values) of 0.42 $\Omega\ K^{-1}$. As a typical sensor was found to read correctly when immersed in liquid nitrogen, the offset, varying between experiments, between the temperature calculated on this basis and that found by extrapolating the British Standard (1984) scale was assumed to be due to poor thermal contact between the sample and the sensor. The sensors are usually placed in holes in the body of the sample cell, but even when greased they may not be in perfect thermal contact

with the cell at low temperatures.

The temperature controller measures the resistance of the sensor by passing a stabilised current through it and measuring the voltage across it. Four-wire connections are used in order to minimize the effect of the resistance of the long, thin wires connecting the sensor to the outside of the cryostat. The difference between the measured resistance and a set value is then used to regulate the voltage applied to the heating coil: the mean power level can be manually adjusted as necessary. The resistance measured is displayed on a panel meter, and a voltage proportional to its value appears at a pair of output connections, so that the temperature variation during an overnight run can be monitored and stored in a data-logger. The temperature was typically steady to within about 0.25° in the timescale of an experiment (up to 40 minutes if bridge measurements were involved). Overnight, the measured sample temperature tended to fall by about 0.5° in 16 hours.

When the top-loading cryostat is used, the temperature controller is connected to the sensor in the base of the cryostat. The sample temperature is monitored by another sensor, embedded in the cell, which is read by a separate device. This consists of a stable current supply provided by a reference diode and operational amplifier, the voltage across the sensor being measured directly by a digital panel meter which displays the resistance in ohm.

4.5 The system for dielectric measurements

4.5.1 Introduction

In order to make dielectric measurements where long time-constants are involved, the 'pulse method' has been used. In this method, a step voltage is applied to the ice sample sandwiched between two electrodes. A capacitor is in series with the ice, and the variation in the charge on this capacitor is measured by a sensitive integrating amplifier. From this variation the time constants and relaxation strengths of the ice can be deduced. The formulae used in these calculations will be given in section 5.3. The method has the advantage of enabling long time constants to be measured relatively quickly, and is more suitable for automation than the conventional a.c. bridge. In order for the method to work satisfactorily, the impedance between the amplifier input and ground must be high.

4.5.2 Hardware

The system which has been developed to measure the dielectric properties of the sample by the pulse method consists of a BBC Master Series Microcomputer, to which is interfaced a unit containing a fast analogue to digital converter (ADC) and a programmable voltage source. A step voltage is applied to the low-impedance side of the sample, and the response at the high-impedance side is amplified by a simple electrometer used as an integrating amplifier. The output from the electrometer is taken to the ADC and the digitised data are passed to the computer.

The relevant features of the microcomputer are as follows. In addition to the 64 Kilobytes of RAM in the central processor, a further 64 K of 'sideways RAM' are available for data storage. The computer has three interfaces for experimental purposes: a four-channel ADC which was not used in the present experiment; a 1 MHz bus for interfacing to fast external devices; and an 8-bit 'user port' which can be used for input and output of TTL signals. A dual disc drive, used in conjunction with the Advanced Disc Filing System, plays an important part in the system.

The electrometer is based on an AD515 electrometer chip used in an integrating mode, and replaces a Keithley 601 Electrometer which was found to have an unsatisfactory response at high frequencies. When leakages in the external circuitry are reduced as far as possible, the drift rate is less than about 1% of full scale in 100 s. The signal from the charging of the specimen capacitance is amplified to a full scale value of 5 V. The instrument is powered by a ±15 V supply taken from the ADC unit. It can be zeroed by means of a well insulated push-button switch which momentarily connects the input and output pins of the electrometer. An external plunger, driven by a battery-powered solenoid and controlled by a 5 V TTL pulse from the computer user-port, enables the button to be pushed remotely. This somewhat clumsy arrangement was adopted because attempts to close the contact by means of a reed switch inside the instrument case seriously affected the perfomance of the electrometer.

The ADC and voltage source are interfaced to the computer via its 1

MHz bus. The ADC has 12-bit resolution and is capable of taking up to 2048 readings at sampling intervals from 8 μs to about 65 ms. (The ADC built into the microcomputer, which was used in preliminary experiments, has a minimum sampling interval of 10 ms). The conversion is triggered by a 5 V TTL pulse from the voltage source, and starts after a programmed delay of between 0.2 ms and 6.5537 s: the converted values are stored in the memory of the device and can then be read into the computer. The voltage applied to the sample is switched on and off from the computer, but its level is controlled by a manual switch and may be 1.5, 3, 6, 9 or 12 V. A 16-bit timer, clocked at 4 μs, is also included in the device.

Because the power supply to the cryogenerator is separate from that to the computer and other equipment, the earth connections in the measuring circuit are kept independent of the cryostat case. The two leads for the dielectric measurement have their screens connected, and are connected to ground via the power supply cable from the ADC unit to the electrometer: the two BNC cables (voltage output and analogue input) connected to the ADC unit have their screens isolated from its case. This arrangement has been found to give satisfactory protection from electrical noise.

A General Radio type 1615-A capacitance bridge is also available, with oscillators and a tuned detector giving a frequency range of 20 Hz to 100 kHz. This allows the measurement of time constants as short as 10 μs.

4.5.3 Software

The program which has been developed to control the experiment and analyse the data is written mainly in BBC BASIC, but substantial portions of machine code are used for the control of the ADC unit.

The values of the sampling interval, number of samples, delay, and duration of pulse for one or two 'shots' of the ADC are calculated from the input parameters and stored in a reserved section of memory together with coded versions of the voltage level and electrometer scale used and the reading of the temperature sensor. The number of readings taken is always a multiple of 256. The values are then written to the appropriate locations in the ADC to bring about a sequence of events as follows. The ADC is first triggered by a pulse from the voltage source, and the timer started. When the time for three conversions at the chosen interval has passed, the voltage source applies a voltage across the sample. When the ADC signals the end of the conversion, the voltage is switched off and the data read into the computer. After an interval equal to the duration of the first 'shot', a second pulse may be applied, the conversion being timed to begin at the point where the previous one finished. In this way, two widely different relaxation times may be measured in one experiment.

A different routine is used when very long sampling intervals are required. The readings are taken in pairs separated by the minimum interval, and one reading from a pair is read into the computer memory. The timer is then used to measure the time to the next pair of readings. In this way, intervals of up to about 0.5 s can be

used, the limiting factors being the stability of the electrometer and the accuracy of the timing routine. The system can be used to measure time constants from about 100 μs to 100 s.

The 12-bit data from the ADC are read directly into an array of 4-byte integers in the computer memory. To save space in the main memory, this array contains only 256 values at a time: when each block of data has been read in it is copied to the sideways RAM, whence it can be retrieved as required. Once the data from the experiment are in memory they can be displayed, analysed or stored on disc.

The data are copied to disc directly from the sideways RAM. Each data file includes a copy of the 48-byte parameter block containing all the information necessary to display, analyse and identify the data, so that a file retrieved from disc can be read into sideways RAM and treated in exactly the same way as a new data set. The files are organised in directories of which the names refer to the sample and the stage of the experiment - for example, directory KP11U1 would contain data from the first heating sequence (U(p)1) for the sample K(OH-doped) P(olycrystalline) 11.

Before analysis, the information in the parameter block is used to convert the data to a convenient form. After subtraction of the base value, found from the first three points measured before the voltage was applied, the four-byte integers are scaled to give real numbers in units of pF (charge per unit voltage), which are stored in a new array. Another array contains the abcissa value (time in

microseconds) for each point. These arrays, together with one containing the calculated values of the function at each point, reside in the sideways RAM and are transferred to the main memory in 256-value sections: a maximum of twelve 256-value blocks of data can be held in the 64 K of sideways RAM. The refinement need not use every point: the operator may elect to take, for example, only one point in four. The data analysis uses a non-linear least squares fitting routine based on the Choleski method. This requires an initial estimate of the parameters, which are then refined in successive cycles until no further significant reduction can be made in the sum of the squared deviations. The functions used contain up to ten parameters; a final level, up to four exponential decays specified by an amplitude and a time constant, and an optional steady drift rate. A graph of the calculated and measured data is displayed before the refinement begins, as an aid to the user in supplying suitable starting values, and also after each cycle.

The program includes a facility for overnight experiments: a measurement with specified parameters is repeated at specified intervals and the data saved on disc. Before each measurement the remotely-operated plunger is used to zero the electrometer. If desired, the data can be fitted to a specified function: the refined parameters from one fit are used as the initial estimate for the next.

CHAPTER 5

THE DIELECTRIC MEASUREMENTS ON KOH-DOPED ICE

5.1 Introduction

The main aims of the dielectric measurements on polycrystalline samples were to investigate the effect of the ordering transition on the dielectric properties of KOH-doped ice, to compare the results obtained by annealing the same sample at different temperatures, and to find the most effective strategy for preparing a sample for a neutron diffraction experiment. The dielectric properties of KOH-doped ice between the melting point and the transition temperature were also investigated in order to identify the mechanism responsible for the effect of KOH in catalysing the transition.

5.2 Sample preparation and experimental method

The polycrystalline samples for the dielectric experiments were prepared as follows. Tap water was passed through an 'Elga' deionizing system (columns SC3, SC6 and SC1) to remove organic and ionic impurities, and the desired amount (usually about 0.5 l) was placed in a polypropylene beaker. The KOH ('AnalaR' pellets) was added, and the solution boiled under reduced pressure in a dessicator for about an hour to remove dissolved air. The agitation of the liquid during boiling provided adequate stirring of the solution. As quickly as possible after the vessel had been brought back to atmospheric pressure, a few drops of the solution were

FIGURE 5.1

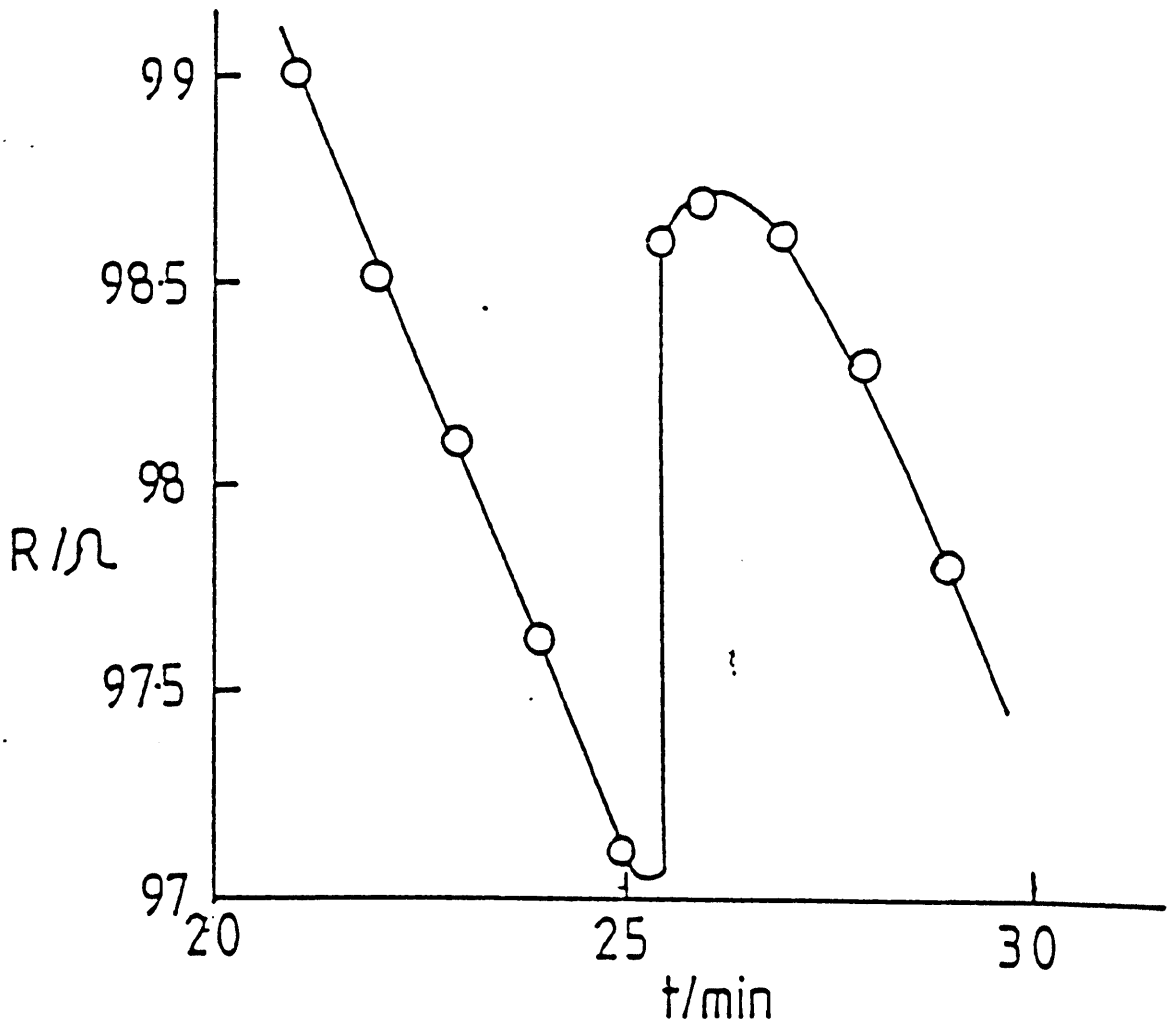

Variation of Pt sensor resistance *R* with time *t* from starting cooling, on freezing of a typical sample

poured into the sample cell, which had previously been mounted in the cryostat with its indium sealing ring in position. The lid of the cell was then sealed and the cryostat cover closed. A rotary pump was used to evacuate the cryostat to a suitable level (about 60 Pa) before the cryogenerator was switched on. Typically, cryopumping would begin within approximately 5 minutes, after which the rotary pump could be isolated, and the pressure would fall to 0.1 Pa in about an hour. The variation of the sample temperature with time, shown for a typical sample in figure 5.1, suggested that the sample usually supercooled by several degrees before freezing, and then froze over two or three minutes. Once freezing had taken place, the sample was cooled at a rate of about 1 degree per minute.

In the first series of experiments (KP1-KP9) the concentration of the solution was estimated by counting the pellets of KOH and noting the approximate volume of liquid. In the second series (KP10-KP14) the KOH was weighed to ±0.1 mg on a chemical balance and the volume determined to ±5 ml by transferring to a measuring cylinder the solution remaining after the sample had been poured out.

Measurements of the dielectric properties of the sample were carried out by the pulse method and in some cases also by using the a.c. bridge. Measurements were taken as the samples were heated and cooled, and also at intervals during annealing below the transition temperature. In all, 13 polycrystalline samples, with KOH concentrations varying from 10^{-3} M to 10^{-1} M, were investigated,

the transition to the ordered phase being observed at least once in each of 11 samples. The failure to observe the transition in the two remaining samples was due to difficulty in cooling the cryostat to a low enough temperature.

The analysis of the experimental data was carried out using the theory discussed in section 5.3.

5.3 Theory

When an electric field is applied to a sample of ice (or any lossy dielectric material), three effects occur: the electronic clouds of the molecules and the internal dipoles become polarised in the direction of the field; and charge carriers move through the material. In the case of ice, the latter two effects are brought about by the migration of charged point defects. The model for the electrical properties of ice which will be described below is due to Jaccard (1959,1964) and Hubmann (1979), to which works the reader is referred for further details.

The high-frequency dielectric constant, ε_∞, is due to the polarization of the electronic cloud surrounding each water molecule. It is essentially independent of temperature, and is small compared to the static dielectric constant ε_s, which is due to the rearrangement of the protons changing the direction of the dipole moment of the molecules.

The charge carriers in the model are the four types of point

FIGURE 5.2

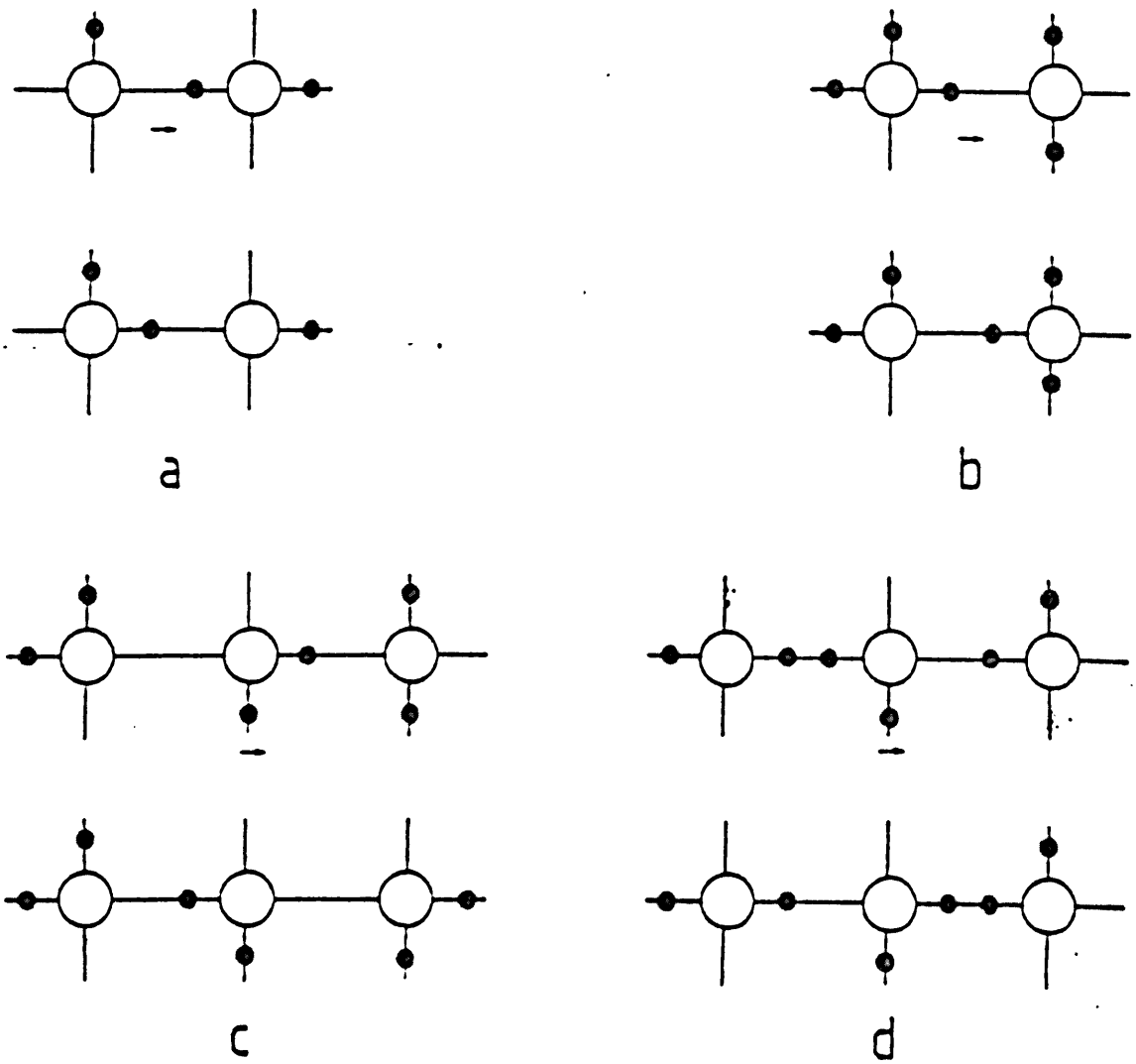

The migration of point defects, shown in 'square ice'
a) OH^- ion
b) H_3O^+ ion
c) L-defect
d) D-defect
The arrow shows the direction of movement of the defect

defect; the OH^- and H_3O^+ ions and the L and D Bjerrum defects. It is assumed that the numbers of each type of defect are small compared with the number of molecules in the crystal, but large enough to be treated statistically. The effect of the migration of the different types of defect is shown schematically in figure 5.2. In the presence of an ionic defect, a proton may move from one end of a bond adjoining the defect to the other, as in figure 5.2 (a) and (b). The ion has thus effectively moved from one oxygen site to the next. Similarly, when an L- or D-defect is adjacent to a molecule, the molecule may rotate (figure 5.2 (c) and (d)). The defect with its charge has thus moved from one bond to another. Although the net effect in either case appears to be to move a proton from one molecule (or bond) to another, the size of the effective charge on a moving defect is not equal to the electronic charge, as the proton has moved by a shorter distance than has the defect. Also, the movement involves the rearrangement of the electronic clouds of the two molecules involved. Since defects can be created in L-D or OH^--H_3O^+ pairs and this process must not create or destroy charge, the effective charges of each member of a pair must be equal and opposite. The charges will be designated by e_{DL} and $e_\pm$ in what follows. L-defects and OH^- ions carry negative charges, D-defects and H_3O^+ ions positive. The passage of a defect of one type through the crystal leaves a trail which cannot be followed by another defect of the same type, unless it has first been restored by the passage of a defect of the other type. If only one type of defect is present, therefore, the crystal will become polarized and a steady current cannot continue to flow: both ions and Bjerrum defects are required if the ice is to exhibit

a d.c. conductivity. If one defect of each type has passed from side to side of the crystal, the net effect is the movement of one proton across the crystal, so that the relation $e_{DL} + e_{\pm} = e$ must be satisfied.

When the crystal becomes polarized in an external field, the configurational entropy is reduced, as the molecular dipoles are no longer randomly oriented. By considering this entropy change in the context of irreversible thermodynamics, the response of the ice to a sinusoidal applied field of angular frequency ω may be found. Hubmann (1979) shows that this may be described as a dispersion of the form

$$\varepsilon(\omega)-\varepsilon_{\infty} = \frac{\varepsilon_s}{1+j\omega\tau_D} + \frac{\sigma_o}{j\omega\varepsilon_o}. \qquad (5.1)$$

The relaxation can be divided into real and imaginary parts, $\varepsilon(\omega) = \varepsilon' - j\varepsilon''$, where

$$\varepsilon' = \frac{\varepsilon_s}{1+\omega^2\tau_D^2} + \varepsilon_{\infty}, \qquad (5.2)$$

$$\varepsilon'' = \frac{\omega\tau_D\varepsilon_s}{1+\omega^2\tau_D^2} + \frac{\sigma_o}{\omega\varepsilon_o}. \qquad (5.3)$$

The parameters are given by

$$\sigma_{\infty} = \sigma_{\pm} + \sigma_{DL} \qquad (5.4)$$

$$1/\tau_D = \Phi(\sigma_{\pm}/e_{\pm}^2 + \sigma_{DL}/e_{DL}^2) \qquad (5.5)$$

$$\varepsilon_s - \varepsilon_{\infty} = \frac{1}{\varepsilon_o\Phi} \frac{(\sigma_{\pm}/e_{\pm} - \sigma_{DL}/e_{DL})^2}{(\sigma_{\pm}/e_{\pm}^2 + \sigma_{DL}/e_{DL}^2)^2} \qquad (5.6)$$

$$\frac{(e_{\pm} + e_{DL})^2}{\sigma_o} = \frac{e_{\pm}^2}{\sigma_{\pm}} + \frac{e_{DL}^2}{\sigma_{DL}}. \qquad (5.7)$$

Here, the conductivities due to the different types of defects ($\sigma_{DL} = \sigma_D + \sigma_L$, $\sigma_{\pm} = \sigma_+ + \sigma_-$) are given by relations

of the form $\sigma_i = n_i e_i \mu_i$, where n_i is the concentration of the charge carriers and μ_i their mobility. The e_i are the effective charges of the defects. τ_D is known as the Debye relaxation time. Φ is a factor proportional to the temperature T, the number of molecules per unit area and the second derivative of the entropy with respect to the polarization, in the case where all configurations of molecules have the same energy in the absence of a field. In the case where all configurations do not have the same energy, Φ would involve the Helmholtz free energy rather than the entropy, as has been discussed in section 3.3.

A special case arises when the condition

$$\frac{\sigma_\pm}{e_\pm} = \frac{\sigma_{DL}}{e_{DL}} \qquad (5.8)$$

is fulfilled. The frequency dependence of the response then vanishes. This is known as the 'crossover' condition, as it occurs at a temperature where the minority and majority carriers exchange their roles.

The concentration of each type of defect will vary with temperature, following relations of the type $n = n_0 \exp(-E/k_B T)$, where E is an activation energy for the formation of a pair of charged defects. There may also be an activation energy for the mobility of certain defects. The effective charges and mobilities of the defects may be determined by experiment. An account of work in this field is given by Hobbs (1974), in the chapter on the electrical properties of ice, and a detailed discussion would be beyond the scope of the present work. In order to determine the

FIGURE 5.3

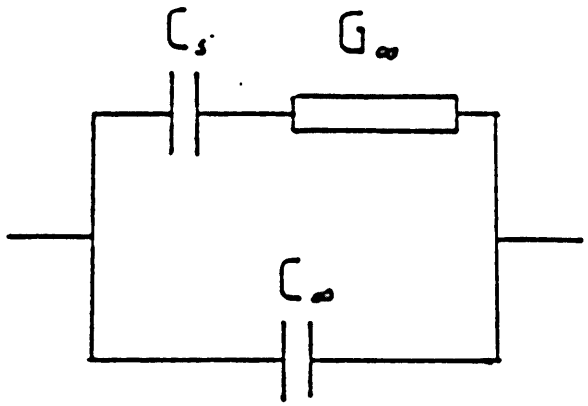

Equivalent circuit for ice with one type of charge carrier

properties of different defects, experiments on doped as well as pure ice are necessary. It is now generally accepted that in pure ice at temperatures between the melting point and about -50°C, the majority carriers are L-defects, which are generated in L-D pairs and have an activation energy for movement: the D-defects are immobile. The minority carriers, H_3O^+ ions, apparently move by quantum mechanical tunnelling of the proton on a bond between the two potential wells, as there is no activation energy for their movement.

If only one type of defect - say OH^- - is present, with an effective charge e_-, the relations 5.4-5.7 simplify to the following forms:

$$\sigma_\infty = \sigma_- \qquad (5.9)$$

$$1/\tau_D = \Phi\sigma_-/e_-^2 \qquad (5.10)$$

$$\varepsilon_s = e_-^2/\varepsilon_o\Phi \qquad (5.11)$$

$$\sigma_o = 0. \qquad (5.12)$$

In this case there is no σ_o term in the relaxation expression: the ice can be modelled by the equivalent circuit in fig. 5.3, where the conductance G_∞ is proportional to the high-frequency conductivity σ_∞, and the capacitances C_s and C_∞ are proportional to the static and high-frequency permittivities, ε_s and ε_∞. The response of this circuit to a sinusoidal applied field of frequency ω can be expressed as a complex capacitance, $C = C' - jC''$, where

FIGURE 5.4

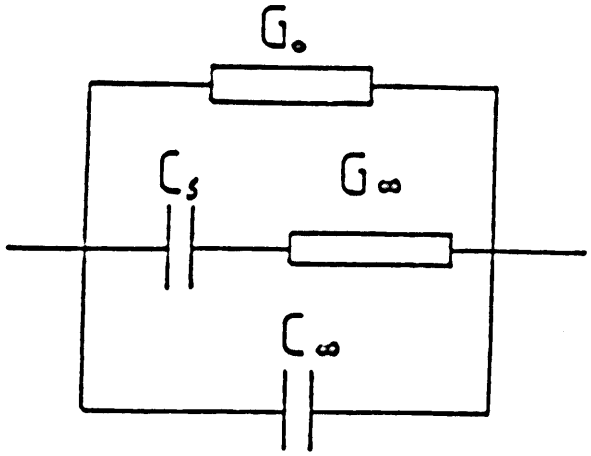

Equivalent circuit for ice with both ionic and Bjerrum-defect charge carriers

$$C' = \frac{C_S}{1+\omega^2\tau_D^2} + C_\infty \qquad (5.13)$$

and

$$C'' = \frac{\omega\tau_D C_S}{1+\omega^2\tau_D^2}, \qquad (5.14)$$

where τ_D is equal to C_S/G_∞. (The complex capacitance C of a circuit is related to the complex impedance Z by the equation $Z=1/j\omega C$). A capacitance bridge may be used to measure the effective parallel capacitance C_P and conductance G of the circuit at a given frequency, which are related to C' and C'' by the equations $C_P = C'$ and $G = \omega C''$. In this simple case, G tends to G_∞ as ω tends to infinity and goes to zero as ω^2 at low frequencies. C_P tends to C_∞ at high freqencies and to (C_S+C_∞) at low frequencies. The relaxation time is given by $\tau_D = 1/\omega_D$, where $C_P(\omega_D) = (C_S+C_\infty)/2$.

Various kinds of plots may be used in the analysis of measurements of such a dispersion. The best known is the 'Cole-Cole' plot, where G/ω is plotted against C_P (equivalent to ε'' against ε'). This gives a semicircle, intersecting the C_P-axis at C_∞ and C_S+C_∞. Any departure from the theoretical form of the dispersion causes distortion or displacement of the semicircle, but these changes are difficult to interpret quantitatively. However, von Hippel, Knoll and Westphal (1971) have devised two alternatives. Plots of ε'' against $\omega(\varepsilon'-\varepsilon_\infty)$ (G/ω against $\omega(C_P-C_\infty)$), and of ε''/ω against ε' (G/ω^2 against C_P) should give straight lines of gradient τ_D.

When the static conductance is included in the model, the

FIGURE 5.5

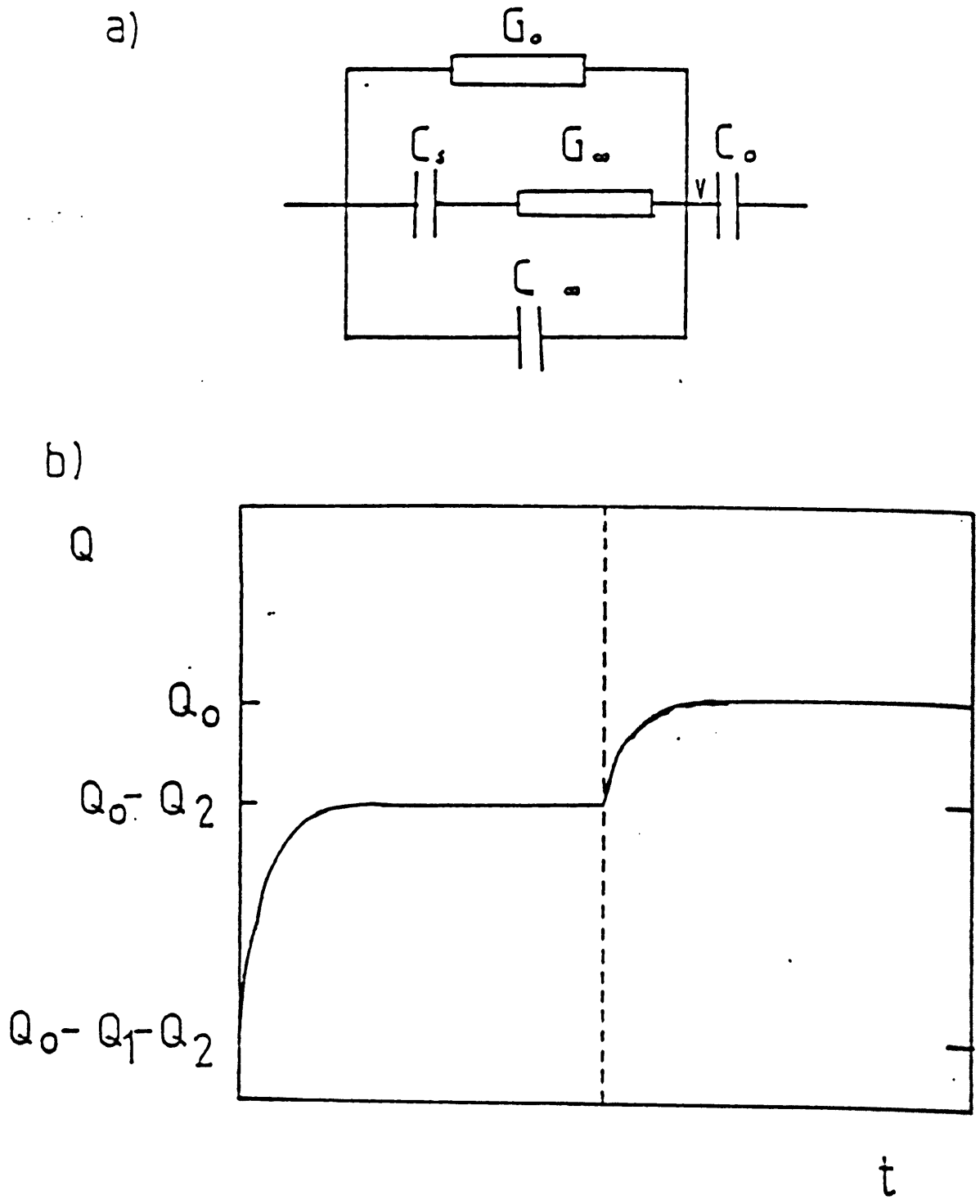

a) Equivalent circuit for ice with a blocking capacitor
b) Response of this circuit to a d.c. step voltage

equivalent circuit is as shown in figure 5.4. The complex capacitance is then modified by the addition of a term G_o/ω to C''. G then tends to (G_o+G_∞) in the high frequency limit and to G_o in the low frequency limit. The crossover condition is represented in the equivalent circuit by putting $C_s=0$, $G_\infty=0$.

In the present work, a blocking electrode - an insulating layer or separate capacitor in series with the ice - has been used. The appropriate equivalent circuit is shown in figure 5.5 (a). The blocking electrode is represented by the capacitor C_o. The response to a sinusoidal applied voltage is modified by an apparent extra relaxation at low frequencies, and there is a shift in the apparent value of the Debye relaxation time. If the response in the absence of the blocking capacitor is described by G and C_p, the full expressions for the measured values G_m and C_{pm} are

$$G_m = \frac{\omega^2 C_o^2 G}{G^2+\omega^2(C_o+C_p)^2} \qquad (5.15) \text{ and}$$

$$C_{pm} = \frac{C_o G^2+\omega^2 C_o C_p (C_o+C_p)}{G^2+\omega^2(C_o+C_p)^2}. \qquad (5.16)$$

If C_o is known, the values of C_{pm} and G_m obtained from bridge measurements can be corrected for the presence of the blocking capacitance by the relations

$$G = \frac{\omega^2 C_o^2 G_m}{G_m^2+\omega^2(C_o-C_{pm})^2} \qquad (5.17) \text{ and}$$

$$C_p = \frac{C_o(\omega^2 C_{pm}(C_o-C_{pm})-G_m^2)}{G_m^2+\omega^2(C_o-C_{pm})^2}. \qquad (5.18)$$

The response of the circuit in figure 5.5 (a) to a step voltage can

be calculated by the use of Laplace transforms. The detailed treatment is given in the Appendix. The voltage at the point V varies with time as

$$V = V_1 \exp(-t/\tau_1) + V_2 \exp(-t/\tau_2). \quad (5.19)$$

The voltage, V_0-V, across the capacitor C_0, is proportional to the charge on the capacitor. This is equal to the integral with respect to time of the current flowing in the network, so that the input of an integrating amplifier between the point O and ground varies as

$$Q = Q_0 - Q_1 \exp(-t/\tau_1) - Q_2 \exp(-t/\tau_2), \quad (5.20)$$

where $Q_0 = C_0 V_0$. This variation is shown in figure 5.5(b), where $\tau_1 \ll \tau_2$, and the scale of the abcissa changes at the point marked. In this case, the three levels indicated on the figure bear the following approximate relations to the circuit parameters:

$$Q_0 \approx C_0 V_0; \quad (5.21)$$

$$Q_0 - Q_2 \approx \frac{C_0 V_0 (C_S + C_\infty)}{C_0 + C_S + C_\infty}; \quad (5.22)$$

$$Q_0 - Q_1 - Q_2 \approx \frac{C_0 V_0 C_\infty}{C_0 + C_\infty}. \quad (5.23)$$

The two time constants are given by

$$\tau_1 \approx \frac{(C_0 + C_\infty)\tau_D}{C_0 + C_\infty + C_S} \quad (5.24)$$

and

$$\tau_2 \approx (C_0 + C_\infty + C_S)/G_0. \quad (5.25)$$

From these approximate relations, or, in the case where the two time constants are not very different, from the exact relations given in the Appendix, the values of C_0, C_∞, C_S, G_∞ and G_0 may be calculated. These capacitances and conductances are related to the corresponding dielectric constants and conductivities of the ice

FIGURE 5.6

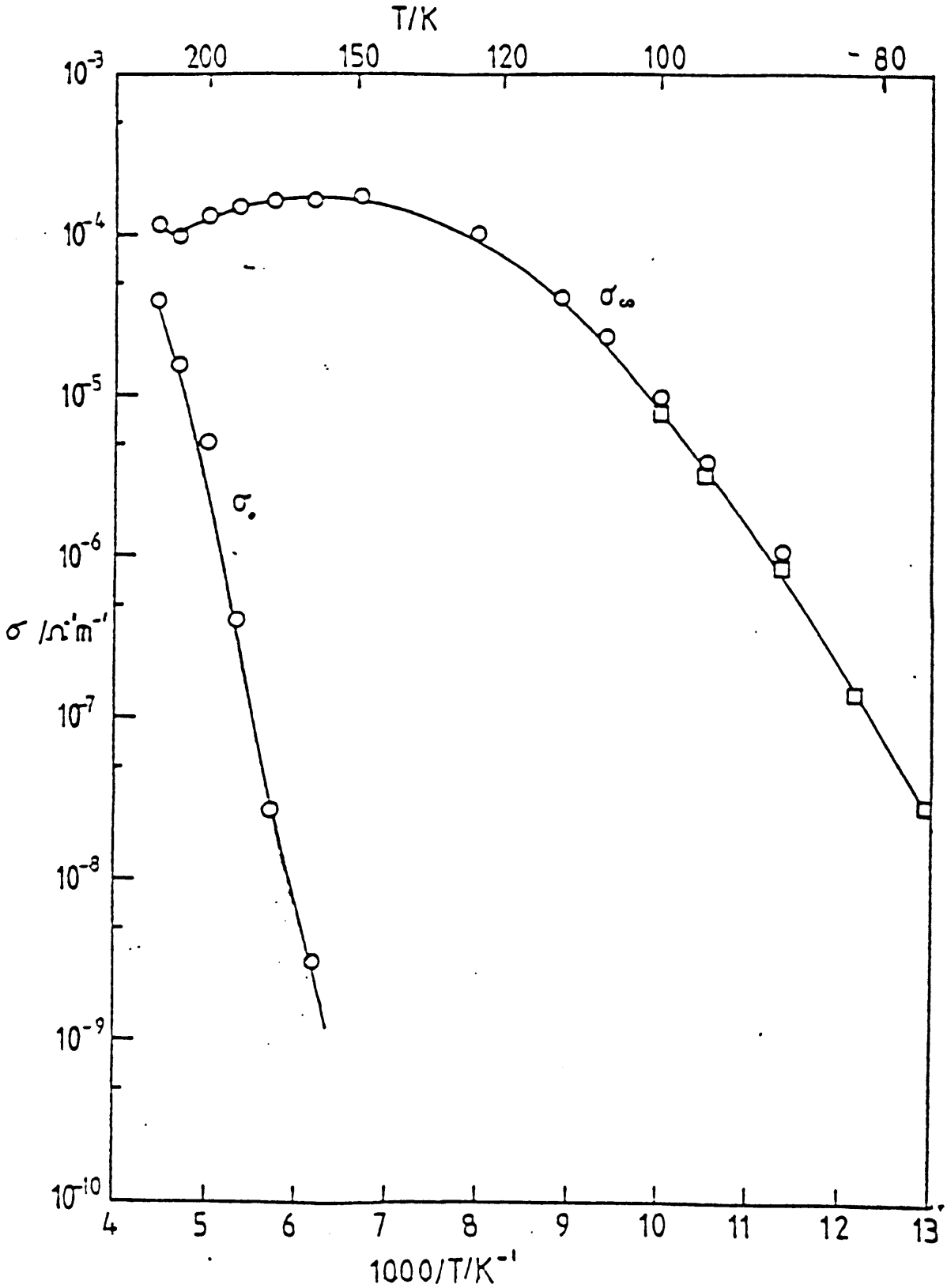

Variation of conductivity with temperature for sample KP1

○ Bridge measurements

□ Pulse method measurements

Following page 78

FIGURE 5.7

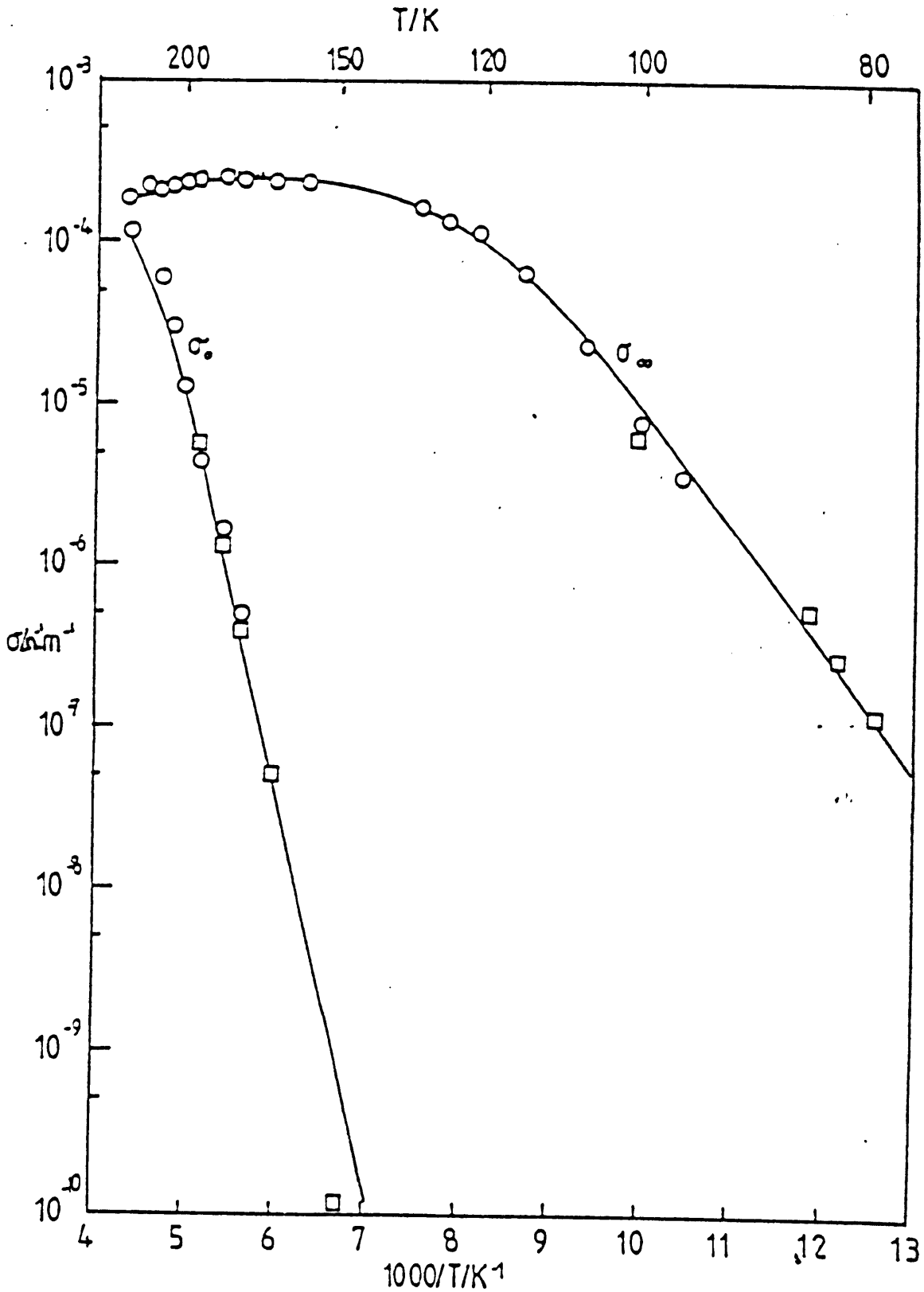

Variation of conductivity with temperature for sample KP10

○ Bridge measurements

□ Pulse method measurements

Following page 76

FIGURE 5.8

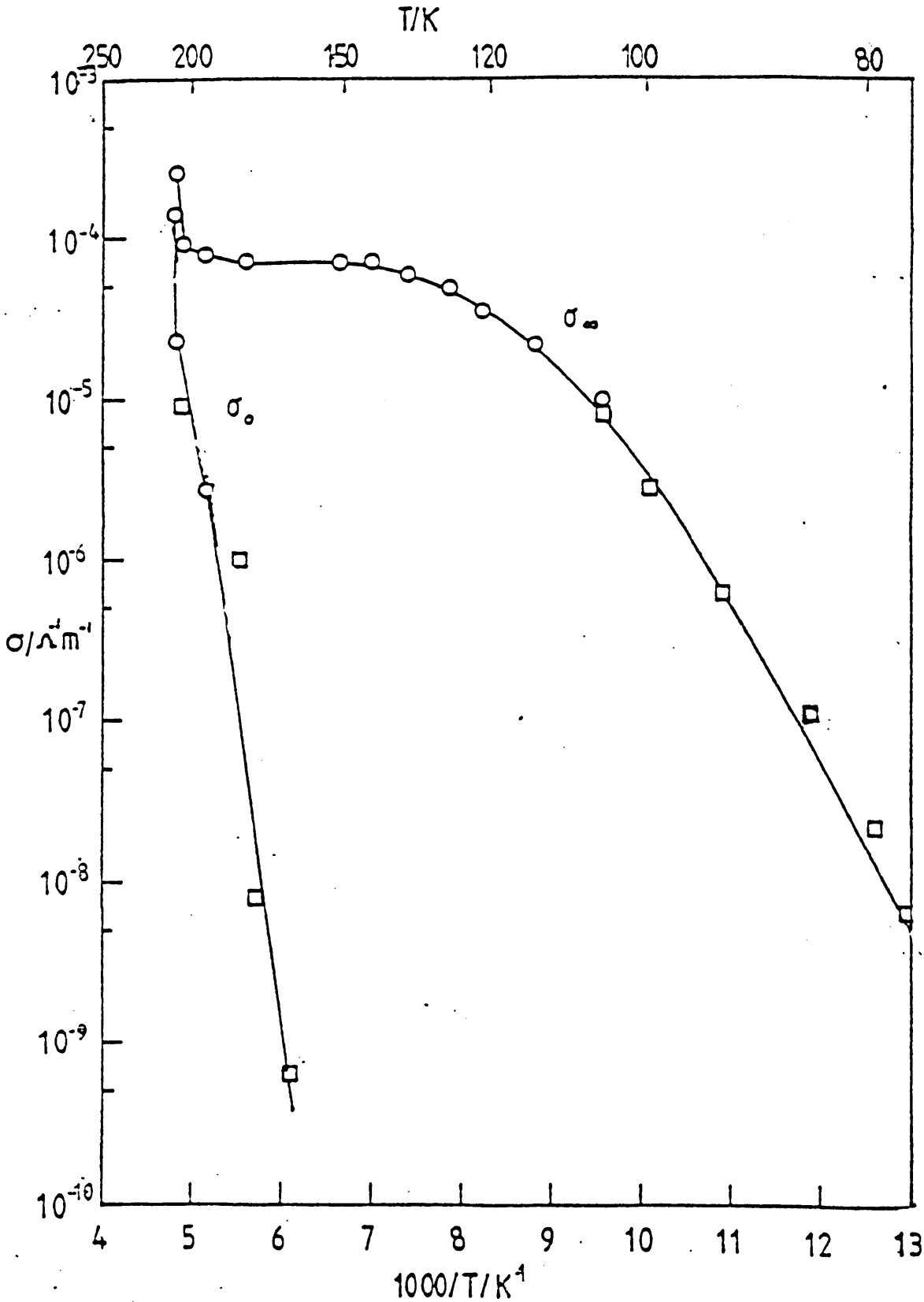

Variation of conductivity with temperature for sample KP12
O Bridge measurements
□ Pulse method measurements

Following page 76

by relations of the form $C = \varepsilon_0 \varepsilon A/L$ and $G = \sigma A/L$, where ε_0 is the permittivity of free space, A is the area of the sample and L is its thickness. Since the high-frequency dielectric constant ε_∞ is essentially constant and known, the value of the factor A/L can be found. In practice, the measured C_∞ often includes a contribution from the 'stray' capacitance of the external circuit. This may be determined by measuring the capacitance of the empty sample cell and finding the difference between the measured value and that calculated from the known geometry.

5.4 Results from measurements above the transition temperature

In three experiments, the electrical properties of KOH-doped polycrystalline samples were studied in detail at temperatures between the melting point and the ordering transition temperature. The aim of these experiments was to determine the mechanism which allows the movement of protons in ice doped with alkali hydroxides at temperatures where in pure ice, or in ice with other types of dopant, the relaxation time is extremely long. No work on the dielectric properties of KOH-doped ice in this temperature range has yet been published: the work of Kawada and co-workers covers only the range below 100 K. Capacitance bridge measurements were extensively used in these experiments, as over much of the temperature range the relaxation times were too short for accurate determination by the pulse method.

5.4.1 General features

Plots of the variation of conductivity with temperature for each of

FIGURE 5.9

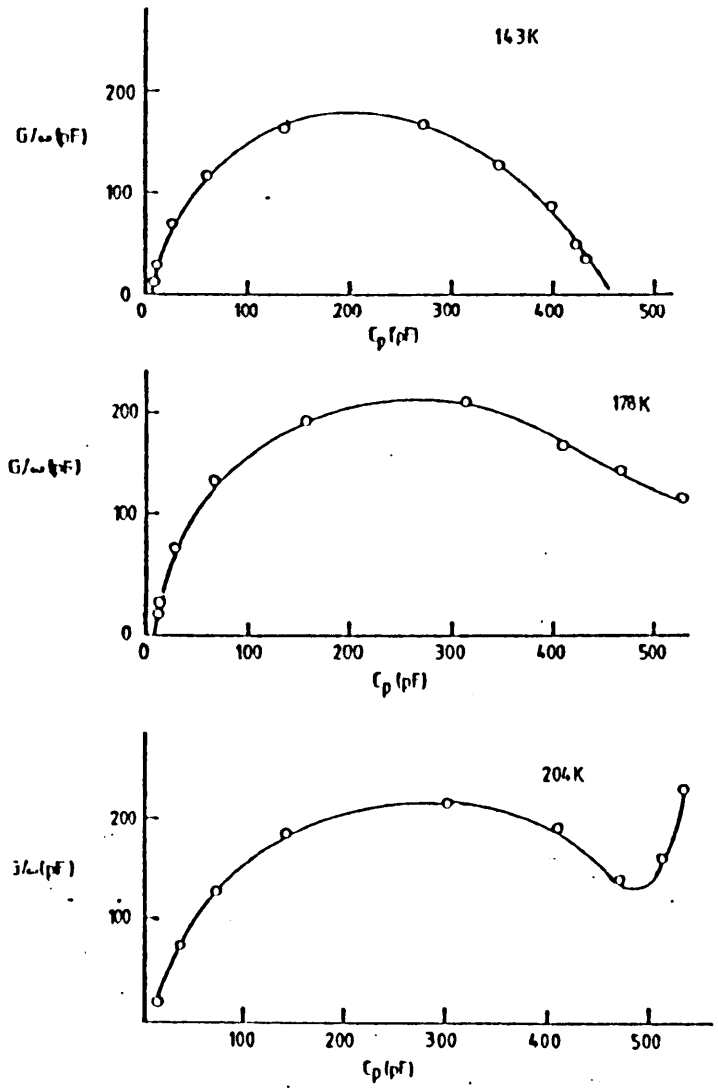

Selected Cole-Cole plots for sample KP12

FIGURE 5.10

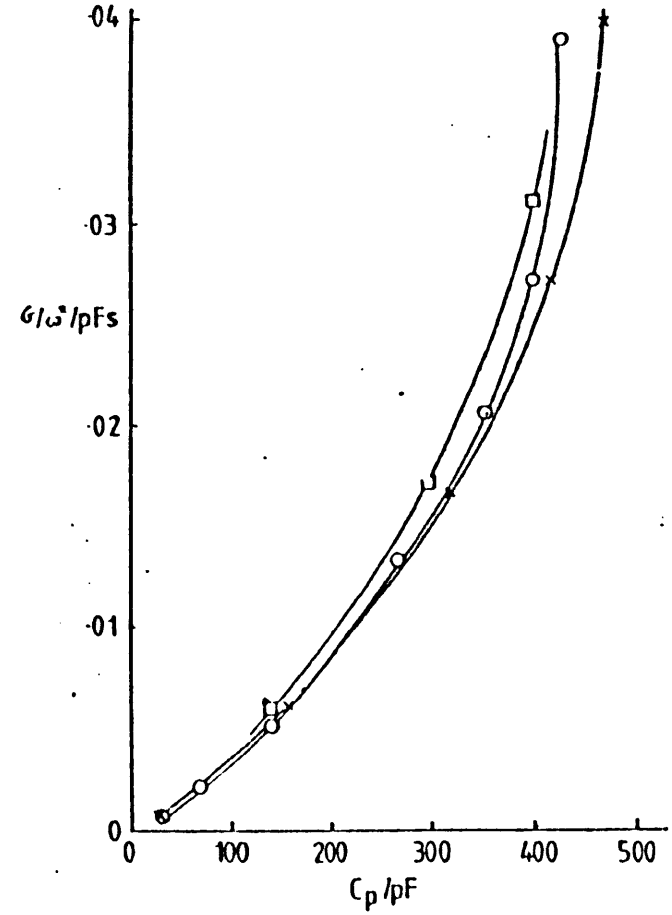

Plots of G/ω^2 against C_P for sample KP12
O 143 K
× 178 K
□ 204 K

Facing Page 78

the three samples, designated KP1, KP10 and KP12, are shown in figures 5.6, 5.7 and 5.8. Certain general features are common to all three sets of measurements. These features were also observed during cooling, but not accurately measured, for all other specimens in which the transition was obtained. The temperature range can be divided into three main regions. In the first region, between the melting point and about 210 K, the ice does not exhibit well-defined relaxation times within the frequency range of the bridge, and it is difficult reliably to establish the high-frequency and static conductivities. Below 200 K, the static conductivity of the sample falls steeply. The high-frequency conductivity σ_∞, however, remains constant or rises slightly as the temperature falls to about 120 K. In the third region, between 70-120 K, the d.c. conductivity has become undetectable, while σ_∞ now falls with decreasing temperature.

Detailed examination of the bridge measurements shows that the ice does not exhibit a simple Debye dispersion even in the region where only the high-frequency response is measurable. The Cole-Cole plots shown in figure 5.9 are flattened in shape, suggesting that there is a spread of relaxation times. Figure 5.10 shows the corresponding plots of G/ω^2 against C_P, which would be straight lines if the Debye relations were obeyed. The curvature of the lines again suggests that a distribution of relaxation times is present.

5.4.2 Behaviour above 220 K

In the higher-temperature region, σ_0 and σ_∞ appear nearly equal, and both fall steeply with decreasing temperature. The simple model

FIGURE 5.11

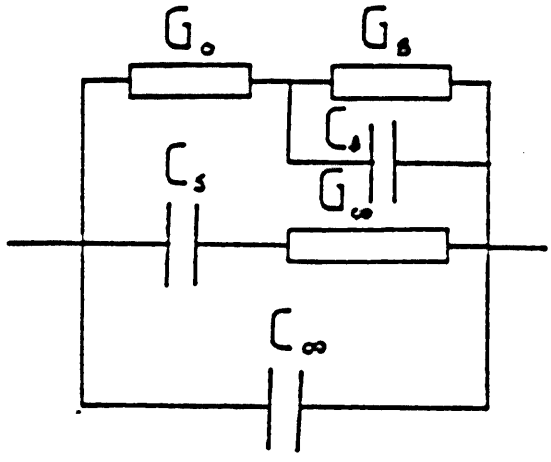

Equivalent circuit for inhomogeneous ice sample

requires that the capacitance (C_P from the bridge measurements) should be independent of frequency and equal to C_∞ when the crossover condition is fulfilled. This was not found to be the case: instead, the capacitance increases steeply with decreasing frequency. While it must be remembered that the corrected values, where $C_{Pm} \approx C_o$, are very sensitive to the value chosen for C_o, the effect cannot be explained away in this manner. If simulated data calculated for a two-relaxation model with a known C_o are 'corrected' assuming a value C_o' for the blocking capacitance, the apparent value of C_P tends to $+\infty$ at low frequencies for $C_o' > C_o$ and to $-\infty$ for $C_o' < C_o$, but does not go through a maximum in either case. The measured data, however, exhibit a maximum in C_P if the value of C_o is deliberately chosen to be too low. It therefore appears that the simple two-relaxation model discussed in section 5.3 is not adequate to describe the experimental results. A model with an equivalent circuit as shown in figure 5.11 has been developed. The extra components, G_B and C_B, may represent a layer in the ice with a lower conductivity than the main sample, either because the dopant is less concentrated or because of the build-up of a carrier-depleted region near the electrode. The complex capacitance of such a circuit in the absence of C_o is given by

$$C' = \frac{C_S}{1+\omega^2\tau_D^2} + \frac{G_o^2 C_B/(G_o+G_B)^2}{1+\omega^2\tau_B^2} \qquad (5.26)$$

$$C'' = \frac{\omega^2\tau^2 G_\infty}{1+\omega^2\tau_D^2} + \frac{G_o G_B/(G_o+G_B) + G_o\omega^2\tau_B^2}{1+\omega^2\tau_B^2}, \qquad (5.27)$$

where $\tau_B = C_B/(G_o+G_B)$.

FIGURE 5.12

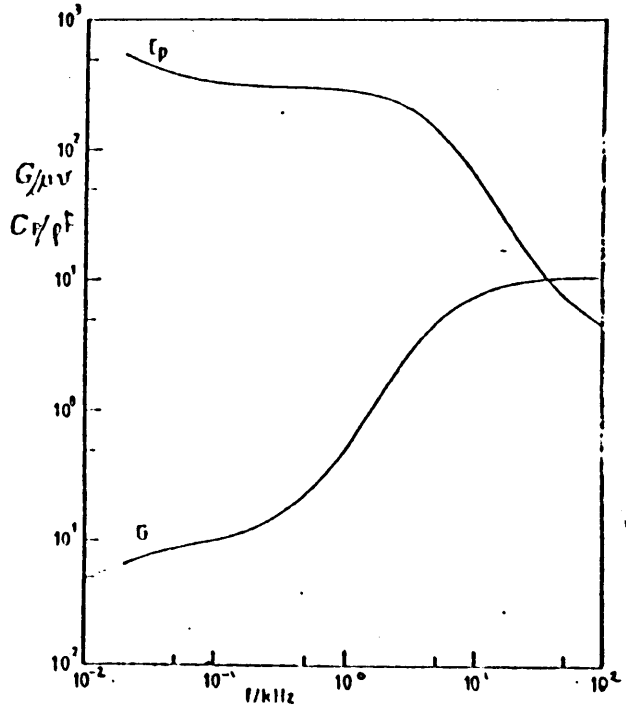

Plots of effective conductance G and capacitance C_F as a function of frequency, calculated for the circuit of figure 5.11 with C_ω=4 pF, C_S=300 pF, C_B=1000 pF, G_o=0.1 μmho, G_ω=10 μmho, G_B=0.05 μmho

FIGURE 5.13

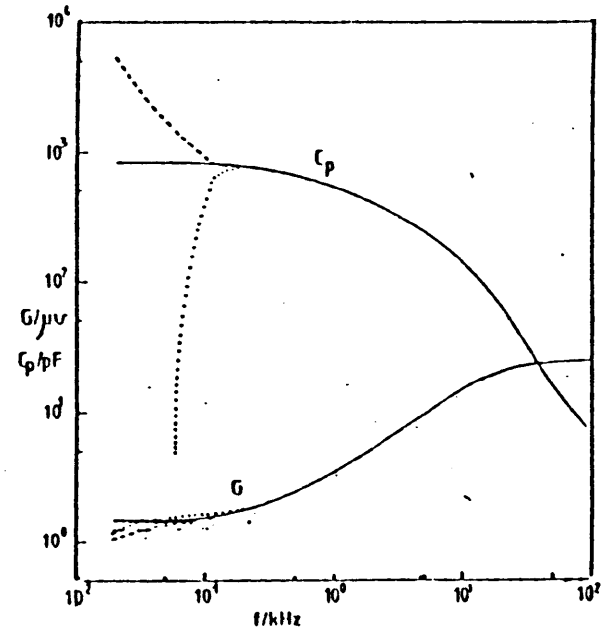

Simulated bridge data for the circuit of figure 5.11 with C_ω=4 pF, C_S=300 pF, C_B=1000 pF, G_o=5 μmho, G_ω=20 μmho, G_B=2 μmho, calculated using C_o = 100 pF, then corrected using C_o=C_o' solid line C_o' = 100 pF dashed line C_o' = 100.5 pF dotted line C_o' = 99.5 pF

Facing Page 80

This response is sketched in figure 5.12 for the case where $\tau_B \simeq 10\tau_D$. Even when the crossover condition is fulfilled, a relaxation is present. The effect of errors in C_o on values obtained from re-converting calculated data are shown in figure 5.13: under appropriate conditions a maximum in C_P can be observed. It seems that such a model might be used in the analysis of the experimental data. However, because of the large errors in the perceived values of C_P which arise from small inaccuracies in the measurement of C_o or C_{Pm}, it has been decided that it is not possible to obtain useful quantitative information when $C_o \approx C_{Pm}$. In practice, this means that no reliable conclusions can be drawn about the behaviour of the samples above about 220 K.

The behaviour of polycrystalline doped samples above about 200 K is complicated by the presence of the concentrated liquid solution which crystallises only at the eutectic transition temperature. In sample KP12, a drift in the dielectric response, fast enough to make accurate bridge measurements impossible, was observed over a period of about 1 hour when the sample was cooled to 205 K. The two sets of plots of the bridge data (figure 5.14), measured before and after this change but at very close temperatures, show the significant change which took place and which was attributed to the eutectic freezing. This sample had an initial KOH concentration of 0.08 M, the highest of the three samples studied, and it appears that much of the KOH was rejected from the ice. Similar effects were observed in some other samples, which were not studied in detail in the higher temperature regions. In samples KP1 and KP10 there is no detectable anomaly at the eutectic transition

FIGURE 5.14

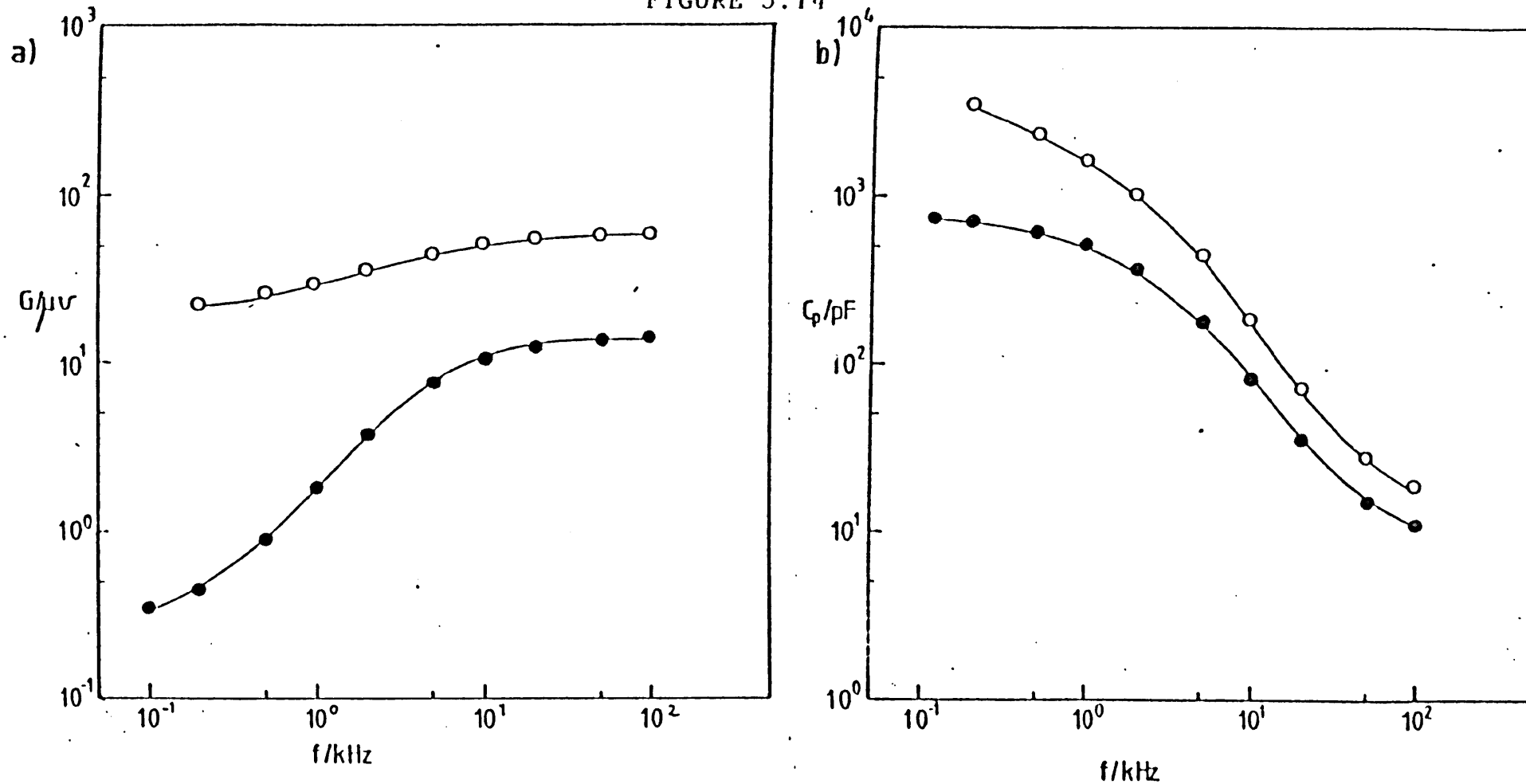

Changes in the corrected bridge data for sample KP12 on freezing of the eutectic solution

● 206 K

O 207 K

a) G as a function of frequency

b) C_P as a function of frequency

Facing Page 91

temperature.

5.4.3 Behaviour in the 70-220 K temperature range

In the second region, where both G_o and G_∞ can be measured, the relations 5.4 and 5.7 can be used to obtain the ionic and Bjerrum-defect contributions to the conductivity, $\sigma_\pm$ and σ_{DL}. Calculations of this kind were performed for samples KP1 and KP10. The values of the defect charges, $e_\pm = 0.626e$ and $e_{DL} = 0.374e$, have been taken from the work of Takei and Maeno (1987). Similar values, $e_\pm = 0.62e$ and $e_{DL} = 0.38e$, are given by Hubmann (1979). Plots of the conductivities as a function of temperature in this region for the two samples are shown in figure 5.15. In each case, the ionic conductivity is almost independent of temperature while the Bjerrum-defect contribution obeys a relation of the form $\sigma \propto \exp(-E/k_B T)$. The values obtained for E from the two sets of data are 0.30±.01 eV for KP1 and 0.40±.01 eV for KP10. As σ_o vanishes, at low temperatures $\sigma_\pm$ is equal to σ_∞.

From the values obtained for σ_∞ in the 'plateau' region, one can attempt to estimate the mobility of the charge carriers using the relation $\sigma_\pm = n_\pm e_\pm \mu_\pm$. For specimen KP1, the concentration of the original solution was approximately (0.015±0.002) M, or approximately $(9\pm1)\times10^{24}$ molecules per m^3. If it is assumed that the KOH was completely incorporated and completely dissociated, this value can be taken as the density of OH^- ions. Using $e_\pm = 0.63e$, and $\sigma_\pm = (1.5\pm0.1)\times10^{-4}\ \Omega^{-1}\ m^{-1}$, the mobility is approximately $(1.7\pm0.3)\times10^{-10}\ m^2\ V^{-1}\ s^{-1}$. A similar value, $(1.0\pm0.1)\times10^{-10}\ m^2\ V^{-1}\ s^{-1}$, is obtained using the concentration,

FIGURE 5.15

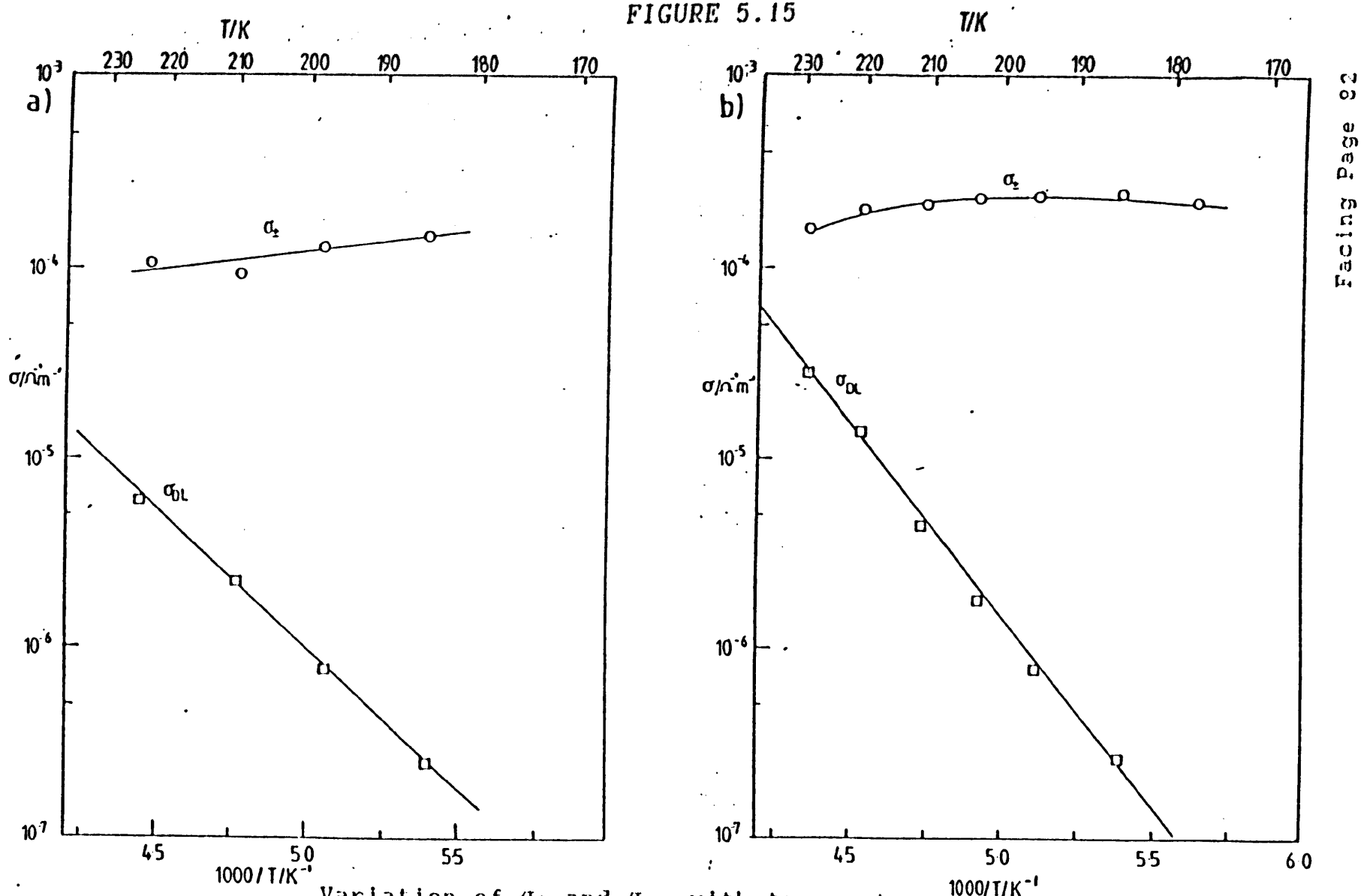

Variation of $\sigma_{\perp}$ and σ_{DL} with temperature
a) sample KP1
b) sample KP10

Facing Page 92

(0.032+0.001) M, and plateau conductivity, $\sigma_{\pm} \simeq (2.0 \pm 0.1) \times 10^{-4}$ Ω^{-1} m^{-1}, for specimen KP10. It therefore appears that in these two specimens the concentration of KOH is not saturated. In specimen KP12, however, the concentration of the original solution was (0.083±0.002) M, or about $(5.0 \pm 0.1) \times 10^{25}$ molecules per cubic metre, and the plateau conductivity is about $(7.0 \pm 0.5) \times 10^{-5}$ Ω^{-1} m^{-1}. Using the value of the mobility obtained from the sample KP1, the effective ionic concentration would be approximately $(4.1 \pm 0.8) \times 10^{24}$ ions per cubic metre. It seems that only about (8±1)% of the KOH in the original solution was incorporated in the ice, while the rest formed a concentrated solution. This conclusion is consistent with the observation of the anomaly at the eutectic transition temperature, described above. It is possible that not all the KOH in samples KP1 and KP10 was incorporated in the ice, in which case the actual value of the mobility would be higher than that given. However, as neither these samples, nor the samples of similar concentration studied by Tajima et al. (1984), show any evidence of a eutectic anomaly, the assumption of complete incorporation seems reasonable. The fact that the conductivity is independent of temperature over a wide range suggests that in this range all the defects are free to move. The mobility of the H_3O^+ ion, which is believed to be the main ionic carrier in pure ice, is still somewhat uncertain. Petrenko, Whitworth and Glen (1983) give a lower limit of approximately 10^{-9} m^2 V^{-1} s^{-1} at -20°C, but Zaretskii, Petrenko, Rhyzhkin and Trukhanov (1987) give a value of approximately 3×10^{-6} m^2 V^{-1} s^{-1}. The measurement of the mobility in this case is complicated by the need to allow for trapping of some of the defects.

FIGURE 5.16

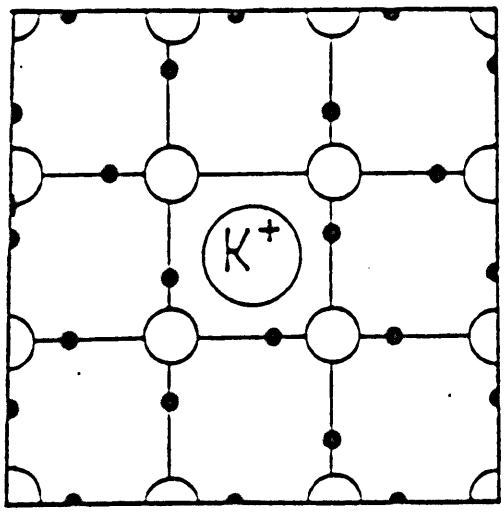

Schematic representation of KOH incorporated in the ice lattice as a K^+ ion, an OH^- ion and an L-defect

In the third temperature region, below about 130 K, the conductivity of the ice begins to fall with decreasing temperature. Between 70 K and about 110 K, it follows an Arrhenius law, with an activation energy of (0.17±0.02) eV.

5.4.4 A suggested model for the dielectric properties of KOH-doped ice above 72 K

The model which is proposed to account for the general form of the conductivity-temperature plots is as follows. The K^+ ion is believed to be incorporated interstitially in the ice lattice, while the OH^- ion occupies an H_2O site. As shown schematically in figure 5.16, this introduces an L-defect and an OH^- defect, which may move independently. The L-defect may be the majority carrier at high temperatures, but becomes the minority carrier below about 220 K. The crossover cannot be reliably measured because of the very high relaxation frequencies in the higher-temperature region. Below 220 K, the OH^- is the majority carrier. It moves by quantum tunnelling: in the plateau region it is completely dissociated, but as the temperature falls below 120 K the ions are held in shallow traps with an activation energy for escape of about 0.17 eV. It is tempting to believe that the L-defects and the OH^- ions are both trapped by the K^+ ion, but there is no direct evidence for this. The feature of the alkali hydroxide doping which makes the ordering transition possible appears then to be the presence of the shallowly trapped OH^- ions, which are not introduced by any other dopant so far studied. Although their mobility is lower than that of the H_3O^+ ions, they are present in sufficient numbers to allow

changes in the proton configuration to take place in a finite time even at 60 K.

The polydispersive form of the dielectric relaxation, which was also observed by Kawada and Dohata (1985), may be due to inhomogeneities in the concentration of dopant in the crystal.

5.5 Results from measurements around the transition temperature

The dielectric properties of KOH-doped ice below, at, and immediately above the transition temperature have been studied in some detail using the pulse method. The general features of the results obtained are as follows.

5.5.1 General features

As the sample is cooled towards the transition temperature, the relaxation time lengthens, obeying a relation of the form $\tau = \tau_0 \exp(E/k_B T)$, where $E \simeq 0.17$ eV. Typically the relaxation time is of the order of 10^{-2} s at 80 K and increases to about 10^{-1} s at 72 K. On cooling slowly below 72 K, this trend continues and the dielectric constant remains at its high-temperature level until the temperature reaches about 65 K. Once the temperature falls below about 65 K, the properties begin to change with time: the relaxation time increases and the static dielectric constant decreases. The sample can then be 'annealed' for many hours, or even several days, as this change continues. When the sample is heated after a period of annealing, the static permittivity increases and the time constant decreases with temperature, even

below the transition temperature. However, when the transition is reached, both quantities show discontinuous jumps.

There are some problems in the interpretation of the data from the pulse experiment when the relaxation time is long compared with the longest possible time over which a measurement can be taken. An attempt to extrapolate an exponential decay to an unknown baseline may result in underestimation both of the amplitude of the relaxation and of its time constant. When the relaxation is compound, the problem is more severe as the slowest part of a distribution of time constants may be ignored altogether. However, the conductance, calculated from the ratio of capacitance to time constant, should always be obtainable. It was found that, where the data from a pulse experiment could be fitted to two or three exponential decays with time constants differing by a factor of ten or less, the mean of the time constants weighted by their associated relaxation strengths was roughly equal to the time constant found by fitting a single exponential term to the same data. In order to save computing time, the latter method was usually adopted even though the single-exponential expression gave a poor fit to the data.

It was noticeable that the response of the ice to a step voltage could usually be quite well described by a single relaxation time when the sample was well above or well below the transition temperature. Very close to the transition, however, the relaxation was definitely spread. This effect may be due to the greater inhomogeneity of a sample in the process of transforming back to the

Table 5.1

Dielectric properties of poycrystalline ice samples immediately above the transition temperature

	Concentration/ M	τ_D/s	ε_s	v
KP1	$(1.5\pm0.1)\times10^{-2}$	1±0.2	400±50	0.91±0.04
KP3	$(1.5\pm0.1)\times10^{-2}$	1±0.2	210±30	0.69±0.03
KP4	$(1.3\pm0.1)\times10^{-2}$	0.2±0.04	400±70	0.90±0.05
KP5	$(1.1\pm0.1)\times10^{-1}$	0.07±0.01	340±40	0.85±0.03
KP6	$(2.3\pm0.1)\times10^{-3}$	0.7±0.1	55±5	0.36±0.01
KP7	$(6.2\pm0.1)\times10^{-3}$	0.1±0.02	230±30	0.72±0.03
KP10	$(3.22\pm0.07)\times10^{-2}$	0.1±0.02	300±25	0.81±0.02
KP12	$(8.26\pm0.18)\times10^{-2}$	0.3±0.05	310±20	0.82±0.02
KP13	$(2.86\pm0.02)\times10^{-2}$	0.3±0.05	230±20	0.72±0.02
KP14	$(1.06\pm0.01)\times10^{-2}$	0.5±0.1	130±10	0.56±0.02

disordered phase.

5.5.2 Behaviour immediately above the transition temperature

The value of the static dielectric constant immediately above the transition varies from sample to sample: in the best specimen it was about 400, in the worst about 50. It is assumed that this variation occurs because the sample consists of a mixture of doped regions, in which the relaxation time is short so that the full intrinsic relaxation strength of the ice is measureable, with 'pure' regions in which the time constant is long compared with the experimental timescale, so that the effective dielectric constant is equal to ε_∞. From the Curie and Curie-Weiss laws obtained by Kawada (1978) and Takei and Maeno (1987), the ideal value of ε_s for a polycrystalline sample at 72 K should be approximately 500. Using the expression of Looyenga, (equn. 3.4), for the effective dielectric constant of a mixture of two phases, the fraction v of effectively doped material in each specimen can be estimated. The results of this calculation are shown in table 5.1., together with the concentration of each sample and the time constant directly above the transition. There is no clear and consistent relationship between the concentration of the original sample and the properties immediately above the transition temperature. However, it appears that the saturation concentration is around 0.02 M: a concentration in the original solution much lower than this gives unsatisfactory results as in sample KP6, while a much higher concentration, as in sample KP5, gives little or no improvement.

In all samples in which the transition was observed, the relaxation

FIGURE 5.17

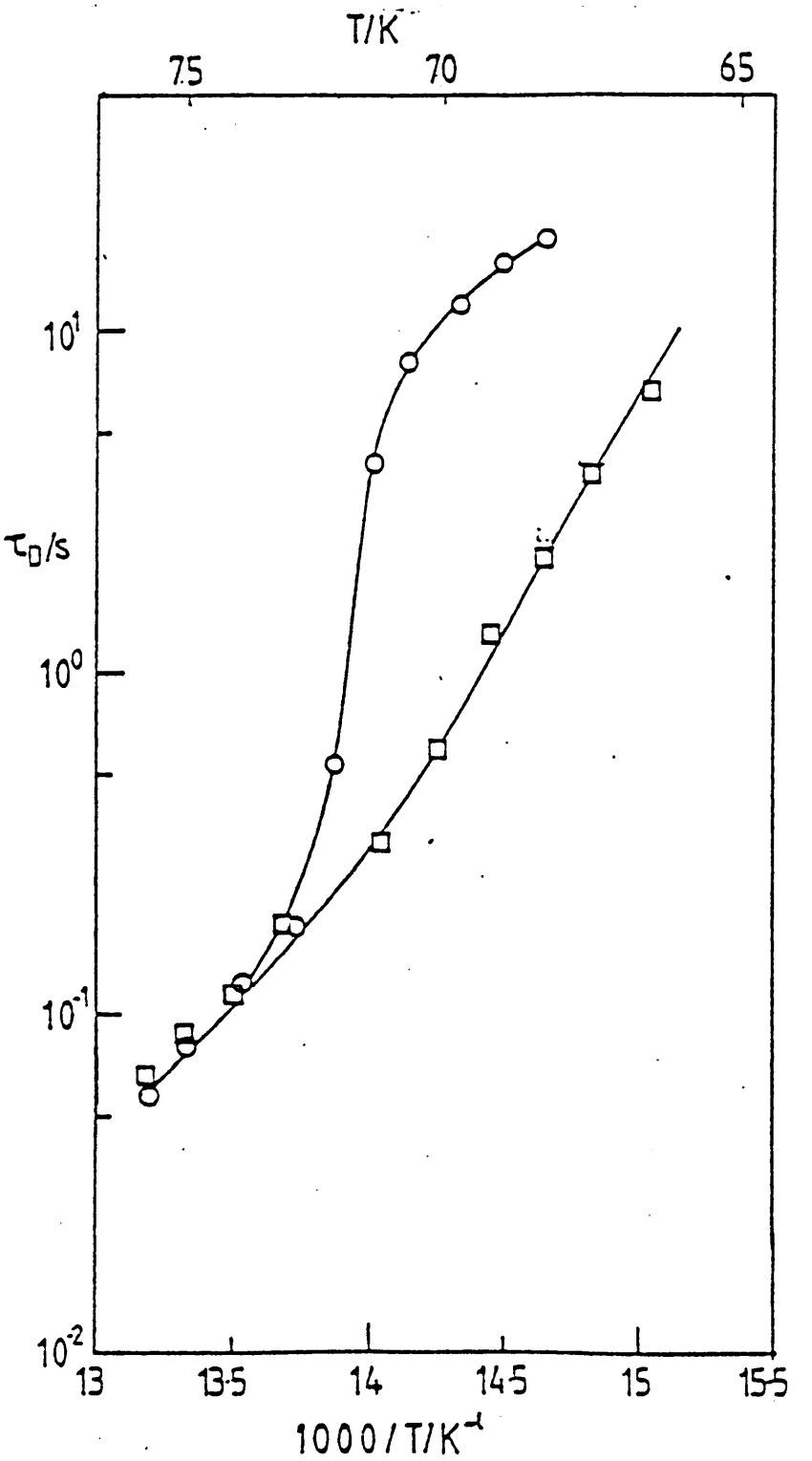

Variation of dielectric relaxation time with temperature for sample KP10 on heating
□ after annealing at 67 K
○ after annealing at 60 K

Facing Page 87

time above the transition temperature varies as $\exp(E/k_B T)$, with E being approximately (0.17±.02) eV. This activation energy is slightly higher than that (0.15 eV) reported by Kawada and co-workers. The value of τ_D at a given temperature above 72 K, in any given sample, was independent of whether the measurements were taken during heating or cooling and of the previous thermal history of the sample. The static permittivity was essentially independent of temperature, within the limits of accuracy of the method, over the range 72-80 K.

5.5.3 Behaviour on cooling and annealing below the transition temperature

When initially cooled below the transition temperature, the samples showed definite supercooling effects. One sample (KP10) was cooled to 66 K and left for 16 hours before heating through the transition temperature: no evidence of transformation was found. The variation of τ_D with temperature on heating in this case, and that for the same sample after being annealed overnight at about 58 K, are shown in figure 5.17.

Once the annealing process has been started by cooling the sample to a low enough temperature for the transformation to begin, it may be more effectively continued by heating again to within a few degrees of the transition temperature. This effect was first observed while measurements were being made on a sample as it was heated after a period of annealing at about 62 K. The relaxation time decreased, and the relaxation strength increased, on heating, but when the sample was left at the higher temperature for a few

FIGURE 5.18

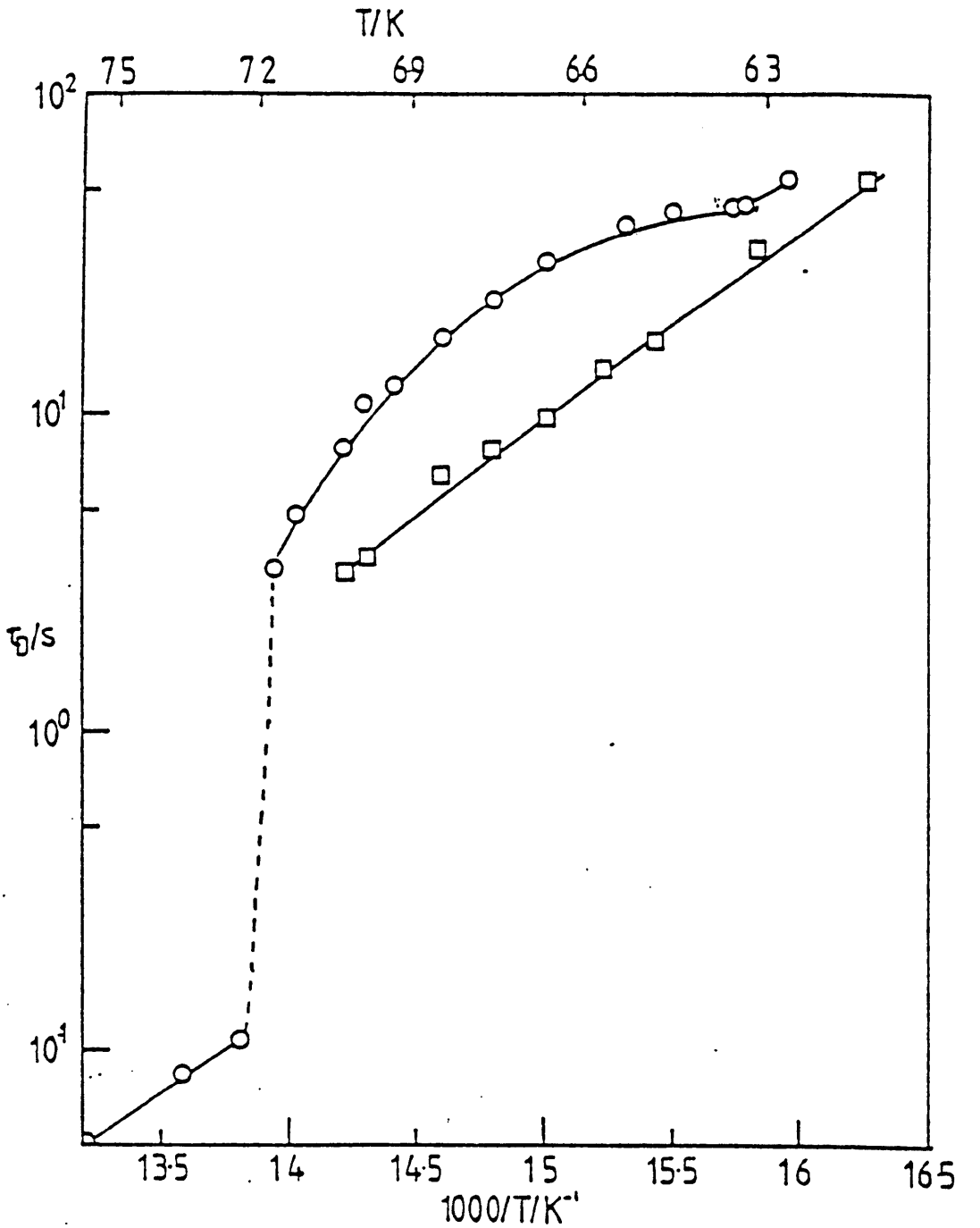

Variation of dielectric relaxation time with temperature on heating for sample KP7
□ after annealing at 60 K
○ after further annealing at 70 K

Facing Page 82

hours, these changes were partially reversed. If the sample was then rapidly cooled and then heated again, the time constant at any given temperature would remain longer, and the permittivity lower, than before the higher-temperature annealing. A good example of this effect was demonstrated in specimen KP7. The values of τ_D obtained during two heating sequences are shown in figure 5.18. The sample was first cooled to 60 K and annealed for 16 hours, then briefly cooled to 50 K and heated again. This thermal shock had no detectable effect on the properties at 60 K. The sample was then heated to 70 K and annealed for 18 hours, during which period the time constant was increased by a factor of three. Finally, after quenching rapidly to 63 K, the sample was heated through the transition temperature. The effect was confirmed in several experiments on different specimens.

The evolution of the electrical properties has been followed overnight, and on one occasion over three days, by taking measurements at regular intervals. The apparent relaxation time of the change becomes longer as the annealing proceeds. Typically, if the dielectric relaxation time is about 10 s, the characteristic time of the evolution is of the order of a few hours. In some cases, a stage is reached at which there is no further significant change in the properties between two measurements. Figures 5.19 (a) to (e) show the variation of conductivity σ_∞ with time for five annealing sequences on the same sample, KP13. In the first sequence (a) the sample was cooled to about 40 K before being annealed at 61 K. In the second experiment (b), the sample was cooled briefly to 60 K, then annealed at 63 K. In the third (c) it was again cooled

FIGURE 5.19

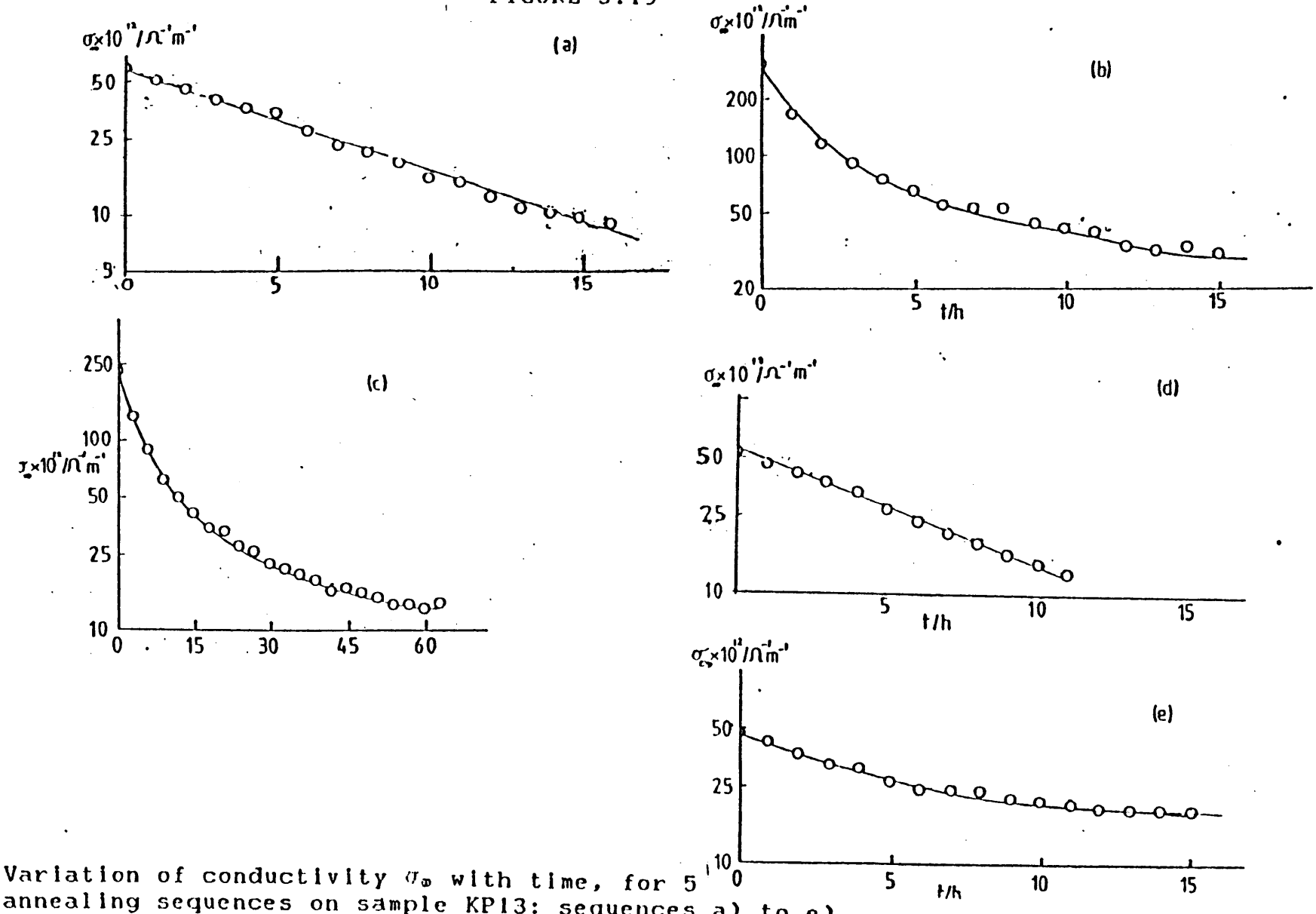

Variation of conductivity σ_∞ with time, for 5 annealing sequences on sample KP13: sequences a) to e) are described in the text of section 5.5.3

Facing Page 89

to about 40 K, then annealed for approximately 70 hours at 65 K. After each of the first two sequences the sample was heated to 120 K to clear any residual nuclei of order. After the third, however, it was heated only to about 80 K, then cooled to 61 K and annealed there for 16 hours to obtain a fourth sequence (d). The rate of change of the conductivity in this sequence is close to that in the first sequence, which suggests that there is no advantage in cooling the sample much below 60 K. The fifth sequence (e) was obtained immediately after the fourth, without first taking the sample through the disordering transition, by annealing at 67 K. Although the rate of change of conductivity in this fifth sequence is comparable to that in the early stages of the third sequence, it is much faster than that in the later stages. This shows the advantage of annealing at a higher temperature once the transformation has started.

5.5.4 Behaviour on heating

The behaviour of a sample as it is heated after annealing for some time below the transition temperature is difficult to interpret because two effects are present which operate in different directions. On heating, the time constant decreases as more defects become available for the relaxation mechanism, and the apparent static permittivity increases. However, as has been described above, unless the sample is already transformed as far as possible, the time constant at any given temperature will be increasing with time and the permittivity decreasing as further ordering proceeds. Because of the continuing transformation to the ordered phase, the activation energy of the relaxation time below the transition is

FIGURE 5.20

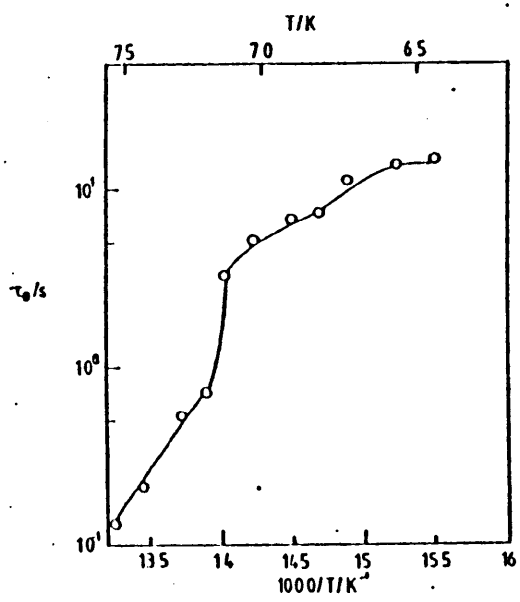

Variation of dielectric relaxation time with temperature for a badly transformed specimen (KP6)

FIGURE 5.21

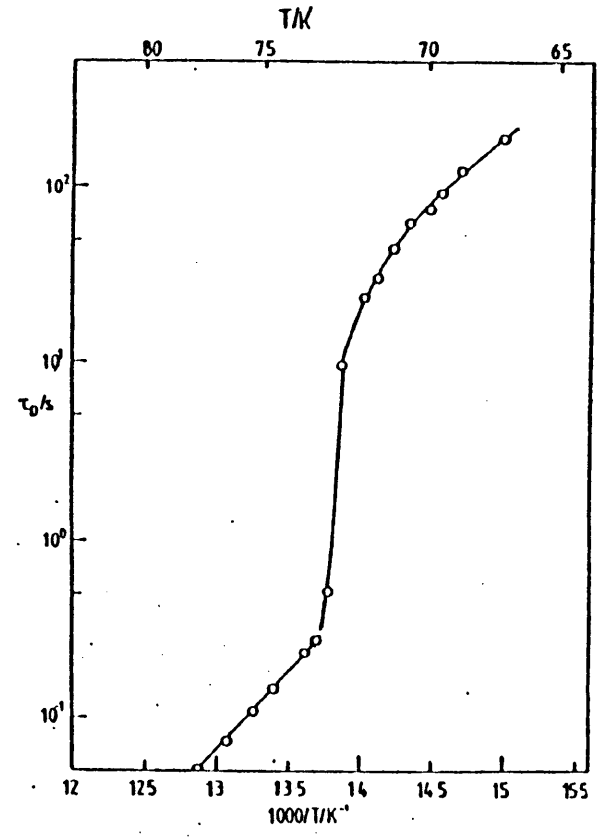

Variation of dielectric relaxation time with temperature for a well-transformed specimen (KP13)

difficult to determine: in a sample which is still transforming rapidly as it is heated, the apparent activation energy will be decreased because a measurement at a higher temperature is on a more ordered sample. An example of the variation of τ_D with temperature in a heating sequence of this kind is shown in figure 5.20. However, in well-transformed specimens the activation energy immediately below the transition appears to be higher than that immediately above. In some such samples an activation energy of about 0.25 eV has been found. An example of a transition of this type is shown in figure 5.21.

When the transformed specimen is heated through the transition temperature, the relaxation time and permittivity revert immediately to their values above the transition and before annealing, the change taking place over a temperature range of about 2 K. Usually the change is sharp, but in one or two cases the transition is not well defined. The ratio of the relaxation times above and below the transition varies with the history of the sample, from less than 10 for a weakly doped or poorly annealed sample to more than 200 for a strongly doped sample annealed for several days.

The dependence of the permittivity on temperature immediately below the transition also varied from sample to sample and between different annealing sequences on the same sample. Some typical examples of this dependence are shown in figure 5.22. If the transformation is assumed to take place in the regions of the sample where the doping is effective, the 'true' value of ε_s in these regions, immediately below the transition temperature, can be

FIGURE 5.22

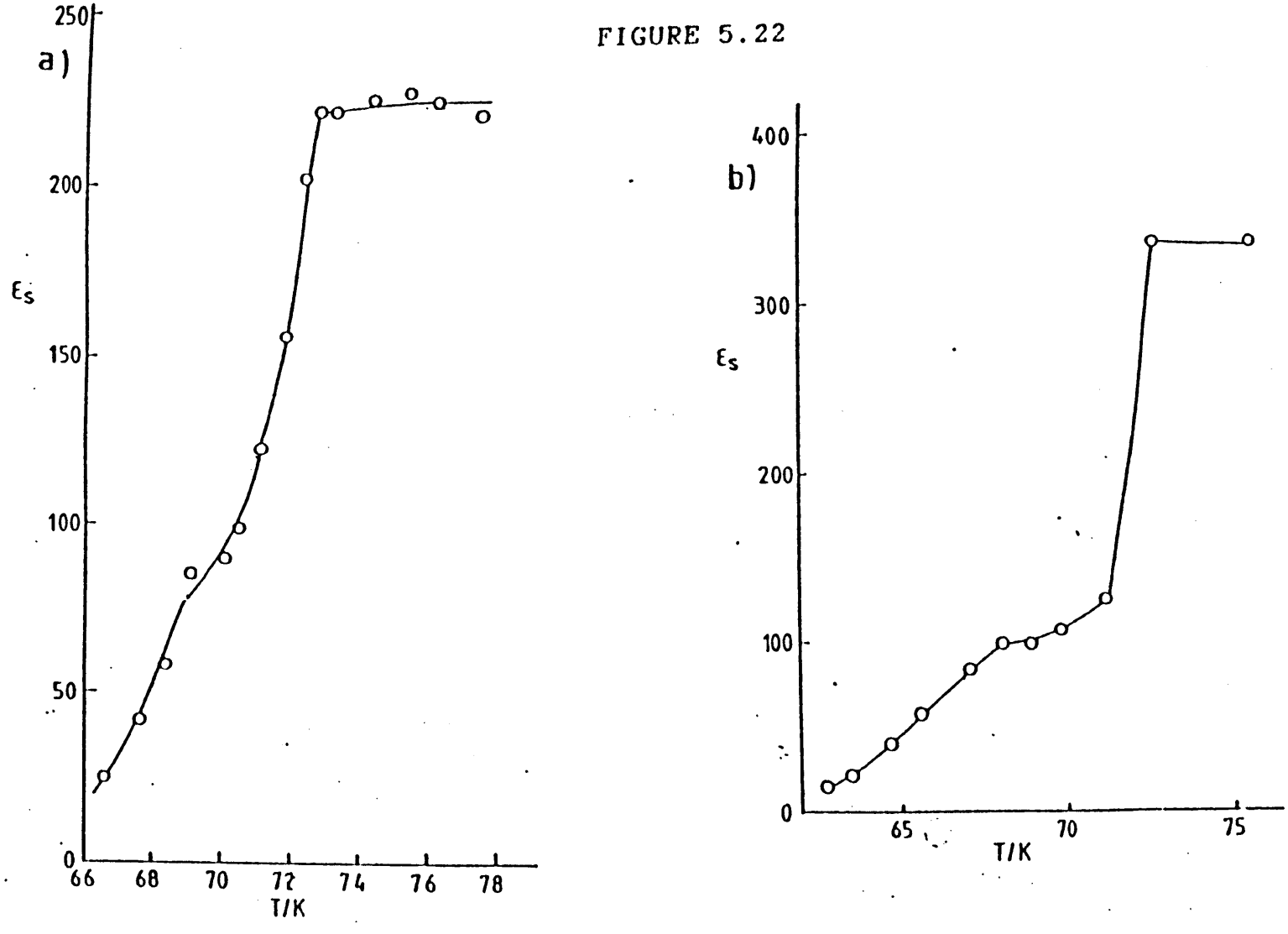

Variation of relaxation strength E_s with temperature on heating after annealing below the transition
a) sample KP13
b) sample KP5

Facing Page 91

calculated by using the values of v, the volume fraction of transformable ice, given in table 5.1. The results of such calculations are shown in table 5.2., together with the values deduced for the fraction w of transformable ice which was actually transformed.

An attempt was made to test the suggestion by Tajima et al. (1984) that nuclei of order might survive after the sample had been heated through the transition. A sample (KP14) which had undergone the transition once was then immediately cooled again from 73 K. The variation of τ_D with temperature on cooling is shown in figure 5.23. The figure also shows the variation of τ_D with temperature on cooling for the same sample when previously heated to 120 K, and a heating sequence after annealing at 58 K. There is no significant difference between the two cooling sequences.

5.5.5 Comment on the results

It appears from these studies of the effect of different annealing routines that the new phase must be nucleated by cooling below some critical level, about 65 K, but that the nuclei subsequently grow at a rate governed by the dielectric relaxation time and hence will grow faster at higher temperatures. This is consistent with the theory given in section 3.3, in which there is a nucleation barrier for the ordering transition which disappears at about 60 K.

The variation of permittivity with temperature shown in figure 5.22 bears little resemblance to the theoretical variation obtained in section 3.3.2. and shown in figure 3.11: instead of a

FIGURE 5.23

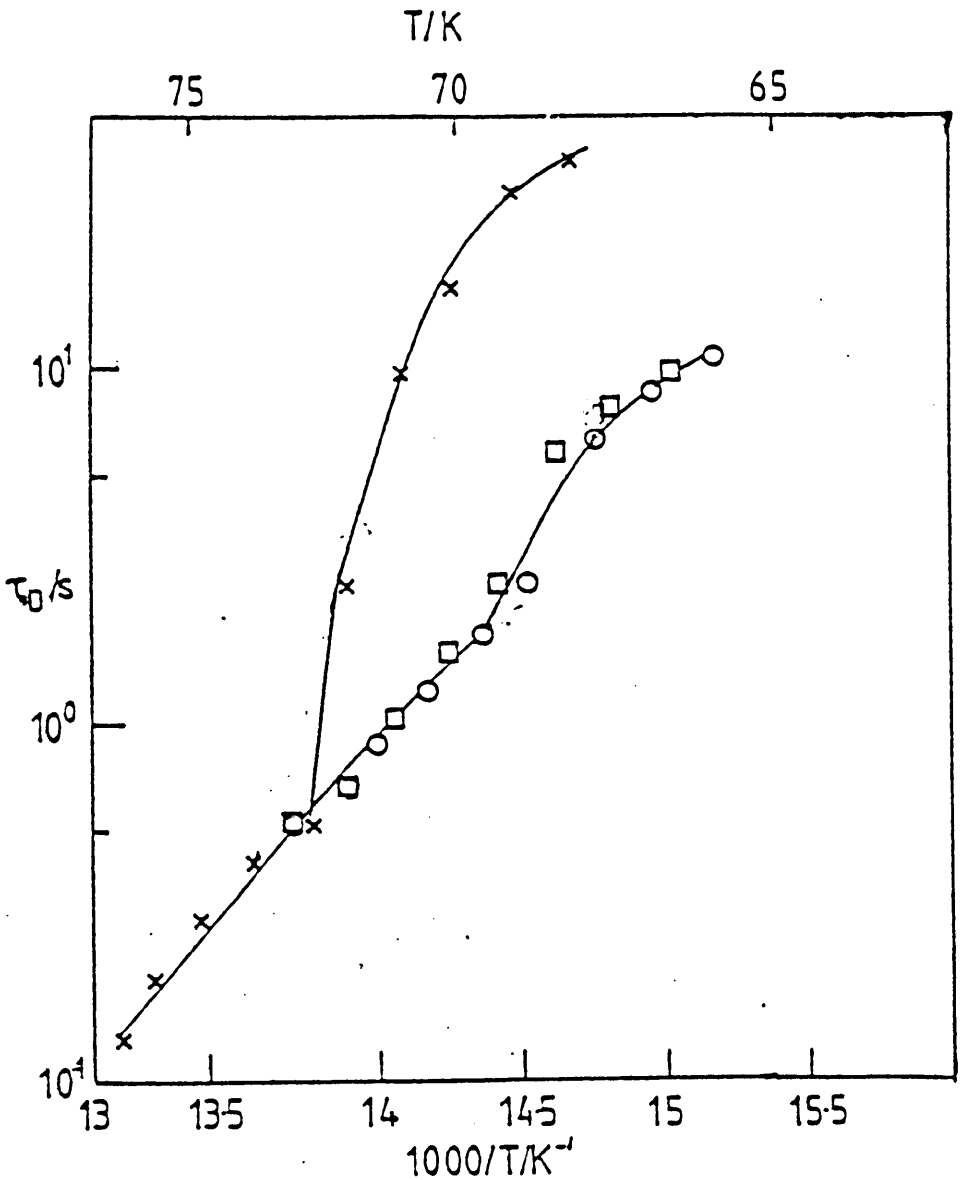

Variation of relaxation time τ_0 with temperature for sample KP14
○ on cooling, cooled from 120 K
□ on cooling, cooled from 73 K after previous transition
× on heating after annealing at 58 K overnight

gentle slope below the transition and a sharp rise as the transition occurs, the experimental observations show a relatively steep rise over several degrees from a low value, with an even steeper but not completely sharp rise around 71-73 K. The spread of about 2 K in the transition temperature is not inconsistent with the calorimetric data of Tajima et al.: it may be exaggerated by slight inhomogeneities in the sample temperature. However, it seems unlikely that at temperatures as low as 65 K parts of the small sample are at 72 K. It is more probable that the apparent low values of the static permittivity are due to failure to extrapolate the long, spread relaxation to its true final value. In other words, because of the increasing time constant in the ordered sample at low temperatures, the fraction of the ice contributing to the measured relaxation is lower than at high temperatures.

Although the measured permittivities and time constants well below the transition may have little absolute meaning, their changes still give a guide to the amount of transformation taking place: since both quantities are liable to be underestimated the fact that they change in different directions must reflect a real change in the properties of the ice. Close to the transition, where the relaxation times are relatively short, the measurements should be reasonably reliable in any case, so that the calculations of table 5.2 have some validity.

The increase in the permittivity and decrease in the time constant on disordering imply a corresponding increase in the conductivity, by a greater factor than that by which the time constant is

Table 5.2

Measured relaxation strengths immediately below the transition temperature, in annealed samples, with the deduced relaxation strength in the 'transformable' portion of each sample and the fraction w of this portion which has undergone the transition.

	ε_s*	ε_s	w
KP3	140±20	170±30	0.51±0.03
KP4	110±20	140±30	0.57±0.04
KP5	130±20	190±40	0.45±0.03
KP6	20± 2	120±20	0.62±0.03
KP7	70±10	140±30	0.57±0.04
KP10	140±10	220±20	0.39±0.01
KP12	150±10	230±20	0.37±0.01
KP13	100±10	200±30	0.57±0.03
KP14	70± 5	240±30	0.36±0.02

reduced. The conductivity depends on the concentration of defects, their mobility and their effective charge. The effective charge should not be affected by the transition, and for a tunnelling process the mobility should also remain essentially constant. It therefore appears that the concentration of free defects in the partially ordered ice must be lower, by up to two orders of magnitude, than that in the disordered phase. No detailed model has been developed for this phenomenon. However, it seems plausible to suggest that the defects become trapped in the ordered regions, with some energy for escape higher than that for escape from the traps present in the disordered state, and are only released when the order is broken down at the transition. Alternatively, one might imagine the defects to become caught in small regions of disorder entirely surrounded by ordered material. As ordering proceeds at a given temperature, the number of available defects is reduced so that the ordering process slows down. When the temperature is raised, more defects are released and the ordering process is speeded up until these extra defects again become trapped.

5.6 Measurements on single crystals

Some attempts were made to investigate the properties of KOH-doped single crystals of ice. The crystals were grown by the modified Bridgman method described by Ohtomo, Ahmad and Whitworth (1987), from degassed solutions of KOH in deionised water. About 1 cubic centimetre of crystal was grown in 24 hours. In order to

FIGURE 5.24

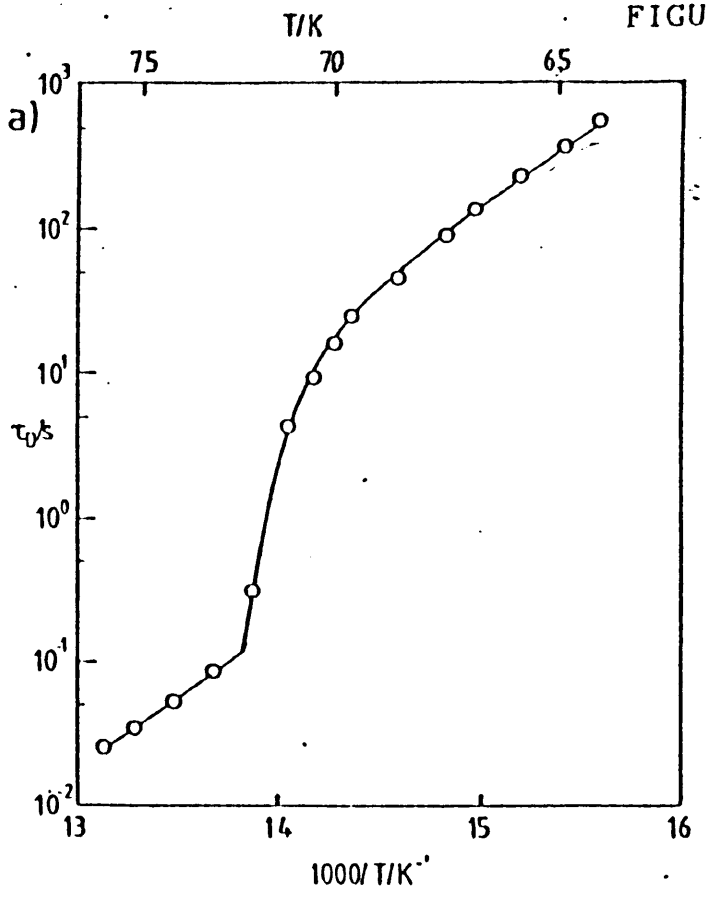

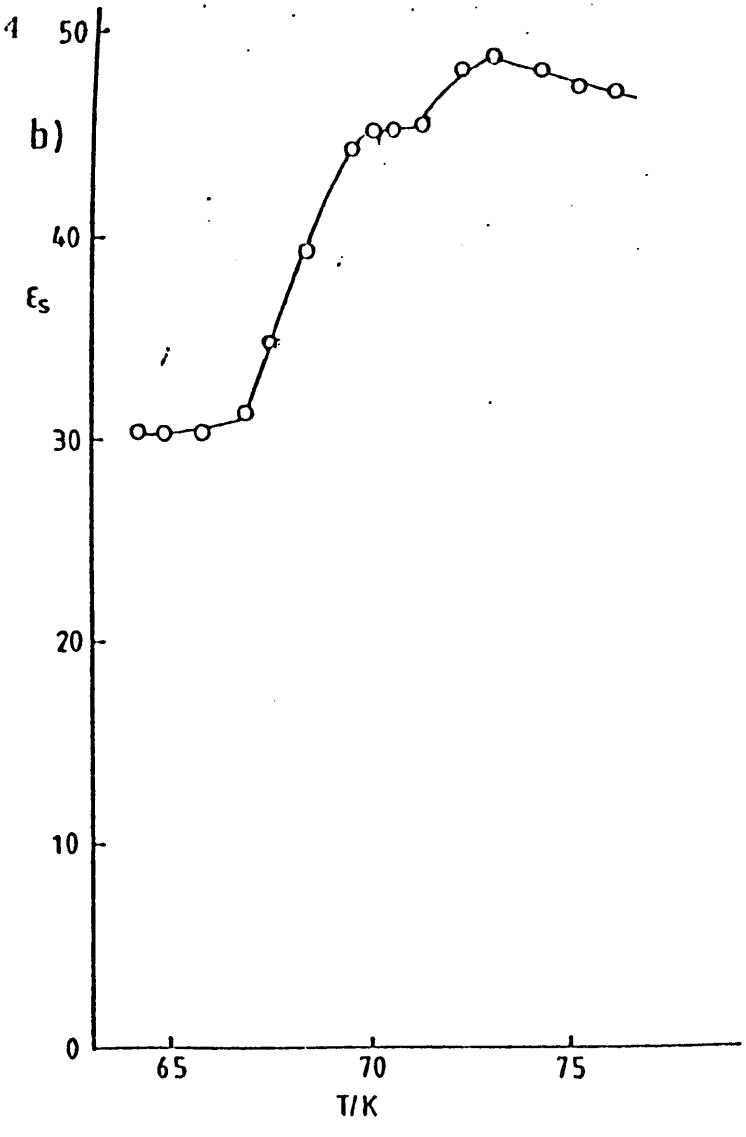

Changes in the dielectric properties of a single crystal specimen on heating after annealing
a) relaxation time τ_D
b) relaxation strength ε_s

Facing page 91

investigate the incorporation of the dopant in the slowly-grown single crystals, two crystals were grown, then sectioned, and the melted sections were analysed for potassium content using an Orion Specific Ion Electrode system, in which the potential difference between two special electrodes dipped in a solution is a measure of the ionic content of the solution. In these crystals, grown from 0.01 M solutions, the concentration of KOH in the ice was at the limit of detection, being less than 10^{-4} M. It therefore appeared that only about 1% of the KOH was incorporated in the ice.

One single-crystal specimen was used for dielectric measurements. The specimen was cut from a crystal grown from a 0.03 M solution of KOH, the concentration being the highest for which a clear crystal could be obtained. The high-frequency conductivity of a specimen cut from the same crystal had been found to be approximately 10^{-5} Ω^{-1} m^{-1} in the 'plateau' region, an order of magnitude lower than the typical value for a polycrystalline specimen. This crystal was grown by Mr D. J. Ives, who also carried out the high-temperature dielectric measurements. By examination in polarised light, it was established that the plane of the specimen used was almost exactly normal to the *c*-axis.

The crystal was shaved to an even thickness of about 2 mm and mounted in the cell used for experiments on powdered samples, described in section 6.3.1. After annealing for several days below 72 K, the variation of τ_D and ε_s shown in figures 5.24 (a) and (b) was obtained on heating. The change in τ_D at the transition suggests that a substantial amount of transformation has taken

place, but the change in permittivity is much smaller than is usual for a well-transformed specimen.

The value of ε_s immediately above the transition temperature is approximately 50. The ideal value, measured parallel to *c*, would be approximately 1000. Using the relation of Looyenga, the fraction of the ice which is effectively doped is calculated to be 0.26. However, if this value is used to calculate the 'true' value of ε_s in the doped regions just below the transition, this is found to be about 800. The expected value, as predicted by the theory in section 3.3.2, for a fully transformed specimen parallel to *c*, would be 20. If the mixed-phase formula is again applied, this means that only about 10% of the doped volume, or 2.6% of the total volume of the ice, is in the ordered phase at this temperature. However, at the lowest temperature where measurements were possible, the estimated value of ε_s was about 550, corresponding to 30% of the doped volume being ordered. Despite the difficulty in interpreting the results, the ordering transition was definitely observed in at least part of this single crystal.

CHAPTER 6

DIFFRACTION AND DIELECTRIC EXPERIMENTS ON POWDERED SAMPLES

6.1 Introduction

The aims of the neutron diffraction work were to determine the structure of ice XI more reliably than had been done by Leadbetter et al. (1985), to attempt to measure the lattice parameter changes associated with the transition, and to compare the results of dielectric and diffraction measurements on the same sample.

ISIS, the Spallation Neutron Source at the Rutherford Appleton Laboratory, produces an intense beam of neutrons with a range of energies, pulsed at 50 Hz. Diffraction measurements use time-of-flight techniques: the time taken by a neutron from a given pulse to reach a detector a known distance from the source depends inversely on its velocity v and hence directly on its de Broglie wavelength, $\lambda = h/mv$, where m is the neutron mass and h is Planck's constant. When a pulse of white neutron radiation falls on a sample, diffracted neutrons will reach a detector at an angle θ at times when the wavelength of the incident beam fulfils the Bragg condition, $2d \sin \theta = \lambda$, for a set of planes. This time is directly proportional to the distance d between the planes. The resolution of an instrument of this type depends primarily on the uncertainty in the length of the flight path, which in turn is governed by the thickness of the moderator in which the neutrons produced by the source are reduced to thermal energies.

The experiments described in this chapter were carried out on the

High Resolution Powder Diffractometer (HRPD), where the flight path is approximately 100 m and the moderator is about 0.25 m thick, so that the uncertainty in the flight path is of the order of 0.25%. Two rotating choppers close to the source ensure that the slow neutrons from one pulse do not overlap with the fast neutrons from the next. The detectors are arranged in concentric rings around the beam at 1 m from the sample, in order to collect neutrons with large values of 2θ. The value of 2θ and the flight path are different for each ring: when the run is complete the data from all rings are converted to spectra in terms of *d*-spacing, which are then summed and converted back to time-of-flight using average values for flight path and 2θ.

Most neutron diffraction experiments on ice have used D_2O, because of the high incoherent cross-section for hydrogen. However, HRPD provides sufficient resolution for satisfactory experiments to be carried out on hydrogenous materials. Also, as was found by Matsuo et al. (1986), the transition to the ordered phase will only occur in D_2O ice which is isotopically pure. Since the necessity for keeping the sample free from H_2O would have made handling much more difficult, particularly when dielectric measurements were required, H_2O ice was used for the two experiments described in this thesis.

6.2 The first neutron diffraction experiment

6.2.1 The sample holder

The cell used for the first neutron powder diffraction experiment

FIGURE 6.1

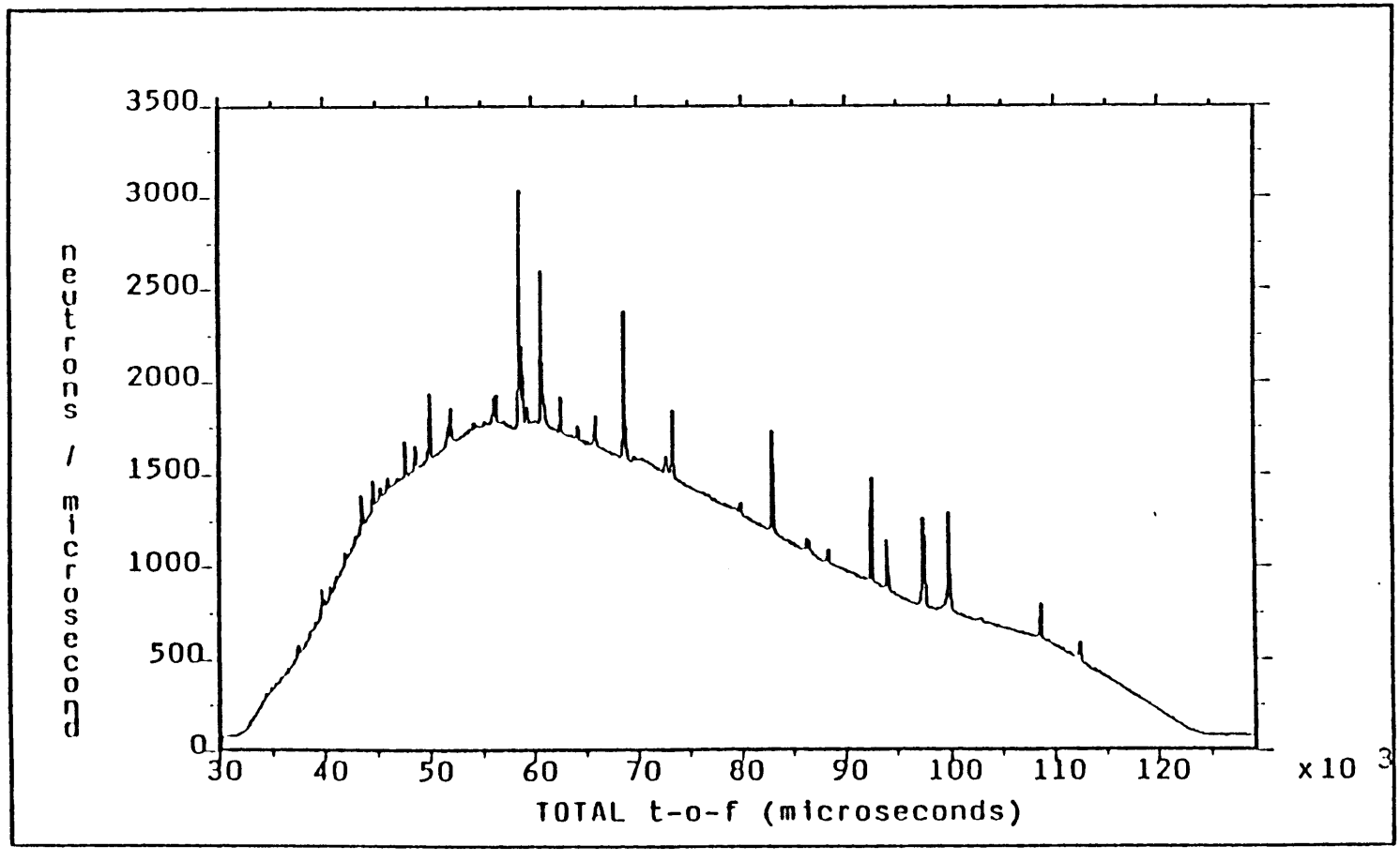

Raw (unnormalised) neutron diffraction profile for powdered ice at 10 K in the first experiment

Facing Page 69

on HRPD was a version of the standard rectangular HRPD powder cell, with an aluminium frame and two aluminium foil windows, the second of which was secured after packing the sample by means of four aluminium strips and twelve small (M 1.6) nuts. The sample was 3 mm thick, thinner than is usual for powder diffraction experiments, because of the high incoherent scattering from the hydrogenous sample.

6.2.2 Sample preparation

The powder sample for the first neutron diffraction experiment on HRPD was prepared as follows. A 0.02 M solution of KOH in deionized water was degassed by boiling under reduced pressure, then transferred to a glass tube, which was sealed and dipped in antifreeze solution at about -30°C. The liquid froze in about 15 minutes. The frozen mass was then removed from the tube by warming the surface and transferred to an open Cold Chamber running at about -30°C. This temperature was chosen because it is cold enough for effective grinding but not too cold for working with gloved hands. The mass was cloudy, suggesting that not all the KOH had been incorporated in solid solution in the ice, and at -10°C enough concentrated liquid solution remained unfrozen to prevent the formation of a fine powder. The powder was obtained by scraping the ice with a knife and grinding the scrapings in a mortar, and was then packed in the rectangular aluminium sample holder. The sample was stored in liquid nitrogen and dry ice before being transferred to the Orange Cryostat (a continuous-flow, liquid helium cooled cryostat) at RAL. The walls of this cryostat were of vanadium, which is virtually transparent to neutrons. The sample

FIGURE 6.2

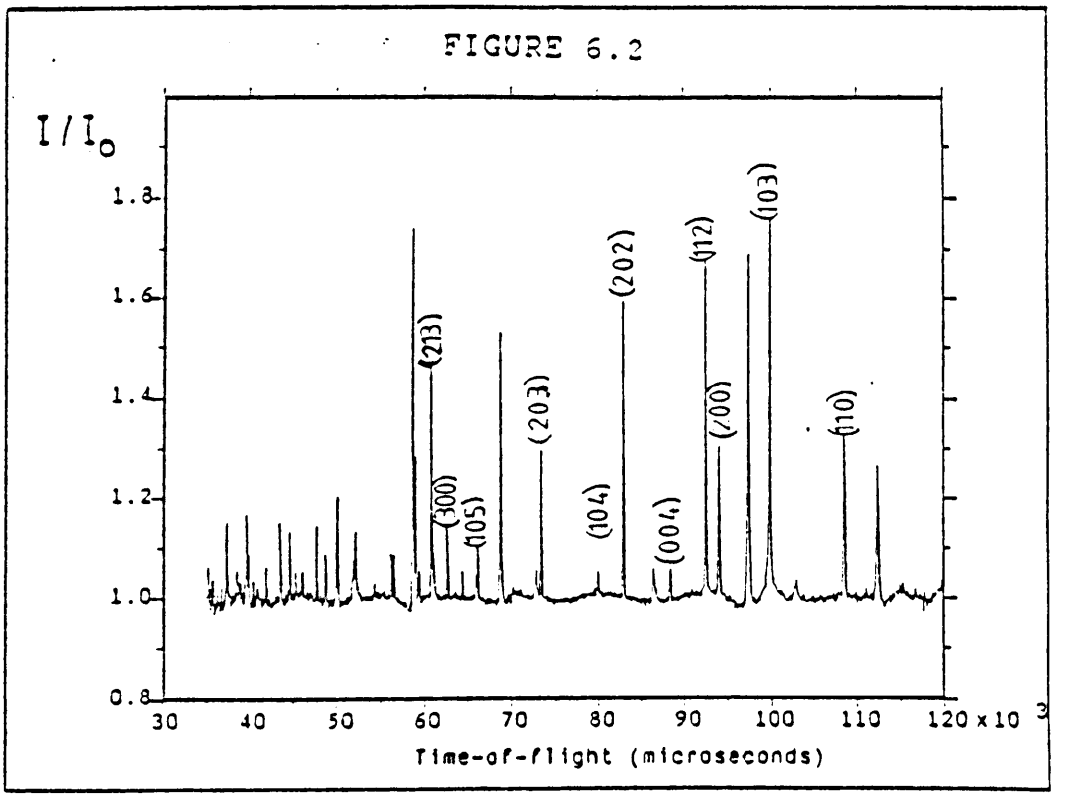

Normalised profile for annealed powdered ice at 10 K, with ice reflections marked and indexed in the hexagonal cell.

FIGURE 6.3

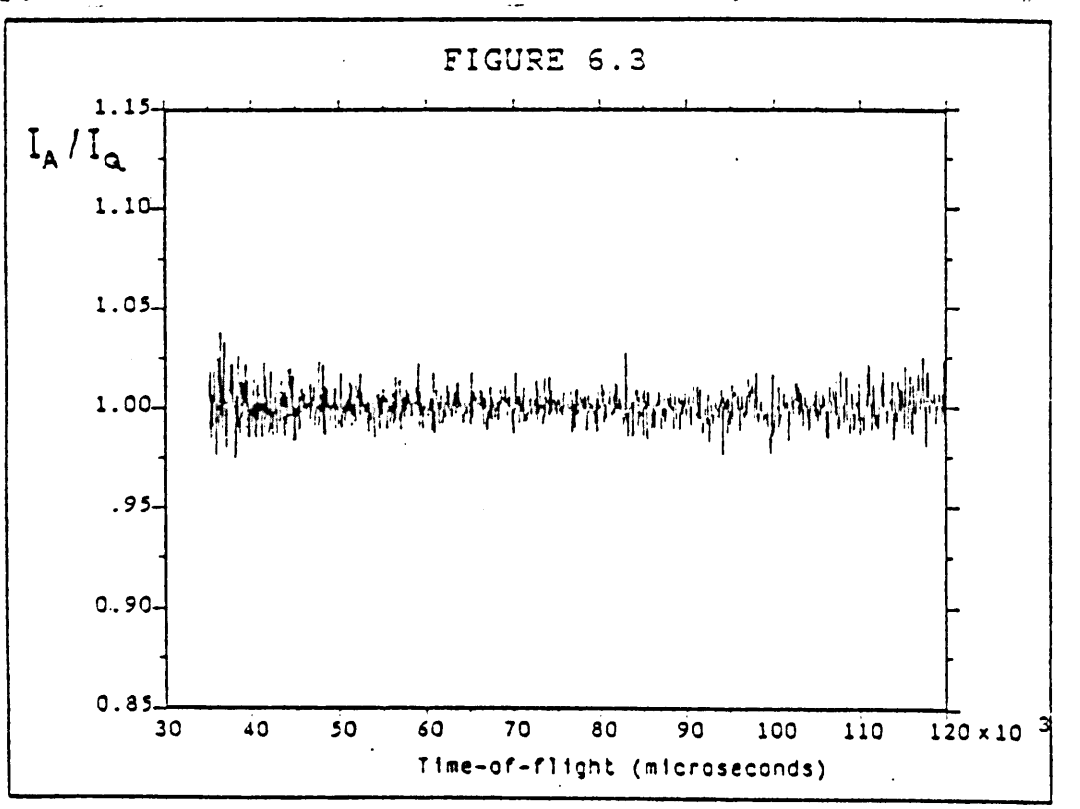

Ratio of normalised profiles for quenched and annealed samples in the first experiment

was maintained in the cryostat at about 62 K, with brief periods at 68 K, for six days. The cryostat was then cooled to 10 K for the first diffraction measurement.

6.2.3 Procedure

Diffraction spectra in the time-of-flight range 30-130 ms (corresponding to reflections from sets of planes with *d*-spacings approximately 0.6-2.6 angstrom) were obtained first on the annealed sample at 10 K and then above the transition at 120 K. The sample was quenched rapidly to 10 K and a further spectrum obtained, in the hope of measuring the expected lattice parameter change due to the transition.

6.2.4 Results

In spite of the high incoherent background due to scattering from hydrogen, a clear spectrum was obtained at each temperature. An example of a 'raw' profile is shown in figure 6.1. Before refinement the profiles were normalized by fitting the background to a 25th order polynomial and then dividing the data by the fitted function. Comparison of the two sets of data at 10 K revealed no significant changes. All profiles were successfully refined using the $P6_3/mmc$ space group and four-molecule unit cell of disordered ice Ih. The refinements were carried out using the Rietveld method, in which the whole profile is fitted to a function calculated from a model which includes parameters for peak shape and background as well as the lattice parameters and atomic coordinates: the programs used were part of the Cambridge Crystallography Subroutines Library and were executed on the VAX 8600 computer at RAL. The lattice

Table 6.1

Lattice parameters for ice, from the first experiment

T/K	10	120
a/angstrom	4.4934±0.0001	4.4958±0.0001
c/angstrom	7.3139±0.0001	7.3189±0.0001
c/*a*	1.6277±0.0001	1.6279±0.0001
2xvolume /angstrom^3	255.776±0.009	256.224±0.009

Table 6.2

Atomic coordinates for disordered ice (first experiment)

a) 10 K

	x	*y*	*z*
H1	1/3	2/3	0.1917±0.0012
H2	0.4441±0.0007	0.5559±0.0007	0.0167±0.0006
O1	1/3	2/3	0.0659±0.0004

b) 120 K

	x	*y*	*z*
H1	1/3	2/3	0.1921±0.0001
H2	0.4418±0.0012	0.5582±0.0012	0.0175±0.0009
O1	1/3	2/3	0.0654±0.0005

parameters obtained are shown in table 6.1 and the atomic co-ordinates in table 6.2.

Figure 6.2 shows the normalised profile for annealed ice at 10 K, with the principal ice reflections marked and indexed in the hexagonal cell for time-of-flight greater than 60 ms. Unmarked peaks, attributed to scattering from the aluminium windows of the cell, were excluded from the profile refinement: these peaks occurred in all three profiles. The dips in the background are due to absorption edges in the aluminium spectrum.

It was evident that no detectable amount of transformation to the ordered phase had taken place. Figure 6.3 shows the ratio of the normalised profiles for the quenched and annealed specimens: it has no discernable features. Simulated diffraction profile calculations for ordered and disordered models suggested, on the basis of extra peaks and changes in the intensities of peaks common to both phases, that changes would have been detectable with as little as 13% transformation, if the lattice parameters and atomic coordinates were unchanged. The resolution appeared to be sufficient for the detection of the lattice parameter changes (of the order of 0.1%) which would be expected on the basis of the work of Yamamuro et al. (1987c) which has been discussed in section 1.2.4.

6.3 Dielectric experiments on powdered ice

After the failure of the first neutron diffraction experiment it

FIGURE 6.4

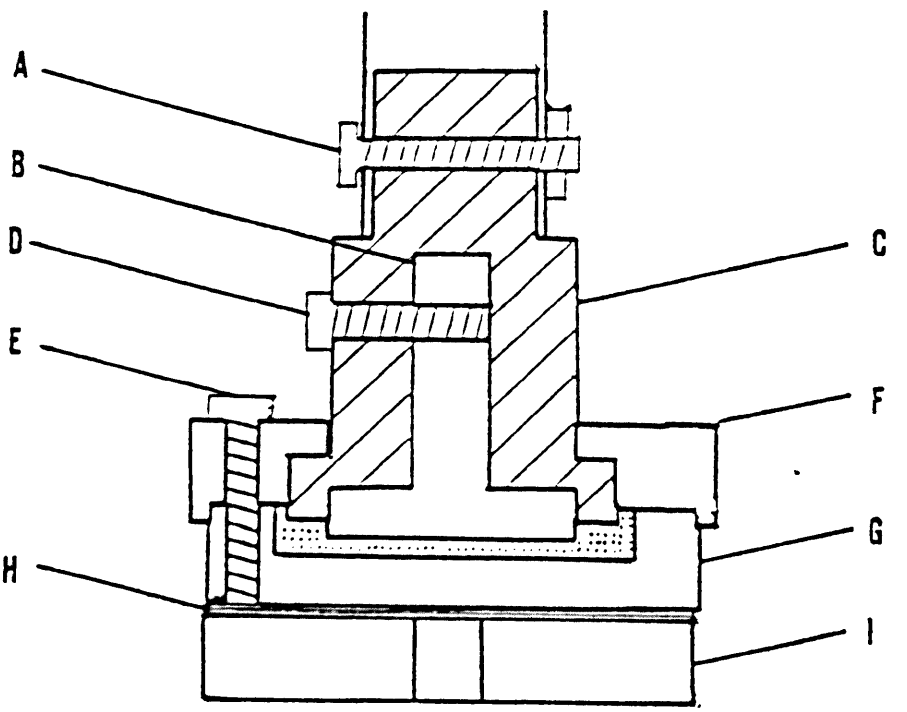

Cell for dielectric measurements on powdered ice samples (twice actual size): the letters refer to the text of section 6.3.1

was necessary to determine the cause of this failure and attempt to remedy it. For this purpose the cryostat was modified to accept frozen samples (as described in section 4.2.2), and a series of dielectric experiments on powdered doped ice was carried out.

6.3.1 The sample holder

For these experiments, a simple cell was designed for use in the adapted cryostat. This cell is illustrated in figure 6.4. The base is a shallow brass dish G, attached by an insulating layer of Araldite and paper H to a brass plate I with a threaded hole to accept the threaded boss on the cryostat bottom. The upper section consists of three parts: a central brass electrode B, a PTFE boss C and a brass lid F. The contact to the upper electrode is made by a screw D passing through the PTFE above the lid, while the contact to the body of the cell, which acts as the second electrode, is held in place by one of the three screws E securing the lid to the base. The upper end of the PTFE boss is attached to the bottom of the centre-stick by a screw A, and its lower end is prevented from rotating with respect to the rest of the cell by two grub screws in the thickness of the lid. The entire upper section can be assembled on the centre-stick before the sample is prepared: the sample is then made up and packed into the base of the cell and the assembly completed by fastening the three screws.

6.3.2 The experiments

A powder sample was prepared in the same way as the one used for the neutron diffraction experiment and was packed in the dielectric cell. The assembled cell was inserted in the cryostat at about

FIGURE 6.5

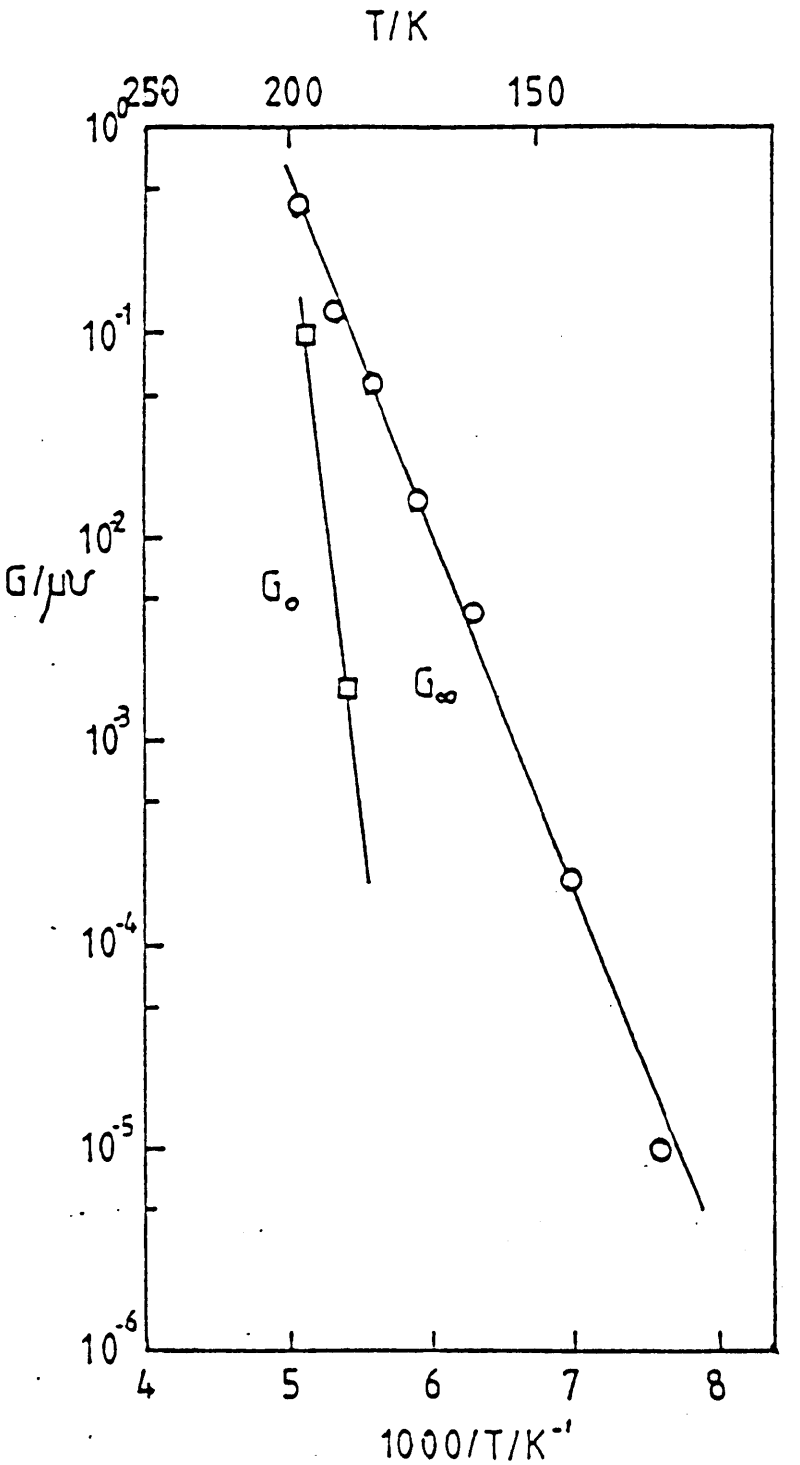

Variation of conductances G_o and G_∞ with temperature, for a polycrystalline sample formed from a powder which had been exposed to the atmosphere and then melted.

-80°C.

Measurements using the pulse method were taken as the sample was cooled. The sample did not show the characteristic behaviour of KOH-doped ice: instead, the Debye relaxation time increased rapidly with falling temperature and became too long to measure at approximately 100 K.

The experiment was repeated with a sample prepared from a 0.1 M KOH solution, with the same result. This sample was annealed for some time around the eutectic temperature without any effect. Annealing at -10°C resulted in a lengthening of the relaxation time and also caused the powder to become coarse and wet.

Evidently, neither of these samples could be made to undergo the transition to the ordered phase. A series of tests was devised in an attempt to find the cause of the problem. At this stage the most probable causes appeared to be contamination of the sample, either before or after powdering, or damage introduced by the powdering process itself.

A sample prepared from the same lump of ice used for the second powder specimen, but broken into coarse pieces in the Cold Room at about -9°C, behaved similarly to the powdered samples.

In order to investigate the possibility that contamination was being introduced at various stages of the process, samples were partly prepared, then melted into the sealed polycrystal cell and

FIGURE 6.6

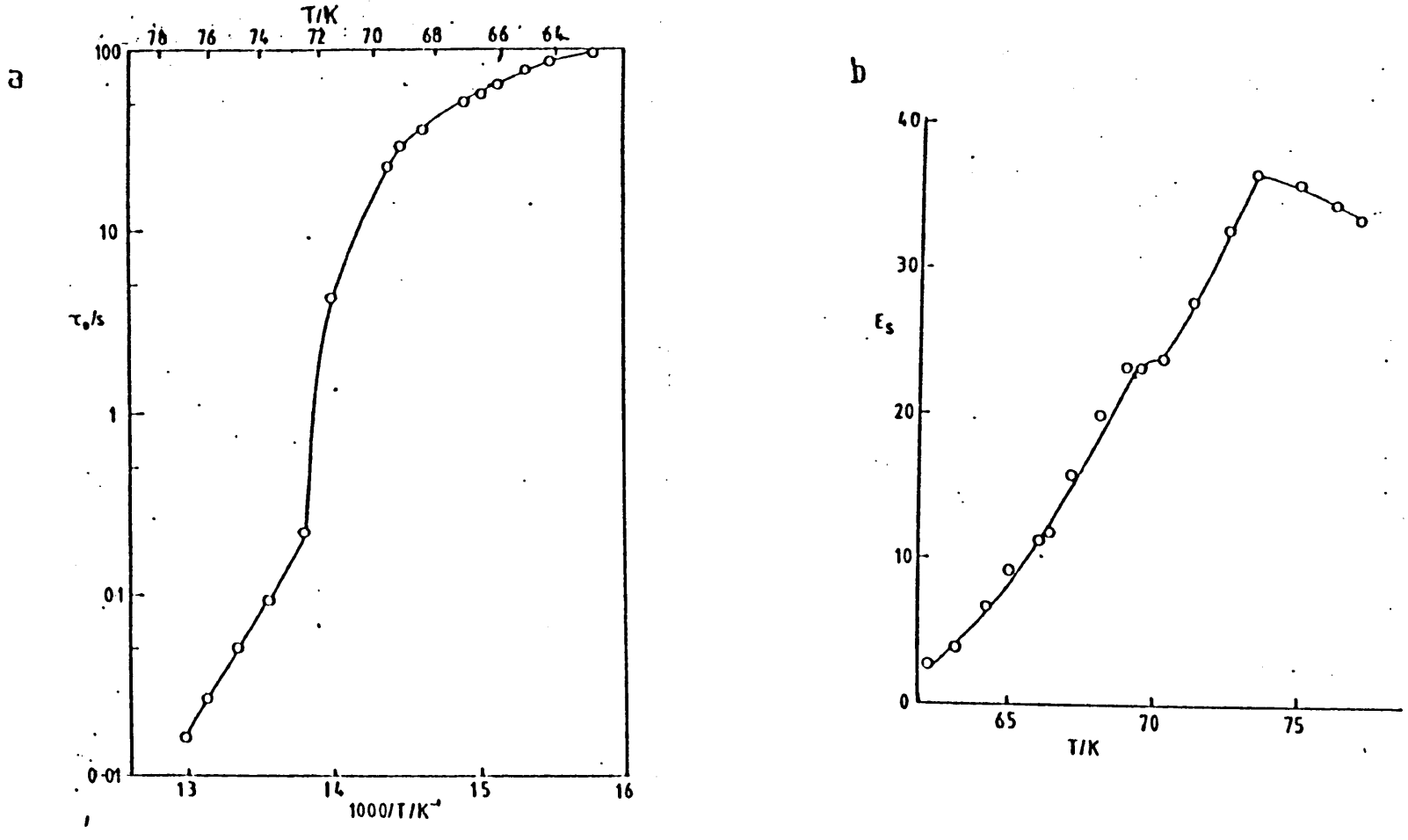

Temperature dependence of the dielectric properties on heating after annealing below the transition temperature, for a powdered sample prepared in a nitrogen atmosphere
a) relaxation time τ_D
b) relaxation strength ε_s

Facing Page 103

refrozen. A sample melted from ice frozen in the glass tube but not powdered was found to transform in the same way as a 'normal' doped polycrystalline sample. However, out of three samples frozen from melted powders, the two which were exposed to the atmosphere for periods of one and two hours after being ground showed behaviour similar to that of the powdered samples. This suggested that the effectiveness of the KOH was destroyed by prolonged exposure to the atmosphere, probably by reaction with CO_2. The variation of G_∞ and G_0 with temperature for one such sample is shown in figure 6.5.

To test this hypothesis, a sample was prepared inside a glove box from which the CO_2 had been removed by exposing a concentrated KOH solution for some hours. This sample was found to undergo a transition to the ordered phase. However, the glove box could only be used in the Cold Room, where the temperature was too high to allow the preparation of a satisfactory powder for diffraction purposes. In order to overcome this difficulty, the Cold Chamber was adapted to form a simple glove box which could be sealed and flushed with nitrogen gas. A sample prepared in this chamber showed a satisfactory transition. The variations of τ_D and ε_s with temperature, as the sample was heated after annealing for about 60 hours, are shown in figure 6.6. The relatively low value of the static dielectric constant immediately above the transition is due to the low packing density of the powdered ice. From the measured value of ε_∞ it was estimated that the packing density was about 35%. If this value is used to calculate the true value of ε_s above the transition, a value of about 470 is

FIGURE 6.7

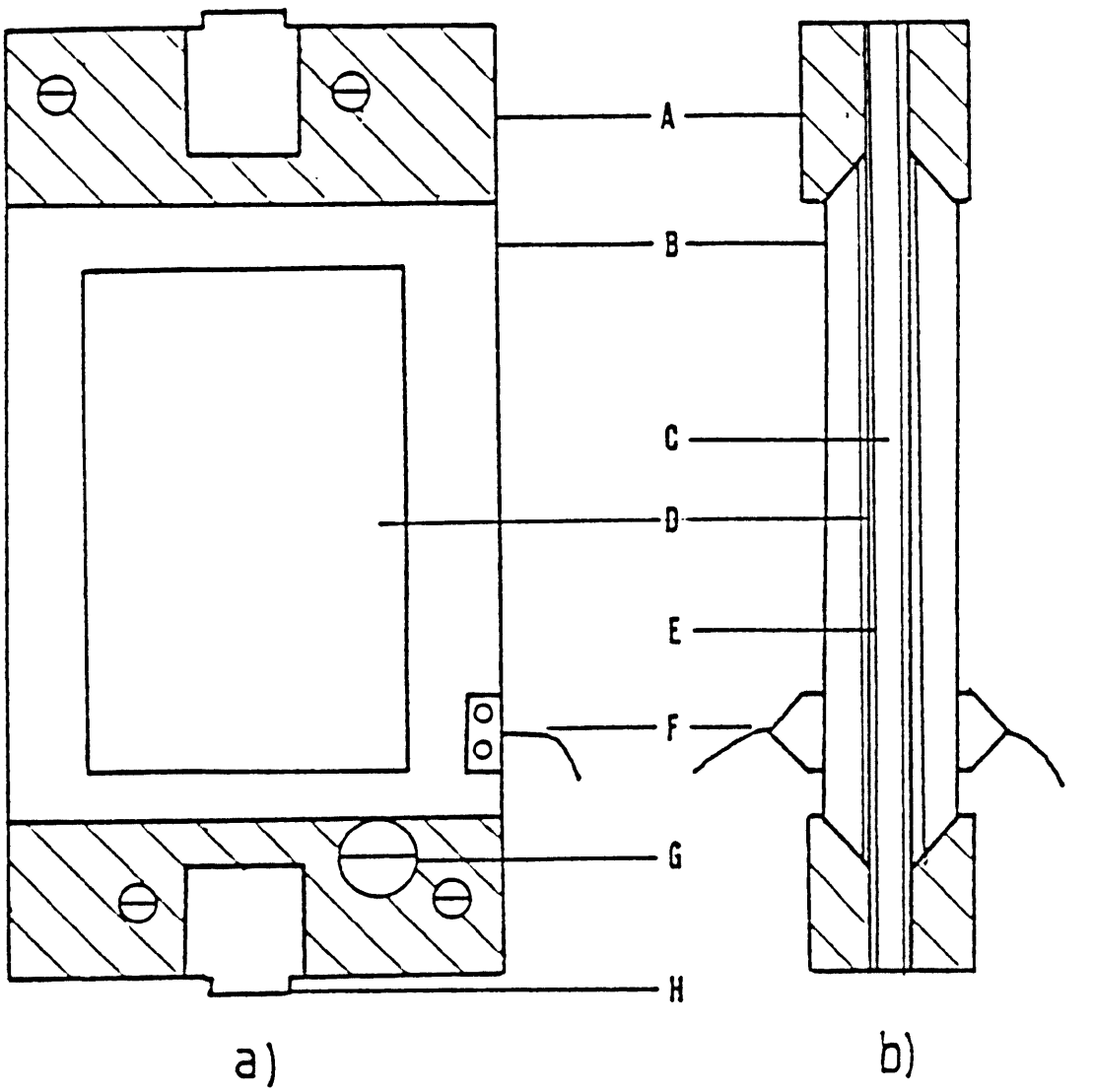

Sample cell for dielectric and powder diffraction measurements (twice actual size)
a) plan view
b) side elevation
The letters refer to the text of section 6.4.1

obtained, suggesting that the sample was effectively doped throughout.

This result is perhaps not surprising. Paren and Glen (1978) found that the dielectric properties of pure powdered ice changed on exposure to the atmosphere in a way which was attributable to contamination by CO_2. The absorption of atmospheric gas will take place more rapidly in a powder than in a solid sample because of the greatly increased ratio of surface area to volume. CO_2 is known to react strongly with alkali hydroxides. It seems likely that the limited success of the experiment of Leadbetter et al. may have been due to the use of solid CO_2 as a coolant during the freezing and grinding of the sample.

6.4 The second neutron diffraction experiment

6.4.1 The sample cell

For the second neutron diffraction experiment a sample holder, illustrated in figure 6.7, was designed to allow dielectric measurements to be taken as the powder sample was annealed and during the experiment. The sample holder was also intended to be easier to assemble than that used for the previous experiment, since it must be handled not only at -30°C but in a nitrogen atmosphere.

The two vanadium foil windows D of the new cell are held in place by aluminium frames B, and form the two electrodes for the dielectric measurement, being isolated from the aluminium body C by

insulating films E, Melinex for the low-impedance electrode and PTFE for the other. Each frame has a lead attached by a solder tag F and two small screws. Two bevelled insulating end-pieces A, each fixed to the body by two screws, hold each frame in place: the frames are prevented from slipping sideways by a single screw G passing through the end-piece and locating in a notch in one edge of each. The filled cell may thus be assembled simply by sliding one window and its frame into place and tightening the locating screw. The cell has tapped holes H at top and bottom. In the Birmingham cryostat the upper hole accepts a threaded boss in the end of the centre-stick, while the lower is screwed to the cryostat base: in the Orange cryostat used for the HRPD experiment only the upper end is attached to the centre-stick. In either case, the body is at ground potential and acts as a 'guard ring', eliminating any problems of stray capacitance. Two side-pieces, fixed to the edges of the body and insulated from the window-frames by Melinex films, contain holes for the heater and sensor intended for temperature control in the RAL cryostat. The centre-stick for the RAL cryostat, which also carried the connections for the heater and temperature sensor, was fitted with two extra screened and insulated leads, connected to the two electrodes by miniature plugs and sockets and terminated outside the cryostat by BNC plugs.

6.4.2 Sample preparation

The sample for the second HRPD experiment was frozen from an approximately 0.1 M solution of KOH formed by diluting the contents of a vial of 'Convol' concentrated solution in deionised water, which was then degassed by boiling under reduced pressure for about

FIGURE 6.8

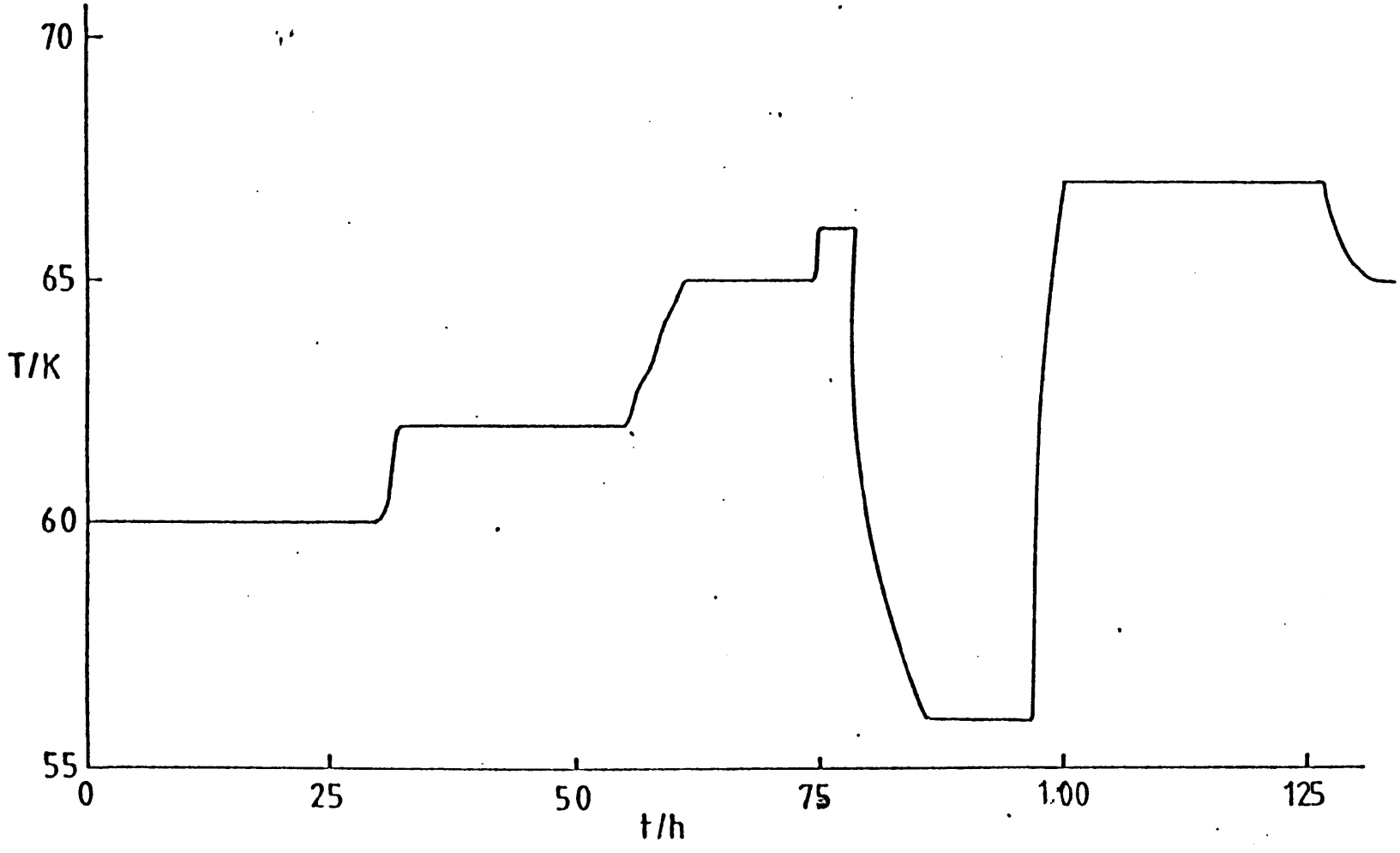

Temperature variation during the first few days of annealing of the sample for the second powder diffraction experiment

Facing Page 105

1 hour. Grinding was carried out in the cold chamber in a nitrogen atmosphere, and the sample holder was assembled before the sealed chamber was opened. The assembled sample holder, complete with the gadolinium mask used to prevent neutron scattering by the frame, was stored in liquid nitrogen until it could be transferred to the RAL cryostat. The connections to the centre-stick were made while the cell was still immersed in liquid nitrogen, so that the sample was exposed to the atmosphere as little as possible, preventing both the reaction of the dopant with CO_2 and the build-up of frost on the cell. The sample was then transferred to the cryostat and heated to about 100 K for a few hours in order to boil off any trapped nitrogen, before being slowly cooled to 60 K to begin the annealing sequence. Dielectric measurements taken during cooling confirmed that the sample was suitable for transformation: at 80 K the relaxation time was approximately 0.03 s and the static permittivity was about 50, an acceptable value for a powdered sample. After the experiment the volume of ice was measured and the packing density found to be approximately 50%. This would imply that the true static permittivity at 80 K was approximately 270, from which in turn the fraction of the ice effectively doped may be estimated at approximately 75%.

The sample was annealed at temperatures between 55-67 K for 12 days before the diffraction measurements were taken: the temperature variation for the early stages is plotted in figure 6.8. Because the use of the heater on the sample was found to produce unacceptable levels of electrical noise, the temperature was controlled using a heater and sensor in the body of the cryostat

FIGURE 6.9

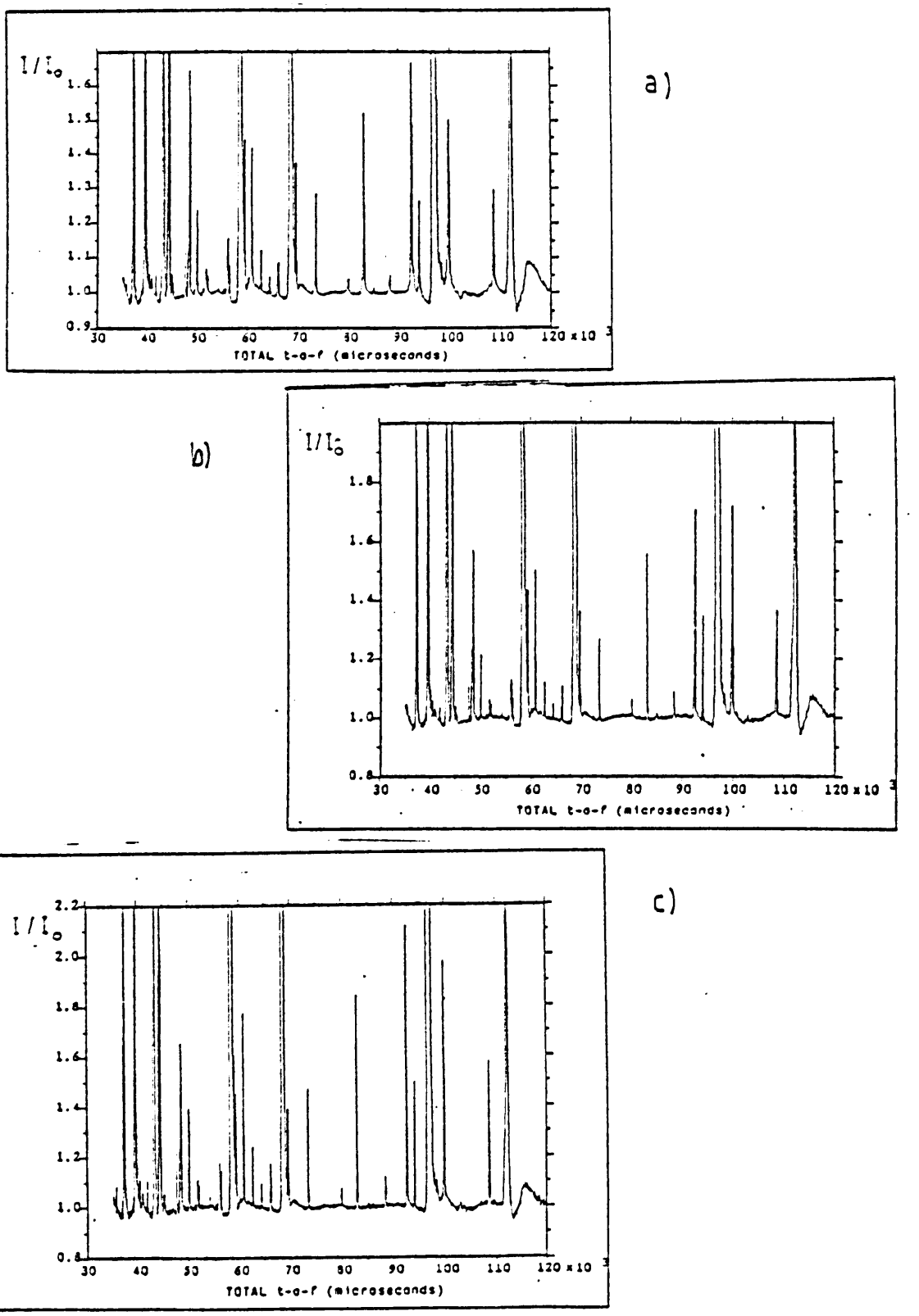

Normalised neutron diffraction spectra for the second experiment
a) at 10 K after annealing
b) at 100 K
c) at 10 K after rapid quenching from 100 K

but monitored using the sensor mounted on the sample can. Except for the excursions caused by the refilling of the cryostat with liquid helium, the measured temperature fluctuated by only a few tenths of a degree about the set temperature. After the initial cooling to 60 K the sample was kept at higher temperatures (65-67 K) as much as possible, so that the transformation to the ordered phase could take place more quickly. Most of the changes in the dielectric properties took place during the first few days of annealing, while over the last six days no significant change occured. Despite the long annealing, the dielectric relaxation did not completely disappear. After the first six days, measurements of the dielectric properties gave $\tau_D \simeq 60$ s and $\varepsilon_s \approx 15$ at 67 K. At the end of the annealing period the sample was cooled to about 10 K and the cryostat was mounted in the neutron beam.

6.4.3 Results

As in the previous experiment, three diffraction spectra were obtained, the first at 10 K after the annealing treatment, the second above the transition at 100 K and the third at 10 K after the sample had been rapidly quenched from 100 K. The time taken to cool the sample from 100 K to 10 K was about 1 hour. Normalised spectra for the three runs are shown in figure 6.9. The very broad, off-scale peaks are due to scattering from the walls of the cryostat, which in this experiment were of aluminium rather than vanadium because no vanadium-walled unit was available. This time the results showed obvious differences, with broadening and splitting of the diffraction peaks in the spectrum for the annealed specimen. As can be seen from a comparison of figure 6.10, which

FIGURE 6.10

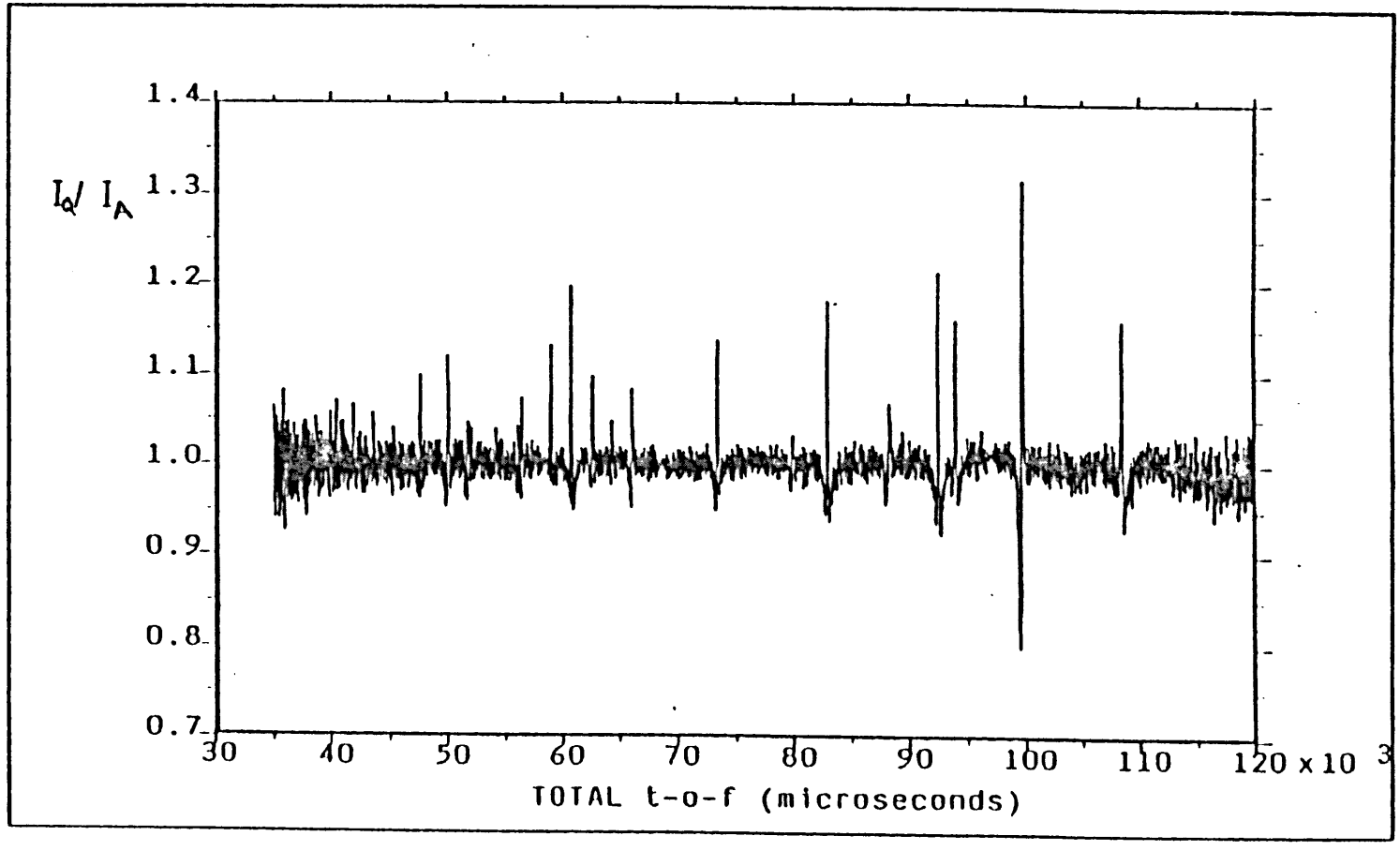

Ratio of normalised spectra for quenched and annealed specimens in the second experiment

Following page 107

FIGURE 6.11

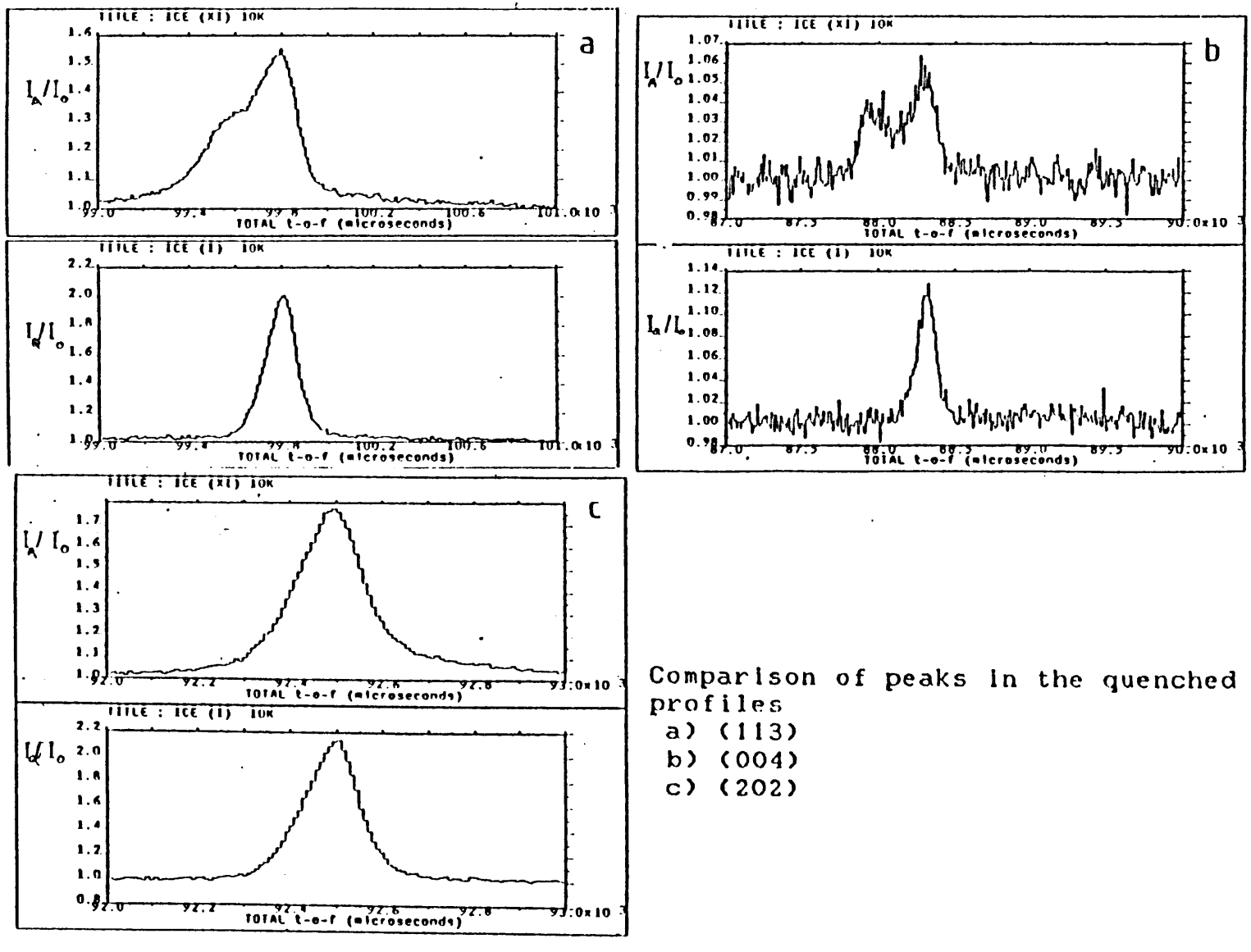

Comparison of peaks in the quenched and annealed profiles
a) (113)
b) (004)
c) (202)

Following page 107

FIGURE 6.12

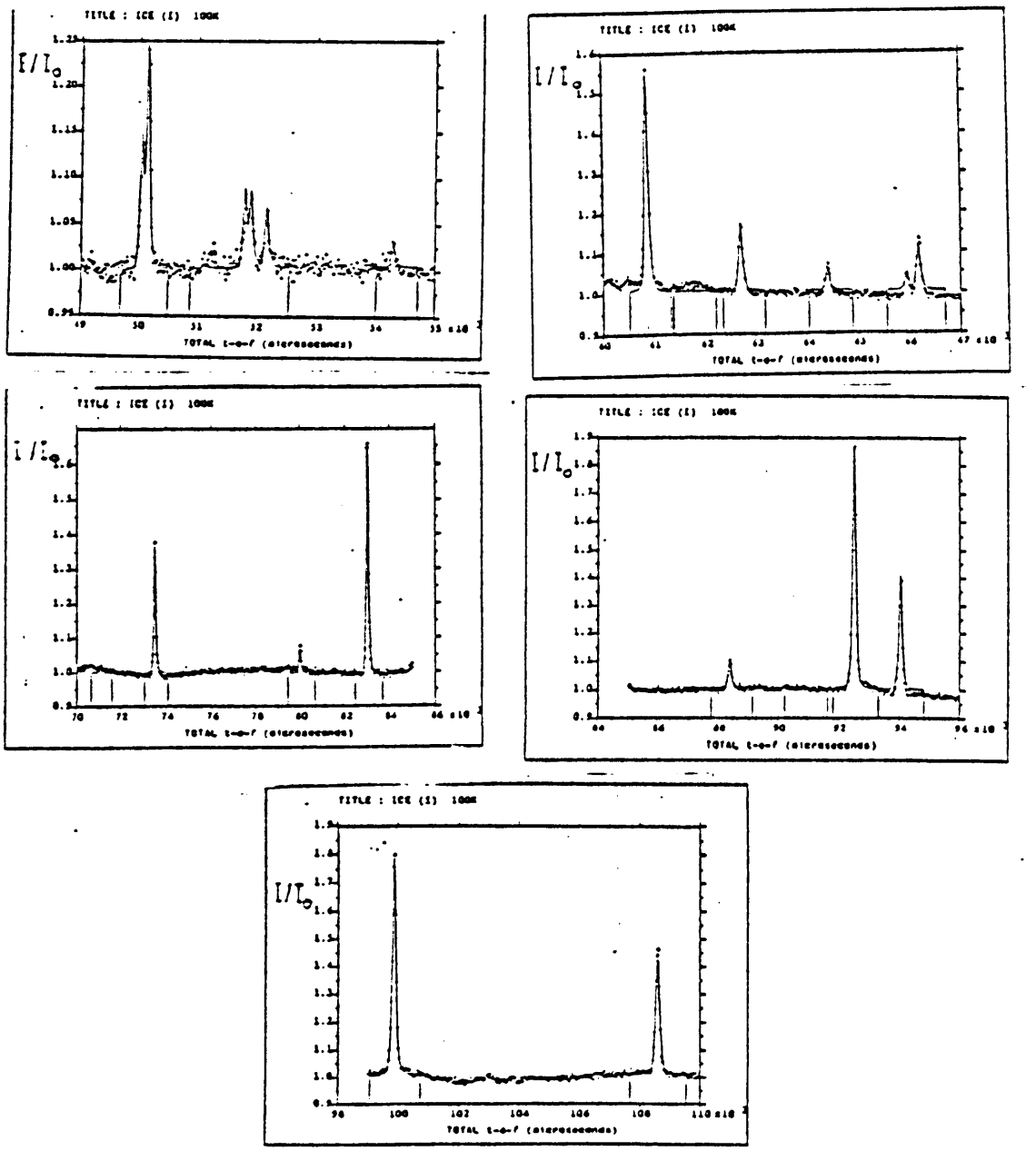

Fitted profile for disordered ice at 100 K: the crosses are the experimental data, the line the calculated function

Following page 107

FIGURE 6.13

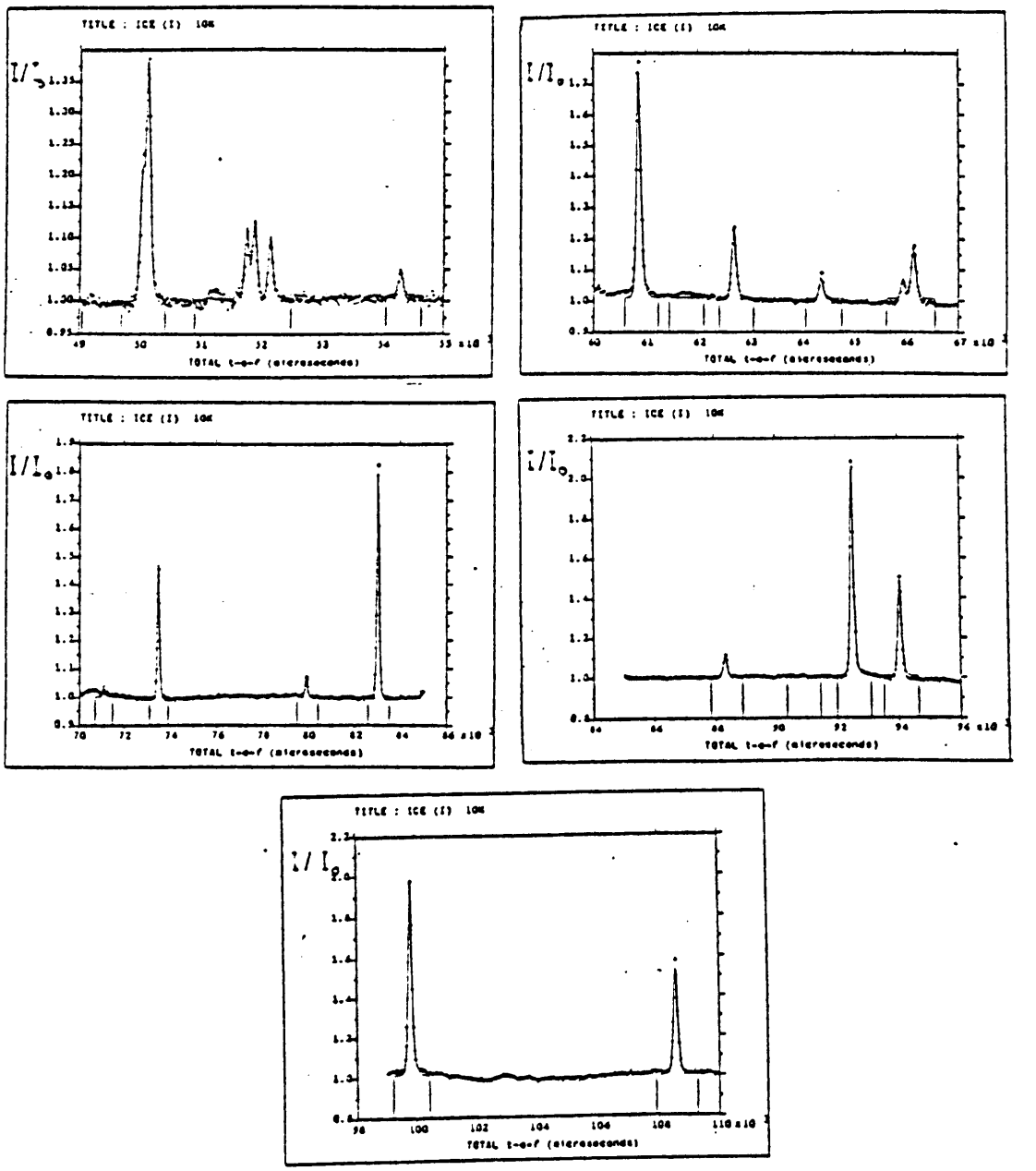

Fitted profile for disordered ice at 10 K: the crosses are the experimental data, the line the calculated function

Following page 107

Table 6.3

Lattice parameters for disordered ice, from the second experiment

T/K	10	100
a/angstrom	4.4933±0.0001	4.4941±0.0001
c/angstrom	7.3105±0.0001	7.3164±0.0001
c/*a*	1.6270±0.0001	1.6280±0.0001
2xvolume /angstrom^3	255.646±0.009	255.943±0.009

Table 6.4

Atomic coordinates for disordered ice (second experiment)

a) 10 K

	x	*y*	*z*
H1	1/3	2/3	0.2003±0.0009
H2	0.4513±0.0004	0.5487±0.0007	0.0177±0.0004
O1	1/3	2/3	0.0635±0.0002

b) 100 K

	x	*y*	*z*
H1	1/3	2/3	0.1973±0.0013
H2	0.4511±0.0007	0.5489±0.0007	0.0188±0.0006
O1	1/3	2/3	0.0650±0.0004

shows the ratio of the normalised profiles for the quenched and annealed specimens, with the profiles in figure 6.9, every peak in the ice spectrum has altered its shape. In particular, the peak indexed as (004) shows clearly resolved splitting, as shown in figure 6.11 (b), while that which would be indexed as (113) in the orthorhombic structure shows a distinct but not completely resolved shoulder (see figure 6.11 (a)). Other peaks, such as the (202) shown in figure 6.11 (c), are broadened but not split.

6.4.4 Analysis

The profiles for disordered ice at 10 K and 100 K were successfully refined using the $P6_3/mmc$ model: the lattice parameters and atomic coordinates obtained are shown in tables 6.3 and 6.4. The background for these profiles was modelled by a fifth-order polynomial of which the coefficients were refined. The regions containing the reflections from the aluminium cryostat were omitted from the refinement. The profiles in the time-of-flight range 35-45 ms were completely dominated by aluminium scattering, so this region was also omitted. The fitted profiles are shown in figures 6.12 and 6.13: the regions excluded from the refinement are not shown.

The changes in the spectrum between the annealed and quenched specimens could only be explained by the assumption that the annealed specimen contained a mixture of ordered and disordered phases, the ordered phase having a different *c*-axis lattice parameter. In accordance with this hypothesis the normalized spectrum for the quenched phase was multiplied by an appropriate fraction (43%) and subtracted from that for the annealed specimen

FIGURE 6.14

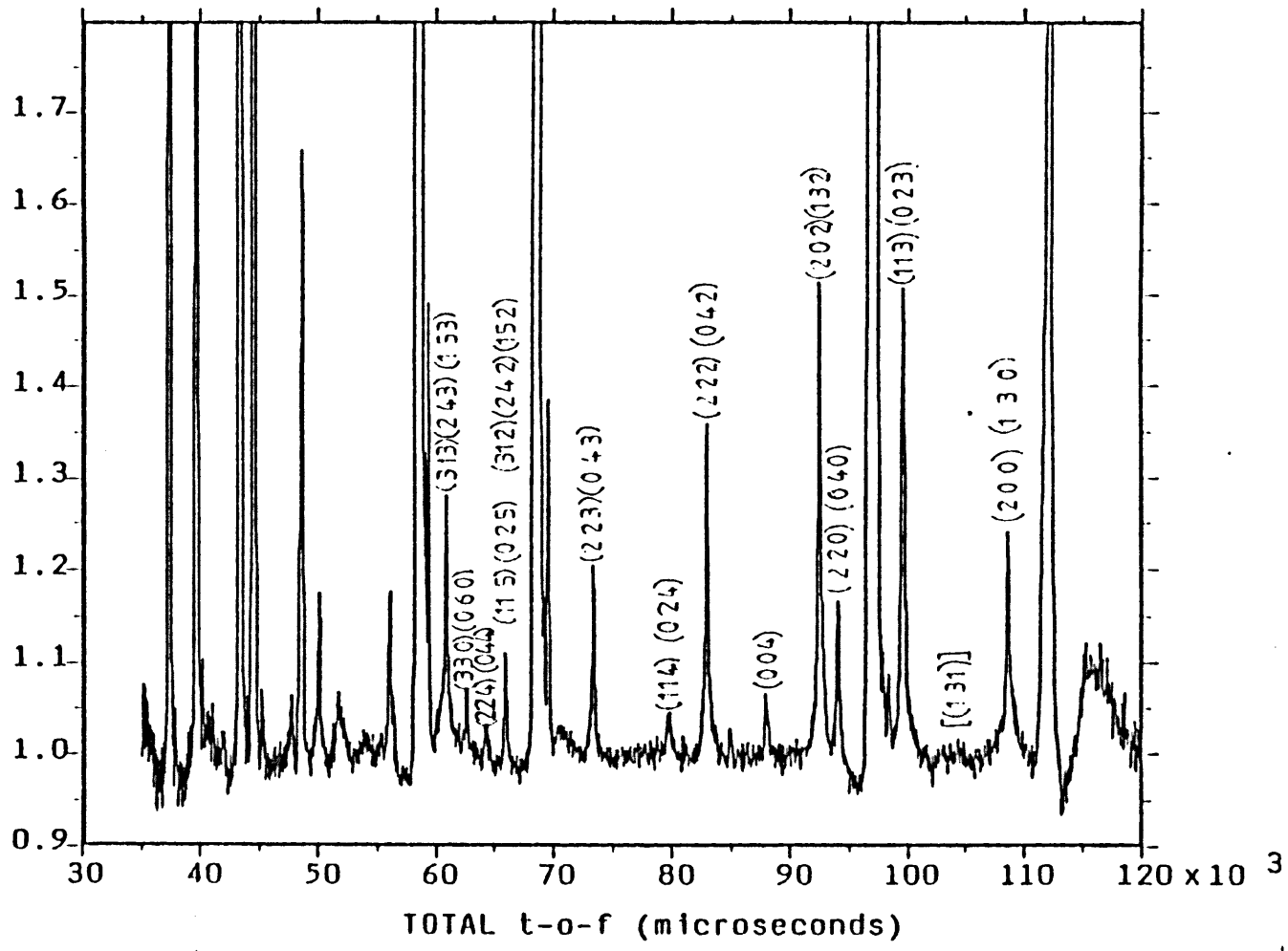

Pure ice XI profile obtained by subtraction of the disordered component from the profile for the annealed sample

to obtain a spectrum for the 'pure' ordered phase. The fraction was determined by trial-and-error, the main criterion being that the '(113)' peak should have a reasonable shape, and is probably accurate to about 2%. The resultant spectrum is shown in fig. 6.14. The peaks are noticeably, and in some cases asymmetrically, broadened compared with those in the 'disordered' spectrum, but none shows a resolved splitting. There are no visible extra reflections, such as might have been expected if a transition had taken place resulting in a lowering of symmetry. In particular, the '(131)' reflection which was the basis for the interpretation of the results of Leadbetter et al. is absent or extremely weak. The signal-to-noise ratio is noticeably worse than that for the two original profiles.

Because of the pronounced broadening of the peaks in the second phase, the background for the 'ordered ice' profile was not refined. Instead, coordinates at background level were measured from the disordered ice profile and used in the refinement of the ordered structure.

An attempt to refine the 'ordered' profile using the $P6_3/mmc$ model was not successful: in the best fit obtained, the shape of the water molecule was unrealistically distorted and the value of χ^2 (a measure of the sum of the squares of the deviations of the data from the model) was high. The obvious next step was to remove the centre of symmetry and attempt to refine in the $P6_3mc$ space group of the 'Rundle' model, where the protons are ordered parallel to the c-axis. However, no improvement in fit could be obtained in

FIGURE 6.15

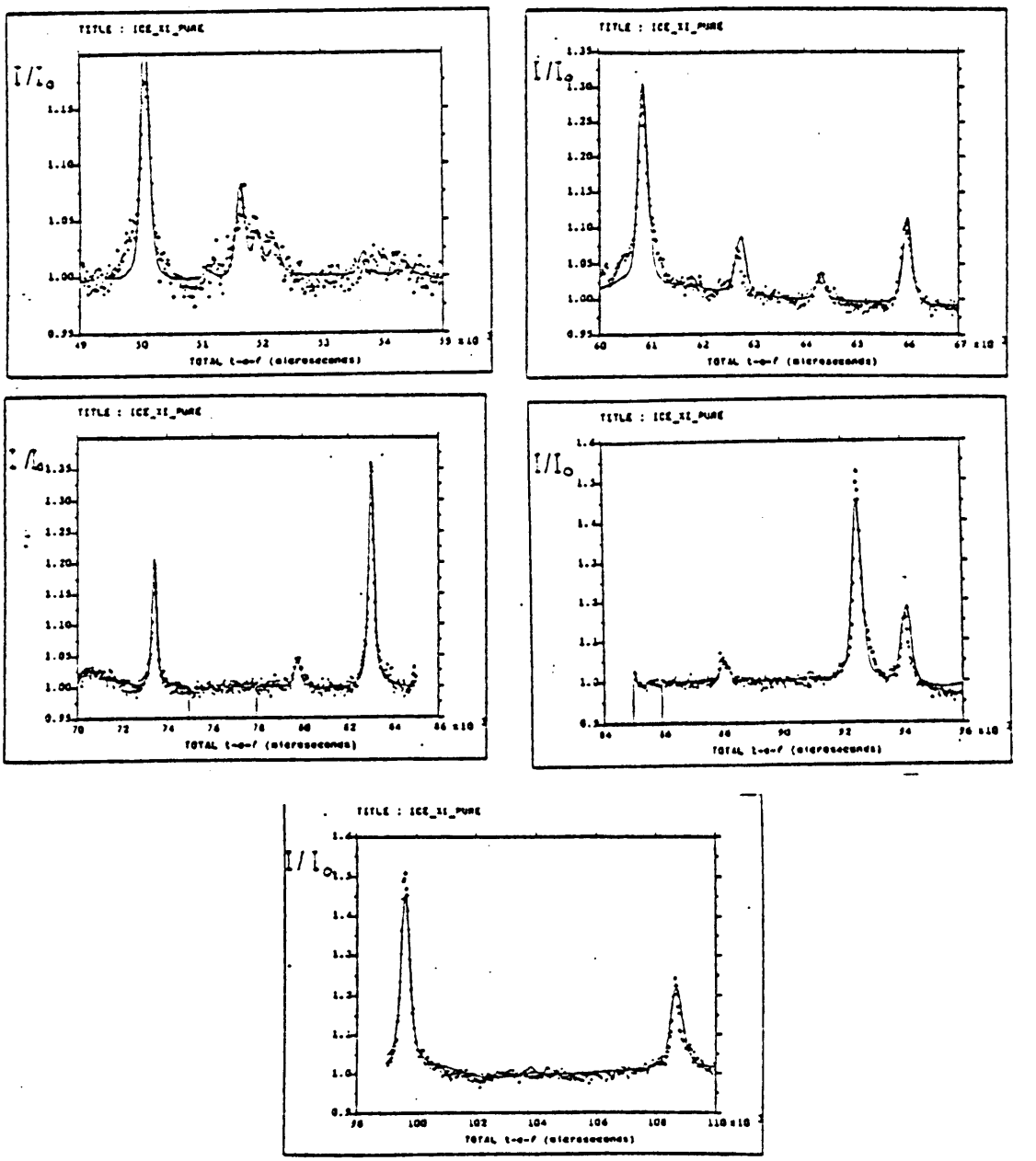

Fitted profile for ice XI at 10 K: the crosses are the experimental data, the line the calculated function

this way. The model was then altered to use the eight-molecule centred cell and the *Cmc*2$_1$ space group, with the protons completely disordered. When the *a* and *b* lattice parameters and the peak shape function were allowed to refine independently, so that the lattice was allowed to distort away from the hexagonal form with $b=\sqrt{3}a$, the fit improved significantly. The final values found for the lattice parameters are shown in table 6.5. A further improvement was obtained by allowing the protons to be partially ordered in the *Cmc*2$_1$ model, using a single parameter to describe the ordering in all of the three crystallographically distinct hydrogen positions. It was found that, by allowing the molecules to move slightly as rigid units within the cell, the extra '(131)' peak in the model could be greatly reduced in intensity and made almost invisible even when the occupancy of the 'correct' proton sites was as high as 0.9. However, no statistically significant improvement in fit could be obtained by the refinement of the atomic coordinates. As only about 15 reflections were available it would in any case be impossible to obtain reliable information on the atomic coordinates if these were all allowed to refine independently.

The final fitted profile is shown in figure 6.15 and the corresponding values for the atomic coordinates in table 6.6.

In order to confirm the structure of ordered ice it is necessary to eliminate other possible structures. Simulated profiles were generated, using the background, scale and peak-shape parameters found from the *Cmc*2$_1$ refinement, for the most symmetrical of the

Table 6.5

Lattice parameters for ice XI

a/angstrom	4.5026±0.0003
b/angstrom	7.7803±0.0006
c/angstrom	7.2884±0.0008
b/*a*	1.7280±0.0002
$a' = \left[\frac{ab}{\sqrt{3}} \right]^{1/2}$/angstrom	4.4973±0.0003
c/*a*'	1.6206±0.0002
vol/angstrom^3	255.32±0.04

Table 6.6

Atomic coordinates and hydrogen site occupancies from the final refinement of the ice XI profile

	x	*y*	*z*	*p*
H1	0	0.6581±0.0014	0.1968±0.0004	0.90±0.02
H2	0	0.5407±0.0014	0.0169±0.0004	0.90±0.02
H3	0.6760	0.7677±0.0014	0.9831±0.0004	0.90±0.02
H4	1/2	0.8263±0.0016	0.8032±0.0004	0.10±0.02
H5	1/2	0.9698±0.0016	0.9831±0.0004	0.10±0.02
H6	0.1760	0.7167±0.0014	0.0169±0.0004	0.10±0.02
O1	0	0.6581±0.0014	0.0627±0.0004	
O2	1/2	0.8263±0.0016	0.9373±0.0004	

possible ordered structures discussed in chapter 2. In figures 6.16 to 6.18 the calculated profiles are compared with the experimental data. A comparison with the simulated profiles in chapter 2 shows that the differences between the profiles for the different structures are much less significant for H_2O ice than for D_2O. This is because the differences are due to reflection from the hydrogen or deuterium nuclei: as the coherent scattering length for hydrogen is only -0.3500, compared with 0.6670 for deuterium, the reflections from hydrogen are weaker. However, most of the simulated profiles show clear differences from the observed data. The monoclinic structure 'G' shows apparent reasonable agreement with the data. However, the structure could not be satisfactorily refined using this model. In particular, no improvement in the fit could be obtained by allowing the monoclinic angle β to vary from 90°. The antiferroelectric structure 'M' proposed by Owston is in clear disagreement with the data. It therefore appears that the data are best explained by the $Cmc2_1$ model.

The peak shape was modelled in the profile refinement by a function containing both Gaussian and Lorentzian terms. The Lorentzian part, $\Gamma=y\lambda^2$, describes the broadening of the peaks due to the finite size of crystallites within the sample, and is proportional to the integral breadth of the peak. y is inversely proportional to the particle size. In the ordered phase, y was found to be (13.8±0.5) microseconds, from which the particle size was calculated to be (560±20) angstrom. This suggests that the ordered regions are reasonably large in extent, containing about 5 million molecules. The mean separation of K^+ ions, assuming a concentration of 0.02

FIGURE 6.16

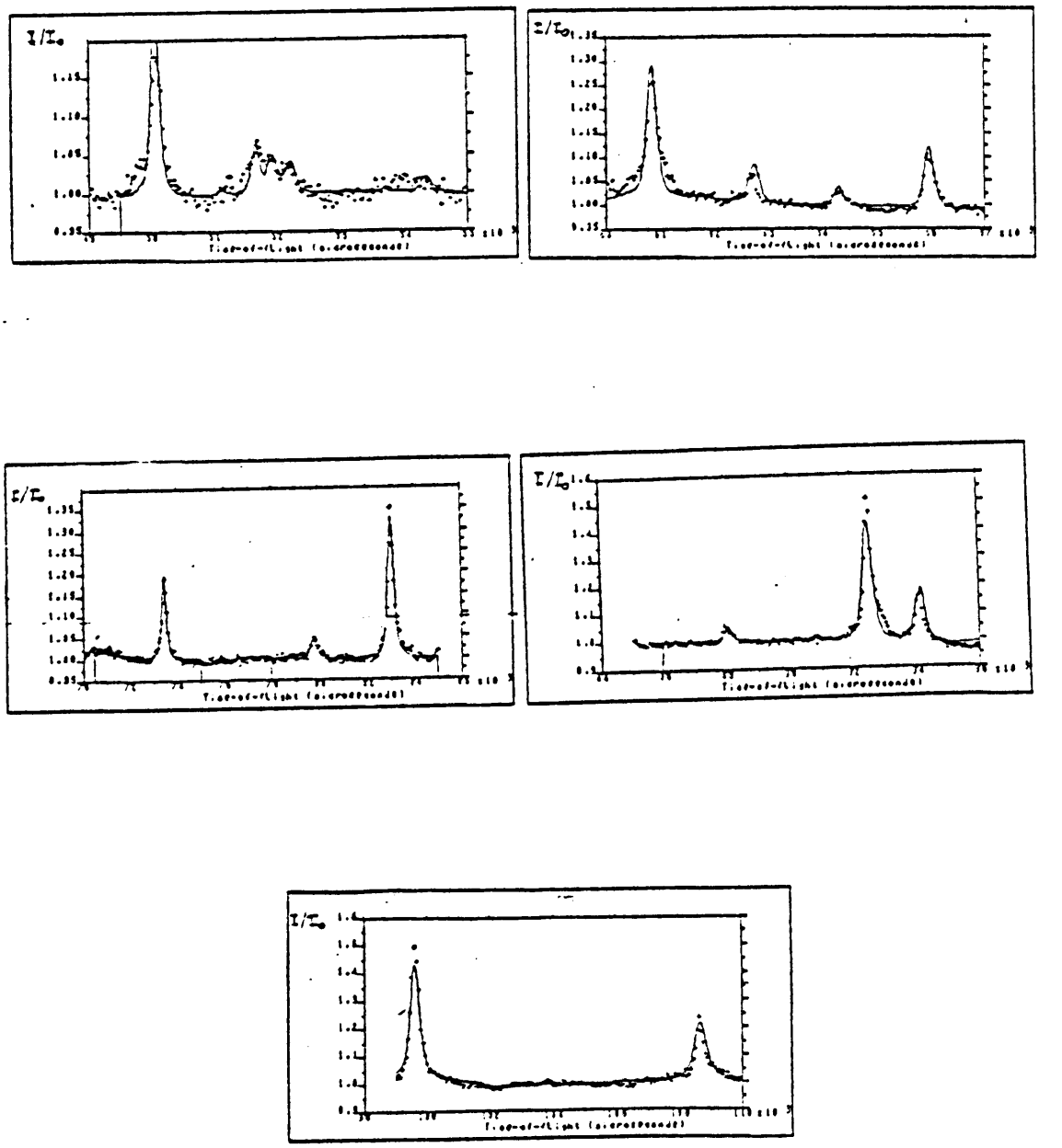

Simulated profile (line) for structure G, compared with the data (crosses)

Following page 111

FIGURE 6.17

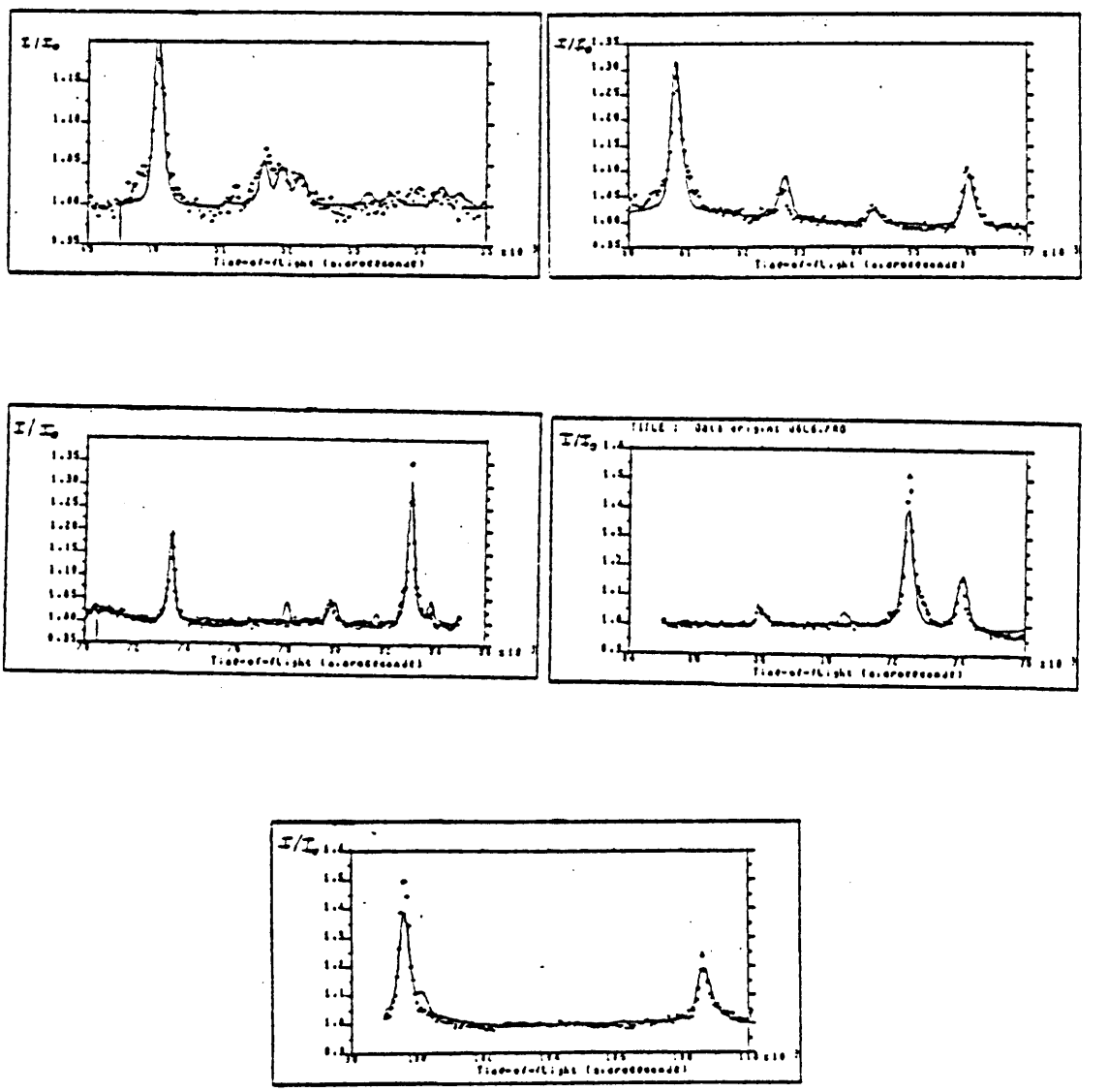

Simulated profile (line) for structure M, compared with the data (crosses)

Following page 111

FIGURE 6.18

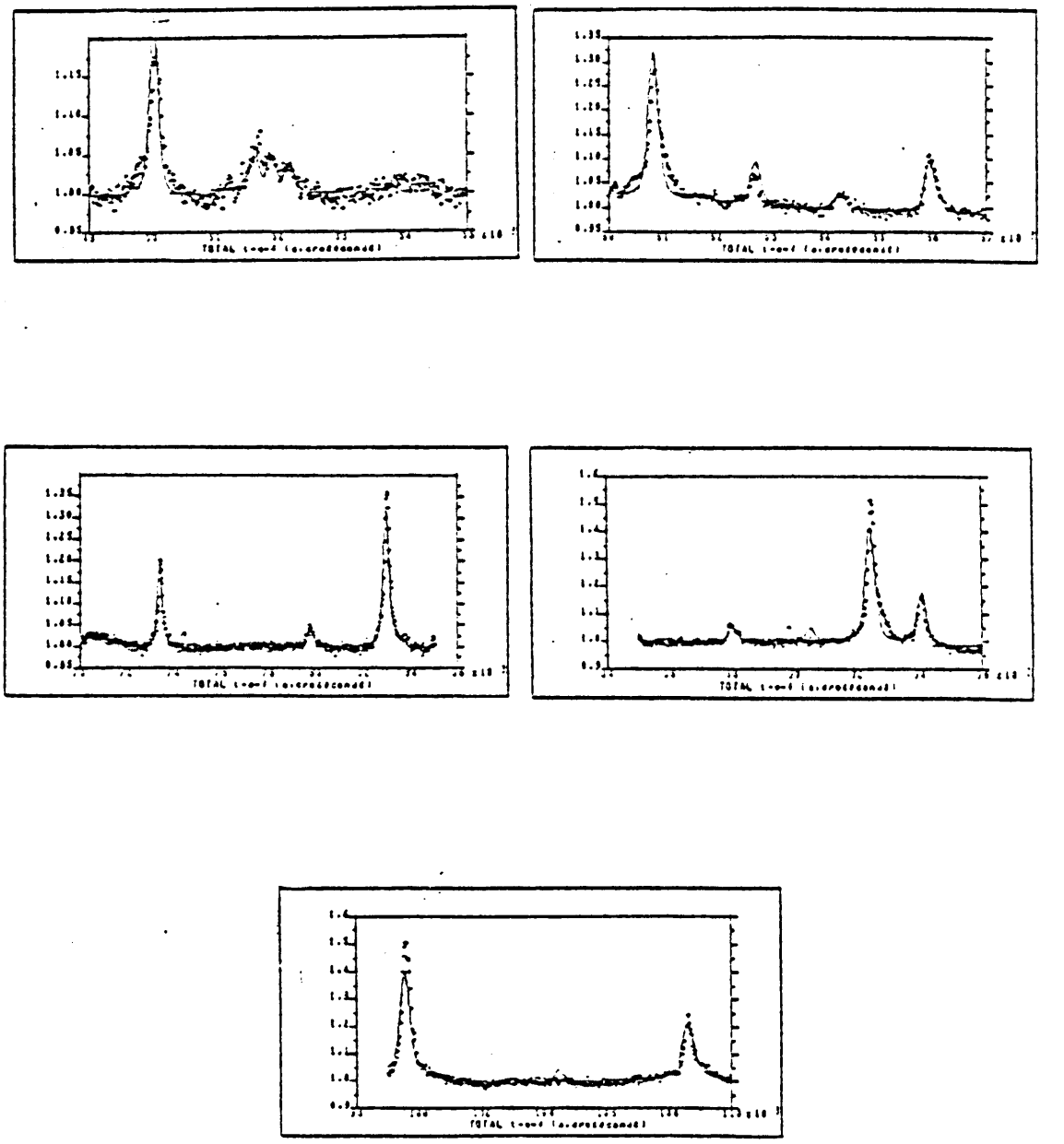

Simulated profile (line) for structure Q, compared with the data (crosses)

Following page 111

M, would be approximately 50 angstrom: it therefore appears that the domains are not simply nucleated on a single K^+. The value of y for the quenched sample was (2.0±0.1) microsecond, giving a particle size of (3800±200) angstrom.

There are interesting and statistically significant differences between the values found for the lattice parameters from the two 'disordered' samples at 10 K: the *c/a* ratio for the quenched phase in the second experiment is lower than for any of the other experiments on disordered ice and lower than the value (1.62778) found by Brill and Tippe (1967) for ice at 13 K. This suggests that there may be a small amount of short-range order present in the quenched phase, either because the nuclei of order were not completely removed by keeping the sample at 100 K for six hours or because some nucleation took place during the rapid cooling to 10 K. Also, very close comparison of the profiles for the annealed and quenched samples reveals a slight shift in the reflections attributed to the disordered part of the annealed sample relative to those in the quenched phase. This may account for some slight anomalies in the subtracted profile. No suitable program was available for carrying out a refinement on the two phases simultaneously. In any case, such a calculation would be difficult when the spectra for the two phases are so nearly superimposed.

The difference in volume between the quenched and annealed ice at 10 K in the second experiment was found to be (0.13±0.02)%. However, if the annealed ice is compared with the truly disordered specimen in the first experiment, the change is (0.176±0.006)%,

which is close to the value found by Yamamuro et al. assuming a homogeneous partial order. Were it not for the strong *c*-axis contraction (a change of (0.30±0.01)%) in the ordered phase, the change would have been difficult to detect even with the resolution of HRPD.

CHAPTER 7

SUMMARY AND SUGGESTIONS FOR FURTHER WORK

7.1 Summary of achievements

The transition to the ordered phase of ice Ih has been studied in several aspects both theoretical and experimental. A theory has been developed relating the entropy loss and the change in the static dielectric constant in the ordering transition to the degree of order achieved. This theory relies on the assumption that the ordered regions are in equilibrium, and is valid only in the temperature region where the Helmholtz free energy has two minima with respect to the order parameter f, the fraction of correctly oriented bonds.

A system has been developed for the measurement of the dielectric properties of ice by the application of a d.c. step voltage to an ice sample. This technique, which is more convenient for the measurement of long relaxation times than the conventional a.c. bridge method, has been used to study the dielectric properties of KOH-doped ice both above and below the ordering transition temperature. Despite some difficulties in interpretation of the data, the method provided a useful means of studying the progress of the ordering transition and of establishing a suitable strategy for preparing a specimen for neutron diffraction. In the higher temperature ranges, the method was used in parallel with a.c. measurements. In the region of overlap, the results obtained by the two methods were in reasonable agreement. The transition was

studied repeatedly in many samples, and several reproducible features of the behaviour were observed.

The mechanism of the proton rearrangement in KOH-doped ice has been established by dielectric measurements to be the movement of OH^- ions, which have a low but temperature-independent mobility and a relatively high concentration even at low temperatures. The mobility of the ions has been estimated by measurement of the conductivity in the extended region where it is independent of temperature.

Detailed investigation of the changes which take place as the ordering proceeds suggests a model for the process. As the sample is cooled, it remains almost entirely disordered until a certain temperature, several degrees below the transition temperature, is reached. This supercooling is consistent with the theoretical prediction of a nucleation barrier for the ordering transition which vanishes when the temperature reaches about 60 K. On cooling below this temperature, nuclei of ordered material are formed and begin to grow, the rate of growth being governed by the availability of mobile defects and so varying with the dielectric relaxation time. As ordering proceeds, the dielectric response of the crystal is altered in two ways. Firstly, the strength of the relaxation is reduced as part of the volume is converted to a phase with low permittivity. Secondly, the conductivity is decreased, either because some ions become trapped in the ordered regions or because their mobility in these regions is reduced. The growth of the ordered regions can be speeded up by increasing the temperature

and so decreasing the relaxation time. At the higher temperature, the ordered regions will be partially disordered, but this effect appears to be reversible. The observed increase in the relaxation strength as the sample is heated several degrees below the transition temperature is probably an artefact of the method, reflecting the decrease in relaxation time, rather than a real effect. In well transformed specimens, an activation energy for the conductivity was measured which was higher than that in the disordered phase.

Most of the samples investigated consisted of a mixture of regions capable of becoming ordered, in which the initial concentration of ions was presumably high, with other regions not so capable. However, the ordering was never complete even in the regions where it was possible. Due to limitations of time it was not feasible to transform all specimens as fully as possible.

The structure of ice XI has been confirmed to be polar and orthorhombic, with the space group *Cmc*2$_1$ and eight molecules in the unit cell, as found by Leadbetter et al. (1985). This was accomplished by a neutron diffraction experiment on a powdered ice sample of which more than half the volume was in the ordered phase, and in which the characteristic behaviour of the ordering process had been observed by dielectric measurements during the annealing period. This was a much more fully transformed sample than that used by Leadbetter et al. in the only other attempt to determine the structure of the ordered phase. The nature of the diffraction profile is consistent with a mixture of ordered and disordered

regions, with a resolvable difference in the *c*-axis lattice parameter and a significant distortion away from the hexagonal lattice of disordered ice. Other possible structures could be ruled out on the basis of comparisons between calculated and experimental diffraction profiles. The order parameter *f* in the ordered regions was approximately equal to 0.9, which is similar to the value obtained if the maximum entropy loss found by the calorimetric measurements of Tajima et al. (1984) is assumed to be that for homogeneous transformation to a partially ordered phase. The ordered regions were relatively large in extent compared with the average separation of dopant molecules. The volume change between the ordered and disordered phases is consistent with that found by Yamamuro et al. (1987c).

7.2 Suggestions for further work

There are several directions in which this research could be extended. The dielectric properties of ice doped with the hydroxides of other alkali metals, in particular lithium and sodium, would be of interest. It would also be interesting to study the dielectric properties of doped D_2O ice and the effect of contamination by H_2O on the defect mobility.

The theoretical model of the partially ordered state and the ordering process is in need of further development, in particular to quantify the effect of ordering on the conductivity of homogeneous and inhomogeneous partially ordered ice. It would also be useful to extend the theory to cover the case of a region which

is partially ordered but not in equilibrium.

The neutron diffraction work could be extended to D_2O ice - which, if a well-transformed sample could be produced, would be much more satisfactory than H_2O ice for this purpose - and also to single crystals. A technique for growing highly-doped single crystals of ice would have to be developed: the result of the one single-crystal dielectric experiment reported in this thesis suggests that it is possible to incorporate an effective concentration of dopant in a slowly-grown crystal. It would also be instructive to attempt to measure by diffraction the change in the degree of order as the transformed sample is heated towards the transition temperature.

FIGURE A.1

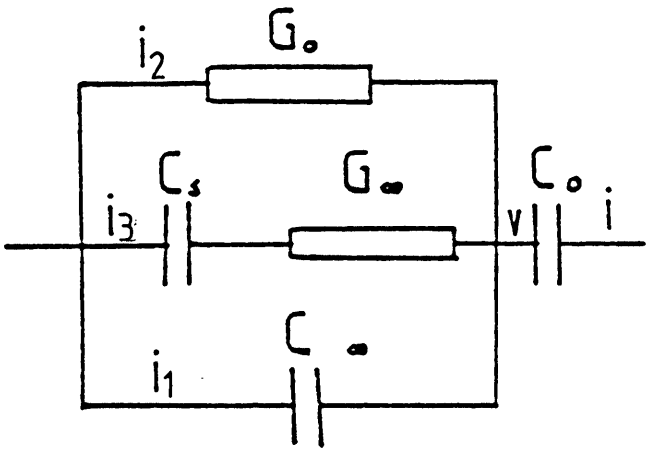

Equivalent circuit for ice with a blocking capacitor

APPENDIX

RESPONSE OF ICE TO A D.C. STEP VOLTAGE

The response to a d.c. voltage step of the equivalent circuit for ice with a blocking electrode may be calculated and interpreted as follows. Let the total current in the network be i and the currents in the three branches be i_1, i_2, i_3 as shown in figure A.1. Then the currents are related to the voltage V at point V by the equations

$$V_o - V = \frac{1}{C_o} \int i \, dt,$$

$$i_1 = C_\infty \frac{dV}{dt},$$

$$i_2 = G_o V,$$

$$\frac{i_3}{G_\infty} + \frac{1}{C_s} \int i_3 \, dt = V,$$

$$i = i_1 + i_2 + i_3.$$

These 5 equations in 5 variables can be rearranged to give

$$V_o = \frac{G_o}{C_o} \int V \, dt + \frac{1}{C_o} \int i_3 \, dt + \frac{(C_o + C_\infty) V}{C_o},$$

$$0 = \frac{i_3}{G_\infty} + \frac{1}{C_s} \int i_3 \, dt - V.$$

We now have two equations in the two unknowns V and i_3. Let $V=y$, $i_3=x$. Then the equations can be rewritten in the form

$$y_o(t) = a \int y \, dt + b \int x \, dt + cy,$$

$$0 = mx + \int x \, dt - ny,$$

where $a = \frac{G_0}{C_0}$, $b = \frac{1}{C_0}$, $c = \frac{C_0+C_\infty}{C_0}$, $m = \frac{C_0}{G_\infty}$, $n = C_s$.

Now take Laplace transforms $L(y) = Y(p)$, $L(x) = X(p)$. For $t<0$, $x=y=0$, while y_0 is a step function, equal to 0 for $t<0$ and to 1 for $t \geqslant 0$.

Using the transforms $L(y_0) = \frac{1}{p}$ and $L\left[\int\int y\,dt\right] = \frac{1}{p}Y$

we obtain the equations

$1 = aY + bX + cpY$,

$0 = mpX + X - npY$,

which can be solved for Y to give

$$Y = \frac{1 + mp}{a + (c+am+bn)p + cmp^2}. \qquad (A.1)$$

This may be written in the form

$$Y = \frac{A_1}{p+\lambda_1} + \frac{A_2}{p+\lambda_2}, \qquad (A.2)$$

which has the inverse transform $y = A_1 \exp(-\lambda_1 t) + A_2 \exp(-\lambda_2 t)$. A_1, A_2, λ_1, λ_2 are the quantities obtained from the experimental data: the function fitted to the data is of the form $C = C_0 - C_1 \exp(-t/\tau_1) - C_2 \exp(-t/\tau_2)$, so $A_1=C_1/C_0$, $\tau_1=1/\lambda_2$, etc. By using the identity of expressions A.1 and A.2, and equating coefficients of p in numerator and denominator, the quantities a, b, c, m and n can be found. They are given by

$$c = \frac{1}{A_1+A_2}, \quad m = \frac{A_1+A_2}{A_1\lambda_2+A_2\lambda_1}, \quad a = \frac{\lambda_1\lambda_2}{A_1\lambda_2+A_2\lambda_1}, \quad b = \frac{1}{C_0} \text{ and}$$

$$n = C_0\left[\frac{\lambda_1+\lambda_2}{A_1\lambda_2+A_2\lambda_1} - \frac{1}{A_1+A_2} - \frac{\lambda_1\lambda_2(A_1+A_2)}{(A_1\lambda_2+A_2\lambda_1)^2}\right].$$

If C_0 is known, the four unknown parameters of the equivalent

circuit may thus be calculated directly from the fitted time constants and relaxation strengths, using the relations

$$C_\infty = C_0(c-1)$$

$$C_S = n$$

$$G_\infty = n/m$$

$$G_0 = a/b.$$

REFERENCES

BARNES, W. H. (1929) The crystal structure of ice between 0°C and -183°C. *Proc. R. Soc.*, A125, 670-693

BARNES, P., BLISS, D. V., FINNEY, J. L. and QUINN, J. E. (1980) Co-operative and quadrupole effects in order-disorder transitions in crystalline ices. *Faraday Discussions of the Chemical Society* 69

van den BEUKEL, A. (1968) Specific heat of ice near the 'ferroelectric' transition temperature. *Phys. Stat. Sol.* 28, 565

BERNAL, J. D., and FOWLER, R. H. (1933) A theory of water and ionic solution, with particular reference to hydrogen and hydroxyl ions. *J. chem. Phys.* 1, 515

BJERRUM, N. (1951) Structure and properties of ice I. The position of the hydrogen atoms and the zero-point entropy of ice. *K. Danske Vidensk.* Skelsk. Skr. 27, 1 [*Science* 115, 385 (1952)]

BRAGG, W. H. (1922) The crystal structure of ice. *Proc. phys. Soc.* 34, 98

BRILL, R., and TIPPE, A. (1967) Gitterparameter von Eis I bie tiefen Temperaturen. *Acta Crystallogr.* 23, 343

CHAMBERLAIN, J. S, MOORE, F. H., and FLETCHER, N. H. (1973) Neutron-diffraction study of H_2O ice at 77 K. In *Physics and Chemistry of Ice*, (eds. E. Whalley, S. J. Jones and L. W. Gold), Royal Society of Canada, Ottawa, p. 283

DAVIDSON, E. R., and MOROKUMA, K., (1984) A proposed antiferroelectric structure for proton ordered ice Ih. *J. chem Phys.* 81, 3741

DAVIES, W. E. A. (1971) The theory of composite dielectrics. *J. Phys. D: Appl. Phys.*, 4, 318

DENGEL O., ECKENER U., PLITZ H., and RIEHL N. (1964) Ferroelectric behaviour of ice. *Phys. Letters* 9, 291

GIAUQUE, W. F., and ASHLEY, M. (1933) Molecular rotation in ice at 10°K. Free energy of formation and entropy of water. *Phys. Rev.* 43, 81

GIAUQUE, W. F., and STOUT, J. D. (1936) The entropy of water and the third law of thermodynamics. The heat capacity of ice from 15 to 273 K. *J. Am. Chem. Soc.* 58, 114

GIGUÈRE, P. A. (1959) On the anomalous thermodynamic properties of ice. *J. Phys. Chem. Solids* 11, 249

HAIDA, O., MATSUO, T., SUGA, H., and SEKI, S. (1974) Calorimetric study of the glassy state: X. Enthalpy relaxation at the

glass-transition temperature of hexagonal ice. *J. chem. Thermodynamics* 6, 815

HANDA, Y. P., KLUG, D. D., and WHALLEY, E. (1987) Phase transitions of ice V and VI. *Journal de Physique* 48, Colloque C1, 435

HENTSCHEL, H. G. E. (1979) The ferroelectric transition in hexagonal ice Ih. *Molecular Physics* 38, 401

HELMREICH, D., (1973) Imperfection-induced phase transformation in D_2O ice Ih. in *Physics and Chemistry of Ice*, (eds E. Whalley, S. J. Jones and L. W. Gold), Royal Society of Canada, Ottawa, p. 291

HELMREICH, D., (1969) Elastic anomalies of ice at low temperatures. In *Physics of Ice* (eds N. Riehl, B. Bullemer and H. Engelhardt), Plenum Press, New York, p. 231

von HIPPEL, A., KNOLL, D. B., and Westphal, W. B. (1971) Transfer of protons through 'pure' ice Ih single crystals. I. Polarization spectra of ice. *J. chem. Phys.* 54, 134

HOBBS, P. V. (1974) *Ice Physics*, Oxford University Press

HOWE, R. (1987) The possible ordered structures of ice Ih. *Journal de Physique*, 48, Colloque C1 599

HOWE, R., and WHITWORTH, R. W. (1987) The configurational entropy of partially ordered ice. *J. chem. Phys.* 86, 6443

HUBMANN, M. (1979) Polarization processes in the ice lattice 1. Approach by thermodynamics of irreversible processes. New experimental verification by means of a universal relation. *Z. Physik B* 32, 127

IDA, M., and KAWADA, S. (1966) Dielectric dispersion of KOH-doped ice at low temperatures. *J. Phys. Soc. Japan* 21, 561

JACCARD, C. (1964) Thermodynamics of irreversible processes applied to ice. *Phys. Kondens. Materie* 3, 99

JACCARD, C. (1959) Etude theorique et experimentale des proprietes electriques de la glace. *Helv. Phys. Acta* 32, 89

KAMB, B., (1973) Crystallography of ice. In *Physics and Chemistry of Ice*, (eds E. Whalley, S. J. Jones and L. W. Gold), Royal Society of Canada, Ottawa, p. 28

KAWADA, S., (1978) Dielectric anisotropy in ice Ih. *J. Phys. Soc. Japan* 44, 1881

KAWADA, S., (1972) Dielectric dispersion and phase transition of KOH-doped ice. *J. Phys. Soc. Japan* 32, 1442

KAWADA, S., and DOHATA, H., (1985) Dielectric properties on 72 K phase transition of KOH-doped ice. *J. Phys. Soc. Japan* 54, 477

KAWADA, S., and SHIMURA, K., (1986) Dielectric studies of RbOH-doped ice and its phase transition. *J. Phys. Soc. Japan* 55, 4485

LEADBETTER, A. J., WARD, R.C., CLARK, J. W., TUCKER, P. A., MATSUO, T., and SUGA, H. (1985) The equilibrium low-temperature structure of ice. *J. chem. Phys.* 82, 424

LONG, E. A., and KEMP, J. D., (1936) The entropy of deuterium oxide and the third law of thermodynamics. Heat capacity of deuterium oxide from 15 to 298°K. The melting point and heat of fusion. *J. Am. Chem. Soc.* 58, 1829

MATSUO, T., and SUGA, H. (1987) Calorimetric study of ices Ih doped with alkali hydroxides and other impurities. *Journal de Physique* 48, Colloque C1, 477

MATSUO, T., TAJIMA, Y., and SUGA, H., (1986) Calorimetric study of a phase transition in D_2O Ice Ih doped with KOD: Ice XI. *J. Phys. Chem. Solids* 47, 165

MINAGAWA, I. (1981) Ferroelectric phase transition and anisotropy of dielectric constant in Ice Ih. *J. Phys. Soc. Japan* 50, 3669

MITSUI, T., TATSUZAKI, I., and NAKAMURA, E. (1974) *An introduction to the physics of ferroelectrics*. Gordon and Breach Science Publishers

NAGLE, J. F. (1973) in *Physics and Chemistry of Ice*, (eds E. Whalley, S. J. Jones and L. W. Gold), Royal Society of Canada, Ottawa, p. 70

OHTOMO, M., AHMAD, S. and WHITWORTH, R. W. (1987) A technique for the growth of high quality single crystals of ice. *Journal de Physique* 48, Colloque C1, 595

ONSAGER, L. (1967) Ferroelectricity of ice? In *Ferroelectricity* (ed. E. F. Weller) Elsevier, New York, p. 16

OWSTON, P. G., (1953) La position des atomes d'hydrogene dans la glace. *J. Chim. Phys.* 50, C13

PAREN, J. G. and GLEN, J. W. (1978) Electrical behaviour of finely divided ice. *Journal of Glaciology*, 21, 173

PAULING, L. (1935) The structure and entropy of ice and of other crystals with some randomness of atomic arrangement. *J. Am. Chem. Soc.* 57, 2680

PETERSON, S. W. and LEVY, H. A. (1957) A single-crystal neutron diffraction study of heavy ice. *Acta Crystallogr.* 10, 70

PETRENKO, V. F., WHITWORTH, R. W., and GLEN, J. W. (1983) Effects of proton injection on the electrical properties of ice. *Philosophical Magazine B*, 47, 259

PICK, M. A. (1969) The specific heat of ice Ih. In *Physics of Ice*, (Eds. N. Riehl, B. Bullemer and H. Engelhardt), Plenum Press, New York, p. 344

PICK, M. A., WENZL H., and ENGELHARDT, H., (1971) The specific heat of pure and doped ice near 120°K. *Z. Naturforsch.* 26a, 810

PITZER, K. S., and POLISSAR, J., (1956) The order-disorder problem for ice. *J. Phys. Chem.* 60, 1140

RUNDLE, R., E., (1955) The structure of ice. *J. Phys. Chem.* 59, 680

SAKABE, Y., IDA, M., and KAWADA, S. (1970) Dielectric dispersion of NaOH-doped ice at low temperatures. *J. Phys. Soc. Japan* 28, 265

SUGA, H. (1985) Phase diagram of ice and discovery of phase XI. *Kotai Butsuri* 20, 135

SUGA, H., and SEKI, S. (1974) Thermodynamic investigation on glassy states of pure simple compounds. *Journal of non-crystalline solids* 16, 171

TAJIMA, Y., MATSUO, T., and SUGA, H., (1984) Calorimetric study of phase transition in hexagonal ice doped with alkali hydroxides. *J. Phys. Chem. Solids* 45, 1135

TAJIMA, Y., MATSUO, T., and SUGA, H., (1982) Phase transition in KOH-doped hexagonal ice. *Nature (Lond.)* 299 811

TAKEI, I. and MAENO, N. (1987) Electric characteristics of point defects in HCl-doped ice. *Journal de Physique* 48, Colloque C1, 121

UEDA, M., MATSUO, T., and SUGA, H., (1982) Calorimetric study of proton ordering in hexagonal ice catalysed by hydrogen fluoride. *J. Phys. Chem. Solids* 43, 1165

WOLLAN, E. O., DAVIDSON, W. L. and SHULL, G. G. (1949) Neutron diffraction study of the structure of ice. *Phys. Rev.* 75, 1348

YAMAMURO, O., OGUNI, M., MATSUO, T. and SUGA, H. (1987a) Heat capacity and glass transition of pure and doped cubic ices. *J. Phys. Chem. Solids* 48, 935

YAMAMURO, O., OGUNI, M., MATSUO, T. and SUGA, H. (1987b) Heat capacity and phase transition of tetrahydrofuran clathrate hydrate. *Solid State Communications* 162, 289

YAMAMURO, O., OGUNI, M., MATSUO, T. and SUGA, H. (1987c) High-pressure calorimetric study on the ice XI-Ih transition. *J. chem. Phys.* 86, 5137

ZARETSKII, A. V., PETRENKO, V. F., RHYZKIN, I. A. and TRUKHANOV, A. V. (1987) Theoretical and experimental study of ice in the presence of a space charge. *Journal de Physique* 48, Colloque C1, 93